UNLV | UNIVERSITY LIBRARIES

1-1-2005

Experimental and finite element studies of shock transmission through jointed hat sections

Karthik Doppala
University of Nevada, Las Vegas

EXPERIMENTAL AND FINITE ELEMENT STUDIES OF SHOCK TRANSMISSION

THROUGH JOINTED HAT SECTIONS

by

Karthik Doppala

Bachelor of Technology in Mechanical Engineering
S.N.I.S.T, J.N.T University, Hyderabad
April 2003

A thesis submitted in partial fulfillment
of the requirements for the

**Master of Science Degree in Mechanical Engineering
Department of Mechanical Engineering
Howard R. Hughes College of Engineering**

**Graduate College
University of Nevada, Las Vegas
December 2005**

UMI Number: 1435604

INFORMATION TO USERS

The quality of this reproduction is dependent upon the quality of the copy submitted. Broken or indistinct print, colored or poor quality illustrations and photographs, print bleed-through, substandard margins, and improper alignment can adversely affect reproduction.

In the unlikely event that the author did not send a complete manuscript and there are missing pages, these will be noted. Also, if unauthorized copyright material had to be removed, a note will indicate the deletion.

UMI®

UMI Microform 1435604

Copyright 2006 by ProQuest Information and Learning Company.

All rights reserved. This microform edition is protected against unauthorized copying under Title 17, United States Code.

ProQuest Information and Learning Company
300 North Zeeb Road
P.O. Box 1346
Ann Arbor, MI 48106-1346

UNLV

Thesis Approval

The Graduate College
University of Nevada, Las Vegas

September 27, 2005

The Thesis prepared by

Karthik Doppala

Entitled

Experimental and Finite Element Analysis Studies of Shock Transmission

Throuth Jointed Hat Sections

is approved in partial fulfillment of the requirements for the degree of

Master of Science in Mechanical Engineering

Examination Committee Co-Chair

Examination Committee Chair

Dean of the Graduate College

Examination Committee Member

Examination Committee Member

Graduate College Faculty Representative

1017-53

ii

ABSTRACT

Experimental and Finite Element Studies of Shock Transmission Through Jointed Hat Sections

by

Karthik Doppala

Dr. Samaan G. Ladkany, Examination Committee Chair
Professor of Civil Engineering
University of Nevada, Las Vegas

and

Dr. Brendan J. O'Toole, Examination Committee Chair
Associate Professor of Mechanical Engineering
University of Nevada, Las Vegas

Shock transfer performance of joints has substantial influence on the dynamics of assembled structures as they induce a large amount of damping into the structure. Study of shock transmission through the various jointed (both mechanical and adhesive) components of the combat vehicle is of particular interest to the army. The principal objective of this work is to develop solutions that enable ARL to generate improved physics-based shock models for lightweight combat vehicles focusing mainly on shock transmission across structural joints. Shock transmission through two identical simple hat sections joined together with different joint configurations like adhesive bonding and bolted joints has been studied to understand the shock response of a full scale light combat vehicle. It was observed that the finite element results from the adhesively jointed double hat sections with spacers (both, continuous and intermittent) show better

congruity with the experimental results when compared to the double hat sections with

bolts.

TABLE OF CONTENTS

LIST OF FIGURES

viii

ix

LIST OF TABLES

ACKNOWLEDGEMENTS

The author is truly grateful to his advisor Dr. Samaan Ladkany and Dr. Brendan J. O'Toole, the Committee Chair Persons, for their guidance, encouragement throughout this investigation.

The author wishes to express his sincere thanks and heartiest gratitude to Dr. Mohamed B. Trabia, Dr. Samir Moujaes and Dr. Gerald Fredrick for their time in reviewing the prospectus, participation of defense, and counseling of the thesis as the committee members.

The financial support provided by the Army Research laboratory (ARL), under project BS3 is thankfully acknowledged.

The author expresses his thanks to the support and help of my colleagues through out this investigation.

CHAPTER 1

INTRODUCTION

1.1 Background

In the world today there is an increasing use of armor piercing projectiles and these constitute a growing threat most eminent to light combat vehicles. Welding, adhesive bonding, and mechanical fasteners are being used for joining various components of the light combat vehicles, especially the body which is subjected to impacts and pressure loads.

Light combat vehicles are at greater risks when they are subjected to impacts (due to projectile hits) and pressure loads (due to mine blasts) when compared to heavily armored combat vehicles. Sensitive equipment present inside the combat vehicles are most vulnerable to ballistic shocks and mine blasts. Shock propagation from the impact region to the vital locations where the sensitive components are present may lead to damage or misalignment, which might result in malfunctioning, and reduction of vehicle performance. Extensive research is in progress to analyze the dynamic response of complex structures involving assemblies, such as a light combat vehicle, as the study helps in understanding and evaluating the structural integrity of such structures when they are subjected to transient loading [1].

1

Joints play a very important role in maintaining the structural integrity of a combat vehicle. Non-linear shock transfer performance of joints has substantial influence on the dynamics of assembled structures as they induce a large amount of damping into the structure [2]. Study of shock transmission through the various jointed (both mechanical and adhesive) components of the combat vehicle is of particular interest to the Army. There is a need to guarantee the survivability and minimize the damage caused to both the primary and secondary electronic systems present inside the combat vehicle. Another area of concern is to reduce or damp the shock transmission caused by a projectile impact. There is an immediate need to develop methodologies for constructing predictive models of structures with joints and shock based dynamic response analysis in order to ensure the safety of critical equipment and hardware [1,3].

1.2 Structural Joints

The design of structural systems involves elements that are joined through bolts, rivets, pins and weldments. Joints and fasteners are used to transmit loads from one structural element to another. In structures, there are three types of joints commonly used, namely, welded, mechanically fastened joints and adhesive bonded joints. Fastened joints include bolts, rivets, and pins. The design of adhesive joints depends on the quantity of the parts to be joined and the amount of overlap necessary for carrying the load [3].

Adhesive joints are being used for joining secondary structures in the automotive industry, which are usually not essential for structural strength and are generally avoided in crucial structures because of their weakness, chemical interaction effects, and dependability [3]. Bolting and welding are still the prevailing fastening mechanisms, used

2

in joining crucial structural parts for most of the machinery in the automotive industry. Adhesive bonding is being widely employed in the aerospace industry to manufacture joints critical for the safety of an airplane [4]. One of the most important reasons for this being its superior fatigue performance compared to conventional joining techniques. Fatigue is considered one of the most important design concerns for aerospace structures [5] and the use of adhesive joints has been enhanced with the ever-growing use of composites in our day-to-day lives.

Nevertheless it cannot be said that one particular type of joint is better than the other as all the joints have their own advantages. For instance adhesive bonding offers improved joint stiffness compared to mechanical fasteners or spot-welds as it produces a continuous bond rather than a localized point contact; this results in a more uniform stress distribution over a larger area. An adhesive is essentially used for dual purposes, it not only provides mechanical strength, but it also seals the joint against moisture and debris ingress. A well-designed joint will absorb energy adequately, and tend to have good noise and vibration damping properties. On the other hand, mechanical joining is easier and more economical and involves less safety and health hazards as most of the current high performance adhesives are epoxy or solvent based systems, which give rise to considerable environmental concerns. Unlike adhesive joints mechanical fasteners are inherently strong in peel and vehicle design takes account of this, particularly with regard to crashworthiness [6].

The complex behavior of connecting elements plays an important role in the overall dynamic characteristics of structures such as natural frequencies, mode shapes, and non-linear response characteristics to external excitations. The joint represents a

3

discontinuity in the structure and results in high stresses that often initiate structural failure [3]. Joints appear to be simple, but as one begins to think about them and start to understand how they work, it becomes apparent how complicated they really are and how difficult it is to precisely quantify their behavior.

1.3 Structural Dynamics of Joints

Little work has been published on the study of shock transmission through jointed structures; however there has been a great deal of work done on both shock propagation in structures and jointed static analysis of joints.

Various finite element models for joints are being developed [7,8] which can accurately predict their dynamic response. Adoption of this type of analysis early in the design phase can influence decisions that improve the structural performance. For example, accurately simulating slip-based mechanisms like sliding friction, clamping forces, bolt-plate interactions [7] are proving to be helpful in crash analysis scenarios. Damping being another important parameter in the design phase of a structure has been studied comprehensively. Detailed finite element models have been developed to establish an understanding of the slip-stick mechanisms in the contact areas of the bolted joints. As compared to material damping, joints act as the main sources of localized non-linear stiffness and damping so it has become imperative to develop models which include the effects of damping stiffness characteristics for calculating the dynamic response of the jointed structures [2, 9].

Y. Songa, C.J. Hartwigsenb, D.M. McFarlanda, A.F. Vakakisb,c,L.A. Bergman [9] have developed an Adjusted Iwan Beam Element (AIBE), which can simulate the

4

non-linear dynamic behavior of bolted joints in beam structures. The same element was used to replicate the effects of bolted joints on a vibrating frame; the attempt was to simulate the hysteretic behavior of bolted joints in the frame. The simulated and experimental impulsive acceleration responses had good agreement validating the efficacy of the AIBE. This element shows its compatibility with the finite element two-dimensional linear elastic beams and is, thus, easily used. Thus AIBE proved to be a universal method of modeling beam structures for non-linear dynamic analysis of bolted joints.

Various methods have been employed to determine the dynamic response of complex jointed structures. Studying the natural frequencies, modal behavior and damping of a structure, which constitute its dynamic characterization, gives us a better understanding of the dynamics of a structure and its reliability [10, 11]. The Frequency Response Function (FRF), which is obtained from Fast Fourier Transform (FFT), is the widely used method for determining the natural frequencies and mode shapes of a structure [12]. Nevertheless it is possible to determine the natural frequencies of a structure using FFT; determining the conspicuous peaks in the FFT analysis does this, the frequencies corresponding to these peaks are the natural frequencies of the structure. Figure 1-1 depicts a sample FFT graph.

5

ACCELEROMETER2
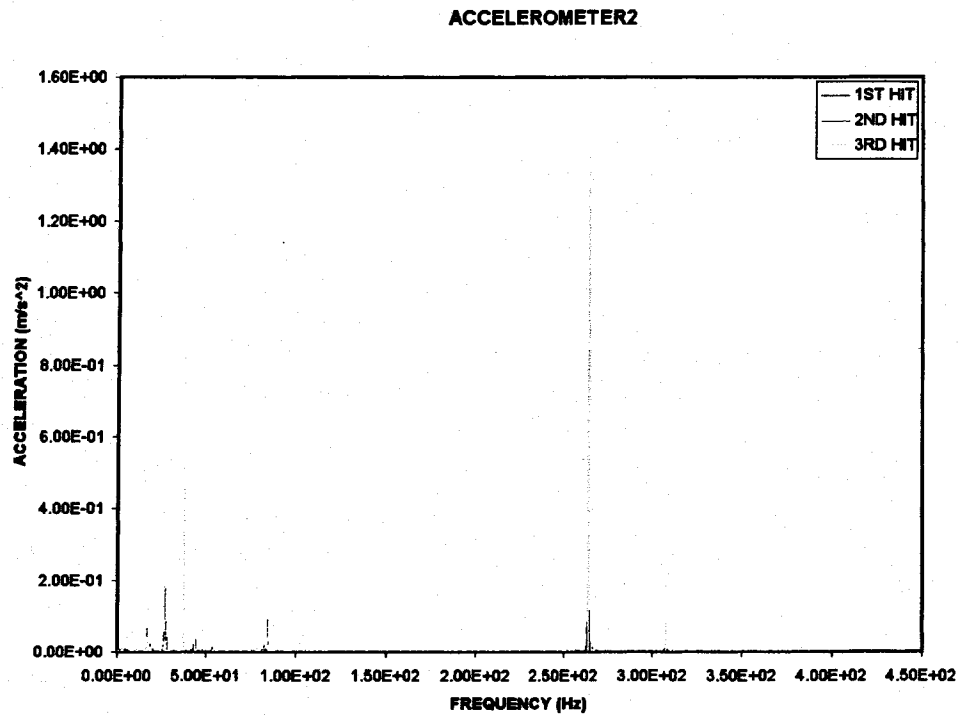
Figure 1-1 FFT graph depicting the peak amplitudes which correspond to the natural frequencies.

Responses measured from impulsive loading (like blast or impact) are typically accelerations, velocities and displacements at the crucial locations on the structure. While comparing the finite element results with the results obtained from experiments, one of these parameters is considered. Figure 1-2 shows a typical comparison graph of these parameters.

6

EXPERIMENT VS FEA
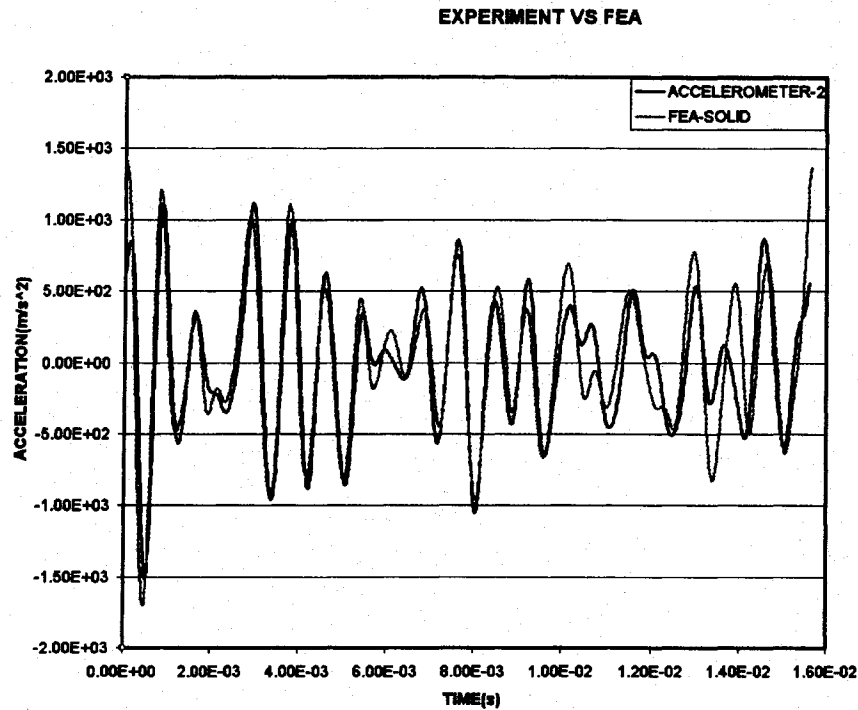
Figure 1-2 FEA and experimental comparisons of acceleration responses

1.4 Objective

The current project is a cooperative venture between the University of Nevada, Las Vegas (UNLV) and the Army Research Laboratories (ARL). The principal objective of research is to develop solutions that enable ARL to generate improved physics-based shock models for lightweight combat vehicles focusing mainly on shock transmission across structural joints. Impact on two identical simple hat sections joined together with different joint configurations, like adhesive bonding and bolted joints, have been identified as a suitable structure to understand the shock response of a full scale light combat vehicle. The objective was to try to create detailed models of structural joints that can simulate the shock transfer across the joint accurately and effectively.

7

This thesis work is one part of the UNLV approach to understanding shock transmission across joints. The following steps have been employed in the thesis to study the response of the jointed hat section:

1. Perform experimental FFT analysis on the jointed hat sections and compare the natural frequencies obtained from the finite element analysis.

2. Perform impact experiments on the jointed hat sections, which will provide input data (force vs. time) and response data (acceleration and/or strain vs. time).

3. Demonstrate that this experiment can be computationally simulated using a detailed 3-D LS-DYNA analysis.

4. Investigate the ability to accurately simulate the structural response for varied joint conditions like bolted joints and adhesive joints.

5. Investigate methods for increasing the efficiency of the analysis by using Shell and Solid element models.

CHAPTER 2

EXPERIMENTAL SETUP AND ANALYSIS OF A SINGLE HAT SECTION

2.1 Experimental Setup

A stand with a circular top is used to suspend the hat section. Steel wires are made to

pass through either side of the hat section and the ends of these wires are tied to the

circular top as shown in Figure 2-1. An impact hammer with a load transducer is used to

trigger the signal and accelerometers are used to record the accelerations at various

locations. A hardware key connected to the computer transmits the signals obtained by

the transducers from the PULSE data acquisition unit to the Pulse software shown

schematically in Figure 2-2.

9
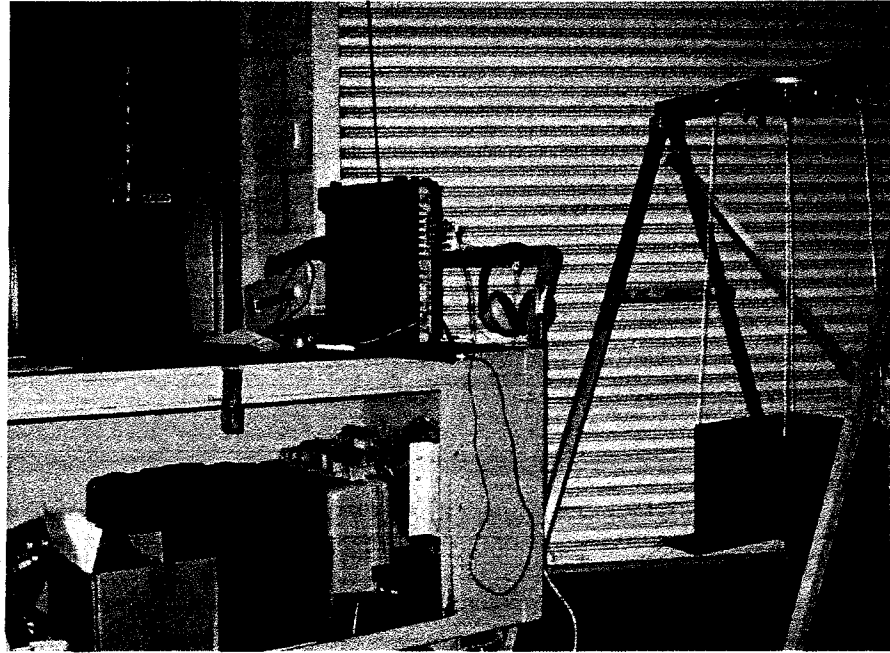
Figure 2-1 Experimental setup

Test Facilities

PULSE System

PC on LAN   "PULSE Viewer Clients"
running PULSE Viewer
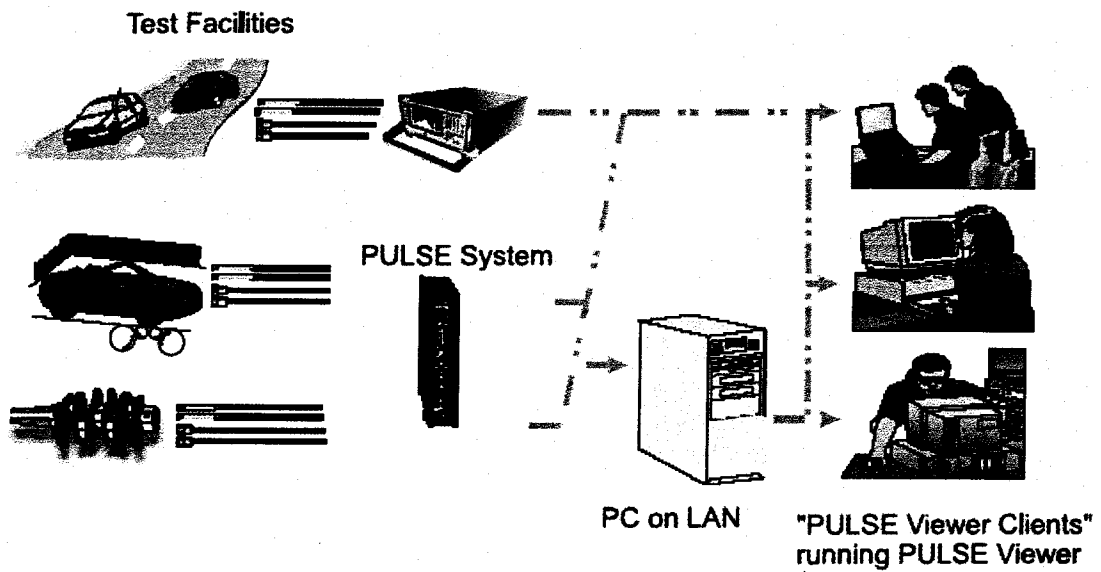
Figure 2-2 Data acquisition from PULSE hardware and software [15].

10

PULSE uses SI units, so the units for the input force and the output accelerations are (N) and (m/s^2) respectively. The PULSE system has six channels; one for the input force transducer and five channels are provided for the output transducers, in this case the output transducers are accelerometers. Specifications of the impact hammer and the accelerometers used are shown in Table 2-1 and Table 2-2 respectively. The accelerometers are mounted on the structure using wax.

Table 2-1 Specifications of the impact hammer [15]
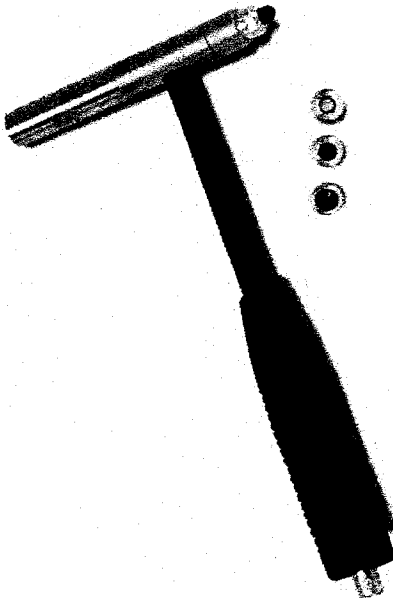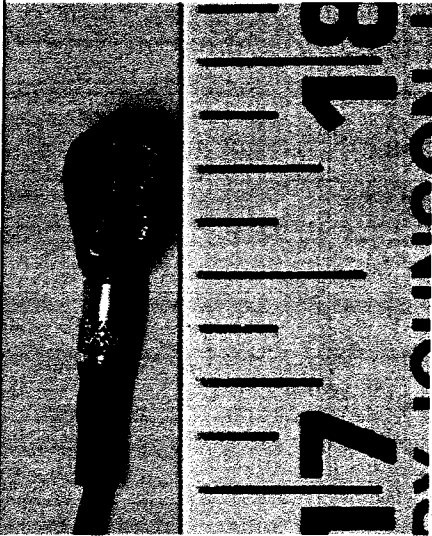
	PCB 086C02 Modally Tuned Impulse Hammer	
	Model #	086C20
	Sensitivity (±15%)	11.2 mV/N
	Measurement Range	±440N
	Frequency Range	1-2.5 kHz
	Mass	0.16Kg

Table 2-2 Specifications of the accelerometers [15]

	PCB 352C22 Piezoelectric Accelerometer	
Model #	352C22	
Sensitivity (± 15 %)	1.0mV/(m/s²)	
Measurement Range	+4900 m/s2 peak	
Frequency Range	1.0 to 2.5kHz	
Weight	0.5g	
Broadband Resolution	0.002 g rms (0.02 m/s² rms)	

2.2 Modal Analysis of the Single Hat Section

The frequency response of the hat section is studied before venturing into the study of shock propagation. The material of the hat section is steel; it has a thickness and length of 0.002654 meters and 0.1533meters respectively. A 3-D model of the hat section with its dimensions is shown below in Figure 2-3.

12
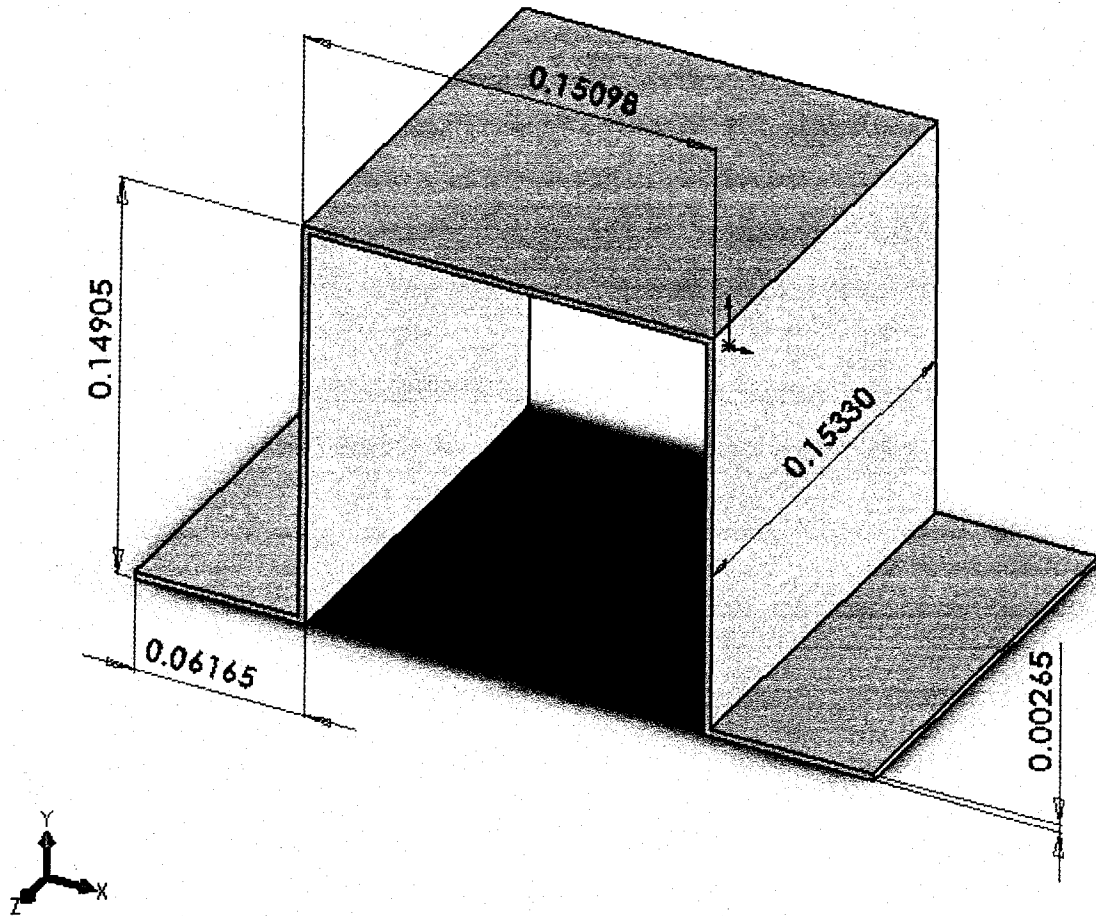
Figure 2-3 Dimensions of the hat section in meters.

2.3 Finite Element Analysis of the Hat Section

The single hat section is first studied by performing modal analysis. The results are then used to help find the natural frequencies experimentally by placing the accelerometers in the most critical places and in the optimum orientations. Material properties of steel used for the analysis are shown below.

13

Density, $\rho = 7780\text{kg/m}^3$

Young's Modulus, E = 200Gpa

Poisson's Ratio, $\nu = 0.33$

Exact shell and solid elements models of the hat section are created in ANSYS, which are shown in Figure 2-4. Modal analysis is performed on these models. The extracted mode shapes are shown in Figure 2-5. One can see that there are certain regions where the hat section deforms periodically when the mode shape is animated, particularly the corners of the horizontal flat plates and the edges of the vertical sides. Exhibiting the largest amplitudes, the accelerometers therefore are located at these locations of the hat section to obtain the natural frequencies experimentally.

14
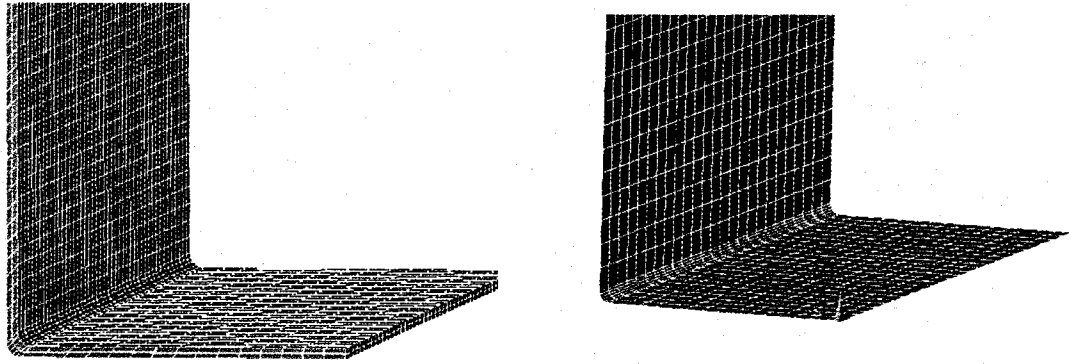
Figure 2-4 Shell and solid models of the hat sections

The solid element model has 31,977 elements and 20,800 nodes and the shell element model has 10,800 elements and 11,067 nodes. There are two elements along the thickness for the solid element hat section as there is a maximum restriction of 128000 elements that can be used in ANSYS and correspondingly three integration points have been incorporated for the thickness of the shell element model.
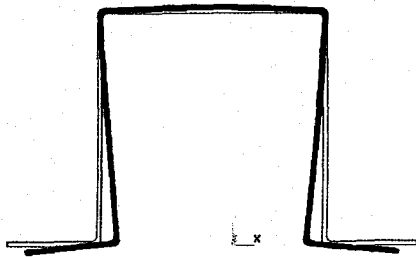
15
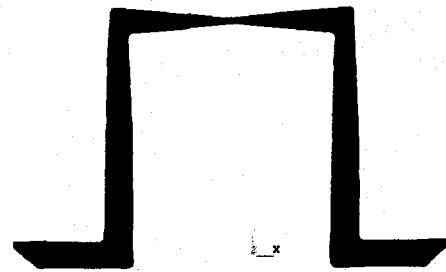
DISPLACEMENT
STEP=1
SUB =10
FREQ=142.711
DMX =2.208

JUN 10 2004
11:07:32

.05.914
..027
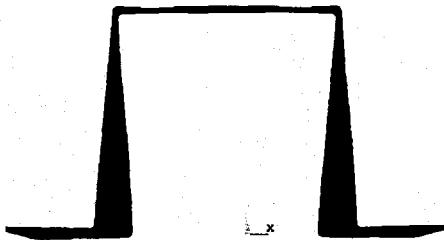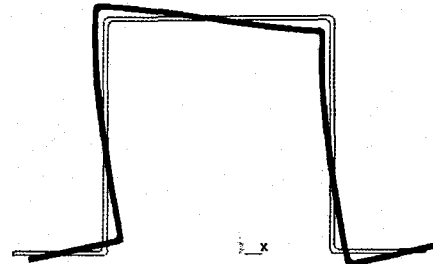
JUN 10 2004
11:06:34

DISPLACEMENT
STEP=1
SUB =11
FREQ=188.056
DMX =1.847
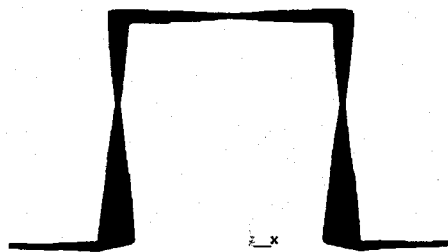
DISPLACEMENT
STEP=1
SUB =12
FREQ=274.172
DMX =2.052
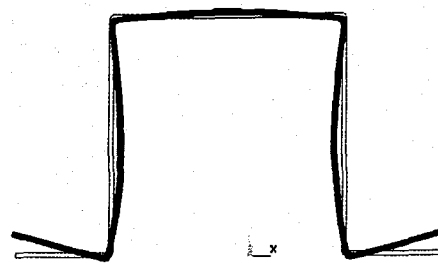
JUN 10 2004
11:09:09

Figure 2-5 First six-mode shapes of the single hat section

16

Experiments are performed on the single hat section by placing the accelerometers at the vertical edges and corners of the horizontal flat plates as discussed previously and shown in Figure 2-6. As seen from Figure 2-6(a) and 2-6(b), the hat section is impacted on the top for the second configuration and is hit on the side of the horizontal flat plates for the first configuration. This is done because the accelerometers used for the experiments are uni-axial thus they cannot record the accelerations in directions other than the direction perpendicular to the face of the accelerometer.

In the first configuration the accelerometers are placed on the horizontal corners of the hat section as shown in Figure 2-6(a) where as in the second configuration the accelerometers are placed on the vertical edges of the hat section that is shown in Figure 2-6(b). In both configurations, accelerometer-1 is placed on the left side and accelerometer-2 is placed on the right side of the hat section.

17
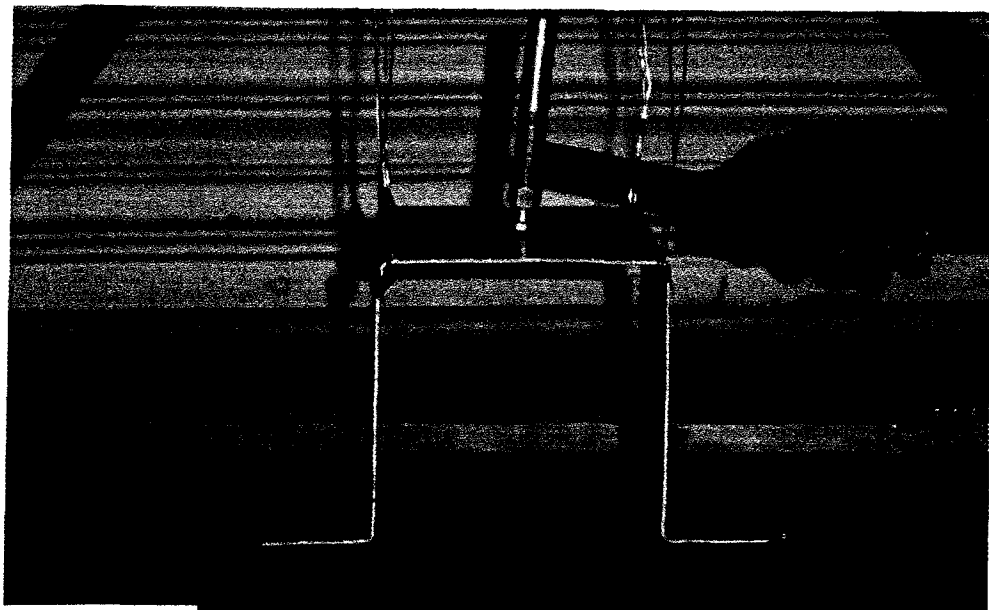
Accelerometer-1   Accelerometer-2

Figure 2-6(a) Impact configuration-1
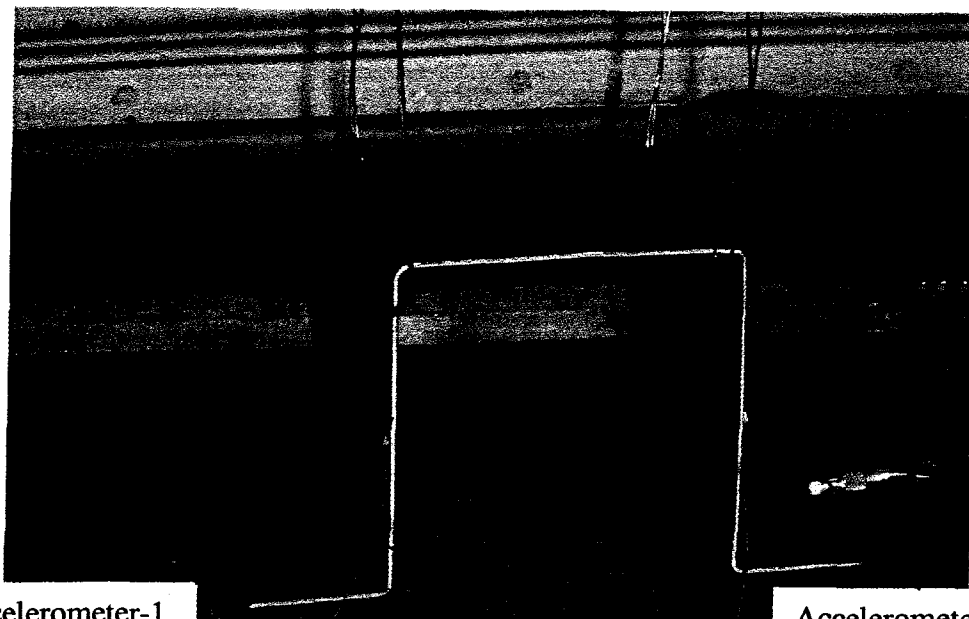
Accelerometer-1   Accelerometer-2

Figure 2-6(b) Impact configuration-2

18

The hat section is impacted in these configurations and Fast Fourier Transform (FFT) analysis is performed. The "y" axis corresponds to the acceleration amplitude, and the "x" axis corresponds to the frequency. The fundamental frequencies are those frequencies with which the hat section vibrates without the influence of any external force. The conspicuous peaks in the FFT correspond to the natural frequencies of the structure. Figure 2-7(a), (b), (c) and (d) show the natural frequencies of the hat section obtained from the accelerometers in both configurations. The hat section is impacted three times to make sure that the frequencies obtained are consistent.

19
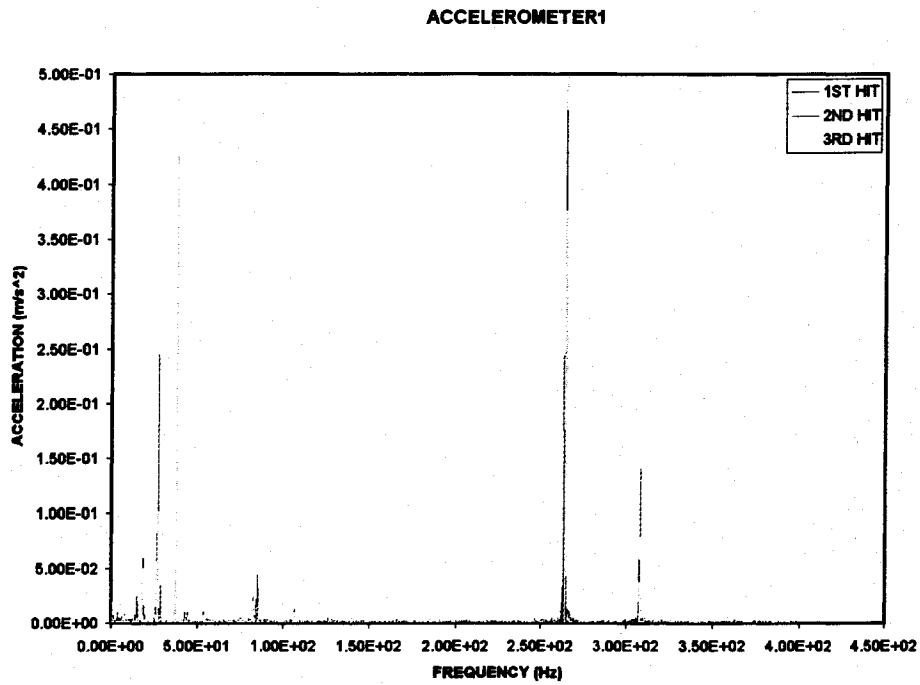
ACCELEROMETER1

Figure 2-7(a) Fundamental frequencies for the single hat section as measured by accelerometer-1 in configuration-1.
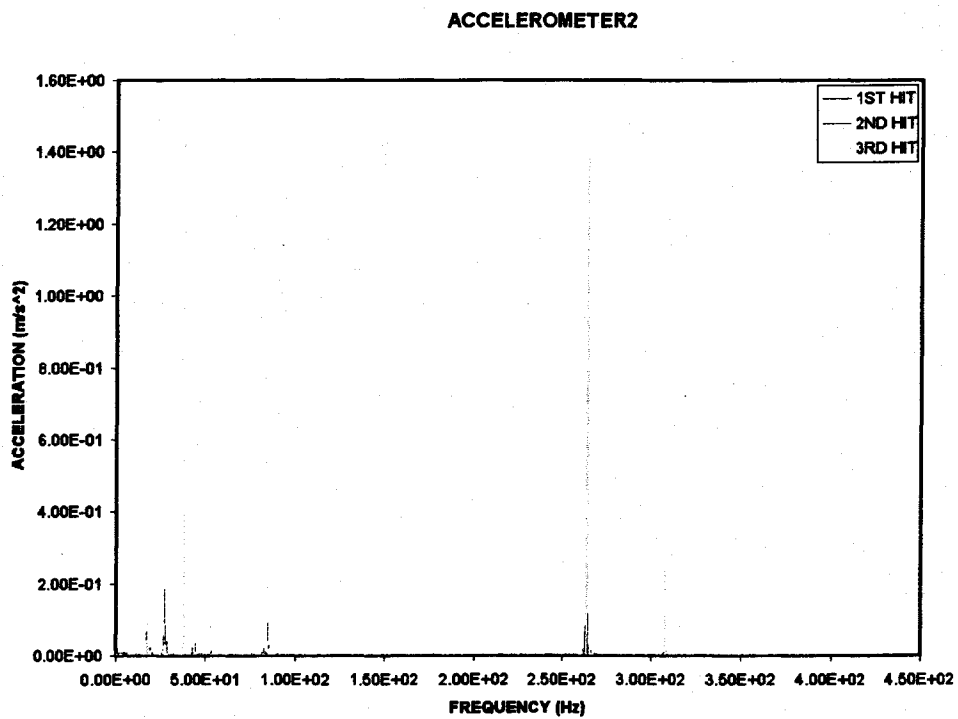
ACCELEROMETER2

Figure 2-7(b) Fundamental frequencies for the single hat section as measured by accelerometer-2 in configuration-1.

20
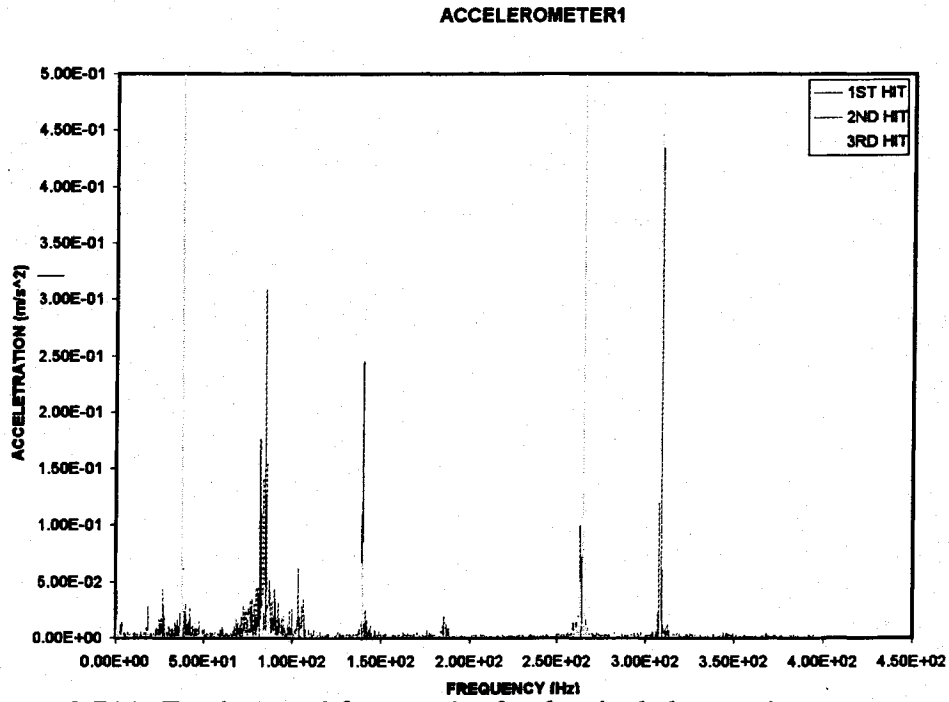
ACCELEROMETER1

Figure 2.7(c)- Fundamental frequencies for the single hat section as measured by accelerometer-1 in configuration-2.
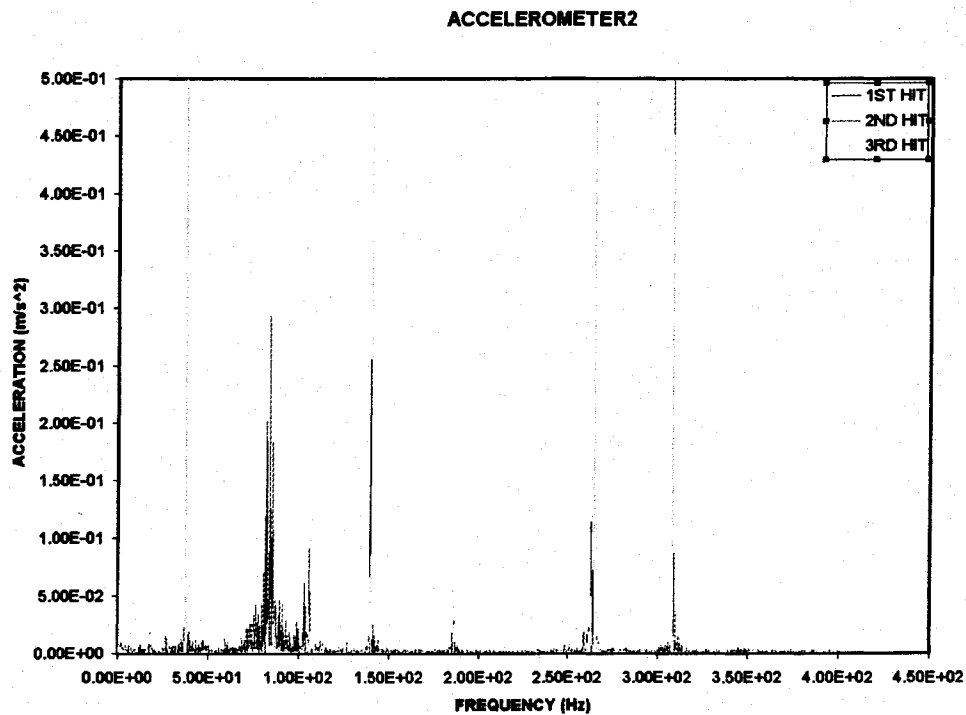
ACCELEROMETER2

Figure 2.7(d)- Fundamental frequencies for the single hat section as measured by accelerometer-2 in configuration-2.

21

There are absolutely no boundary conditions applied to the finite element models of the hat section. The effect of the steel cables supporting the hat section in the experimental phase is also neglected. The first six natural frequencies obtained from the finite element analysis are neglected as they characterize rigid body motion. Comparison between the values of natural frequencies obtained from the experiments and the finite element analysis, which includes both solid and shell element models of the hat section, is shown in Table 2-3. The reason behind recording the first thirteen natural frequencies is the fact that the default settings in the PULSE system are set to 400Hz, which was not changed while doing the experiments. If required, higher frequencies can also be recorded.

Table 2-3 Comparisons of experimental and finite element results

MODE #	EXPERIMENTAL (Hz)	SHELL MODEL (Hz)	SOLID MODEL (Hz)	% ERROR IN SOLID	% ERROR IN SHELL
7	34	38	38	11.5	11.71
8	84	81	81	3.28	2.93
9	104	105	105	1.07	1.83
10	140	141	142	0.85	1.93
11	186	187	188	0.68	1.10
12	264	273	274	3.44	3.85
13	308	317	322	3.10	4.71

It can be seen form the above table that the experimental and finite element analysis results show an analogous pattern. The natural frequency analysis discussed above is used as a benchmark for future experiments. As can be seen from the FFT graphs, either of the configurations can be used for obtaining the natural frequencies. The

only difference between the configurations is the amplitude, which might be more in one case than the other depending on the orientation of the accelerometer. Nevertheless the peaks corresponding to the natural frequencies are conspicuous in both configurations. The use of two accelerometers is to confirm the proper functioning and accuracy of the accelerometers as both of them pick up the same natural frequencies notwithstanding the fact that the amplitudes are slightly different.

2.4 Shock Transmission through a Single Hat Section

Acceleration response to an impact is measured with the help of the accelerometers .The load curve generated by the impact hammer is extracted from PULSE and is applied to the finite element models. Acceleromerter-2 is placed right behind the point of application of impact, which is at the center of the vertical side of the hat section as shown in Figure 2-9 and acclerometer-1 is placed at the center of the opposite vertical side. Initial finite element analysis is performed using four elements in the solid element model, and five integration points was used in the thickness of the shell element model.

23
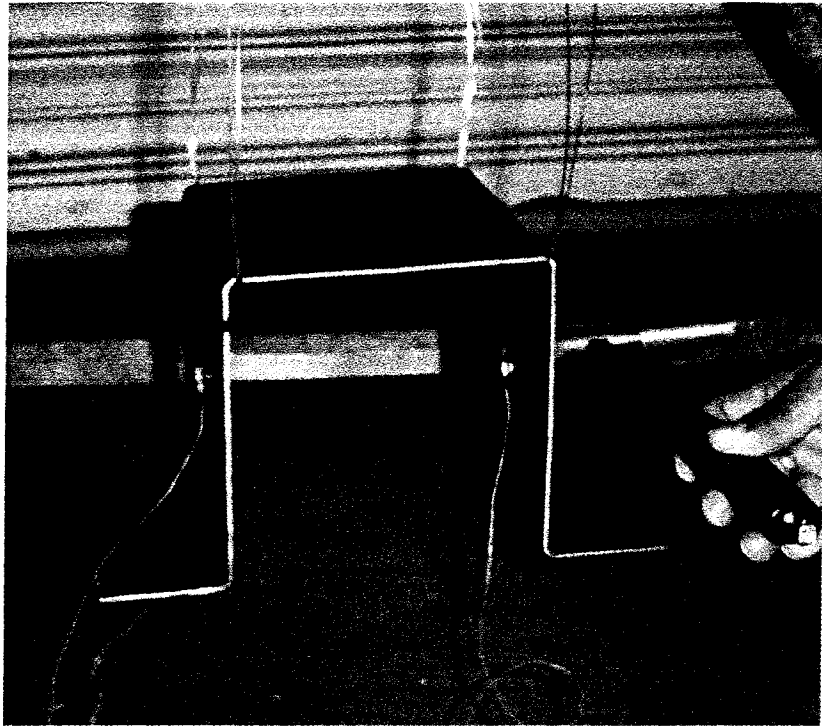
Figure 2-8 Placement of the accelerometers and point of impact

The finite element analysis software, ANSYS [16] and HYPERMESH [17] are used for modeling and meshing all the models. The input deck is written to LS-DYNA [18] for the dynamic shock analysis. Run time for the analysis is 0.016 seconds and the sampling rate used for the finite element analysis is equal to the value of sampling time used in the experiment which is 4,084,937/second which is the default value as well as the maximum value in the pulse software. Initially no filtering was done on the data obtained from the finite element analysis.

24
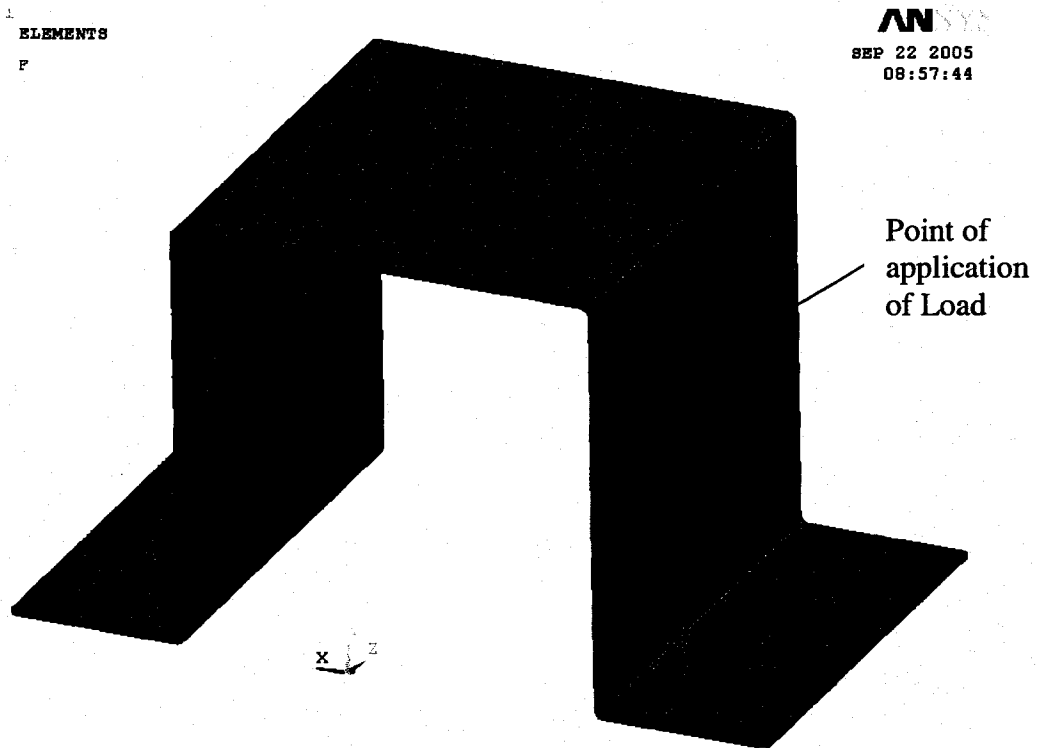
Figure 2-9 Point of application of load in the FEA model

Better results can be obtained by increasing the mesh densities in the finite element models but this would result in an increase in the run time. Figure 2-10 shows the comparison between the experimental data obtained from experiment with the finite element data obtained from models using three and four elements along the thickness. It can be observed that the FEA model with four elements along the thickness shows better proximity with the experiment. In both the solid and shell element models, default element formulations are used which are Fully Integrated Solid and Belytschko-Tsay respectively. The input load curve for the analysis obtained from the experiments is shown in Figure 2-11.

25
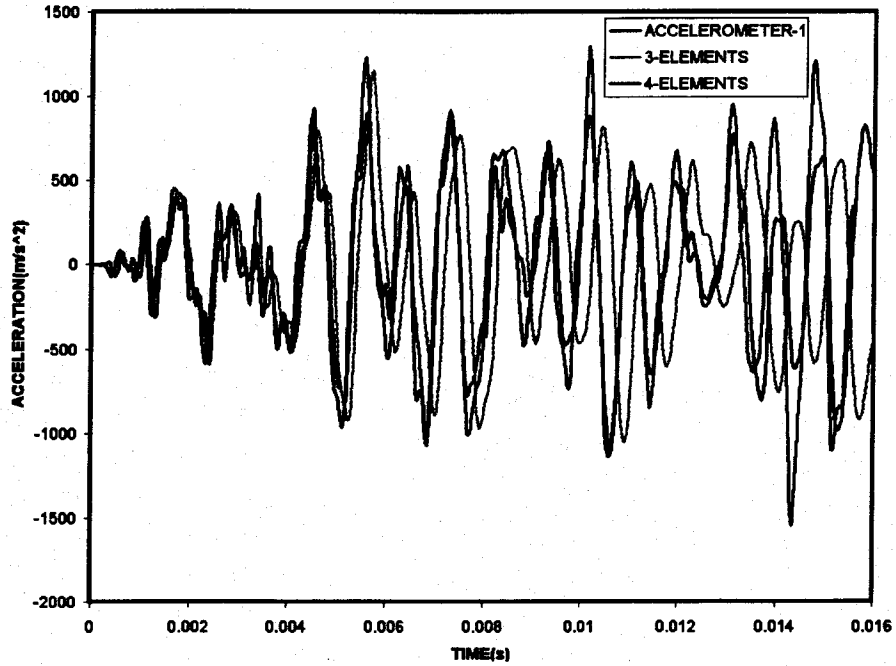
Figure 2-10(a) Finite element analysis comparisons using solid elements with experimental results (Acceleration Vs Time) obtained from aceelerometer-1
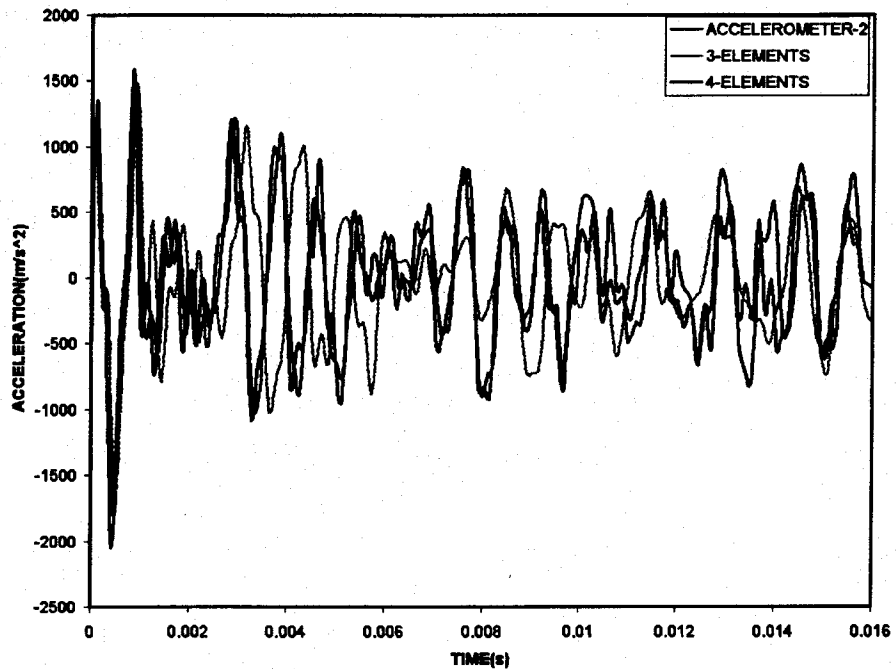
Figure 2-10(b) Finite element analysis comparisons using solid elements with experimental results (Acceleration Vs Time) obtained from aceelerometer-2

26
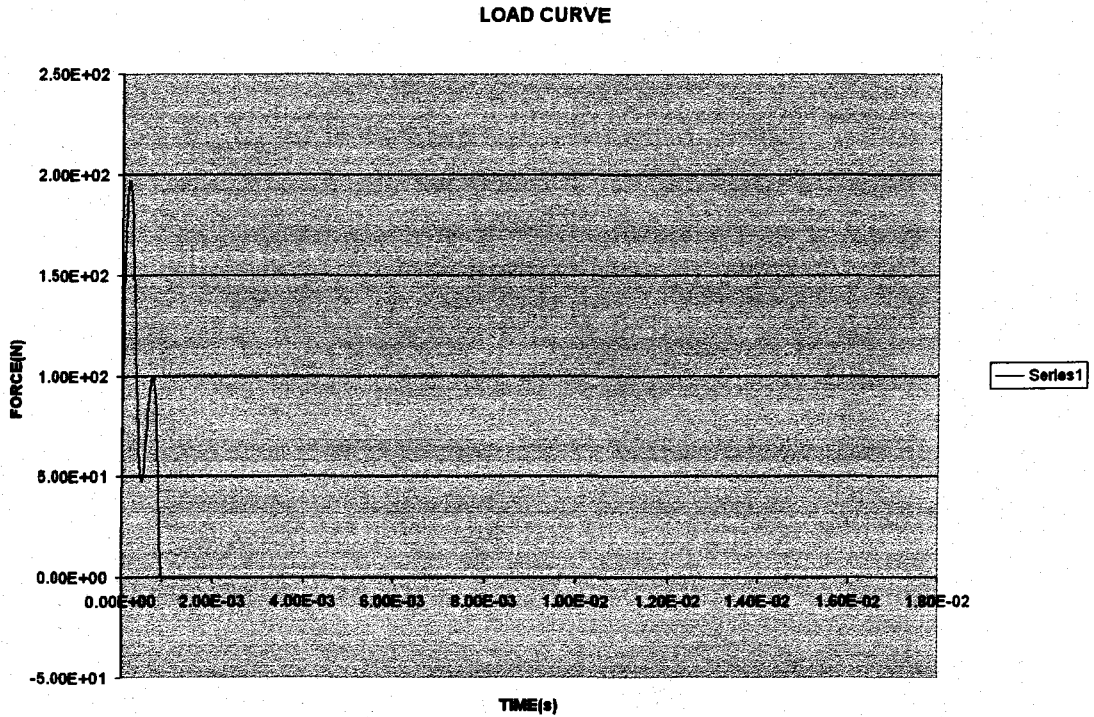
LOAD CURVE

Figure 2-11 Load curve used in FEA

2.5 LS-DYNA Input Cards

2.5.1 Material Card

Material properties in LS-DYNA are defined in the material card. Density of the steel was determined by measuring the mass and dimensions of the hat section and other material properties were obtained from matweb.com using the calculated density. Material card used for steel in the analysis is *MAT_ELASTIC which is shown below.

```
*MAT_ELASTIC
$       MID        RO        E         PR        DA        DB        K
$
         1 0.773E+4  0.200E+12  0.300000        0.0       0.0       0.0
```

27

MID in the material card defines the material identification number and RO defines the density. E and PR define the Youngs modulus and Poissons ratio respectively. DA, DB and K are the axial damping factor, bending damping factor of the beam element and bulk modulus. DA and DB are applicable when beam element is used and K is used only when dealing with fluids.

2.5.2 Input Card for the Load Curve

For defining a load on a point in LS-DYNA the input card, *LOAD_NODE_POINT is used which is shown below.

```
*LOAD_NODE_SET
$    NODE        DOF     LCID        SF        CID
$
      1           1       1         1.000       0
```

NODE refers to the identification number of the node on which the load is being applied and DOF refers to the applicable degree of freedom the direction in which the load is applied. SF and CID define the scaling factor and coordinate system id respectively. LCID defines the identification of the load curve that is applied on the structure.

2.5.3 Control Cards

Most control cards are optional cards and are used to change defaults and activate solution options like mass scaling, adaptive remeshing and implicit solution [15]. *CONTOL_TERMINATION, which is shown below, is one of the cards that is invariably used in most explicit analysis as it defines the end time.

28

```
*CONTROL_TERMINATION
$          ENDTIME     ENDCYC      DTMIN     ENDENG     ENDMAS
$
         0.160E-01          0    0.00000    0.00000    0.00000
```

ENDTIME defines the termination time of the analysis after which the analysis

stops and ENDCYC defines the termination cycle, which is optional and is used if a

specific cycle is reached before termination [18]. DTMIN is the reduction factor for

initial time step size to determine minimum time step. ENDENG is the percent change in

energy ratio for termination of calculation. DTMIN is the reduction factor for initial time

step size to determine minimum time step. ENDENG is the percent change in energy

ratio for termination of calculation and ENDMAS is the percent change in the total mass

for the termination of calculation [18].

2.5.4 Database Card

These are optional cards, but are necessary to obtain output files containing

results information [18]. *DATABASE_NODOUT card defines the time step at which

output data is outputted. *DATABASE_HISTORY_NODE defines the node/nodes

whose results information is to be outputted.

```
*DATABASE_NODOUT
$          DT      BINARY
$
   1.530E-05          1


*DATABASE_HISTORY_NODE
$         ID1        ID2
$
        38772      11644
```

29

DT in the nodout card refers to the time step where as BINARY refers to the flag foe binary file. In the history node card, ID1, ID2 refer to the identification numbers of the nodes whose data is to be outputted.

The LS-DYNA input cards described above are some of the important in put cards used in the analysis of all the finite element joint configuration models. Due to this reason they are not mentioned in the later chapters where only the relevant input cards are discussed.

2.6 Comparisons of FEA and Experimental Results.

Graphs of the acceleration response from accelerometer-1 and accelerometer-2 are shown in Figure 2-12(a), (b). Node number 38,772 corresponds to the location of Accelerometer-1 and node number 11,644 corresponds to the location of acceleromerter-2 on the solid element model. The model has a total of 42,400 elements and 54,315 nodes. Figure- 9 shows the application of load on the finite element model.

30
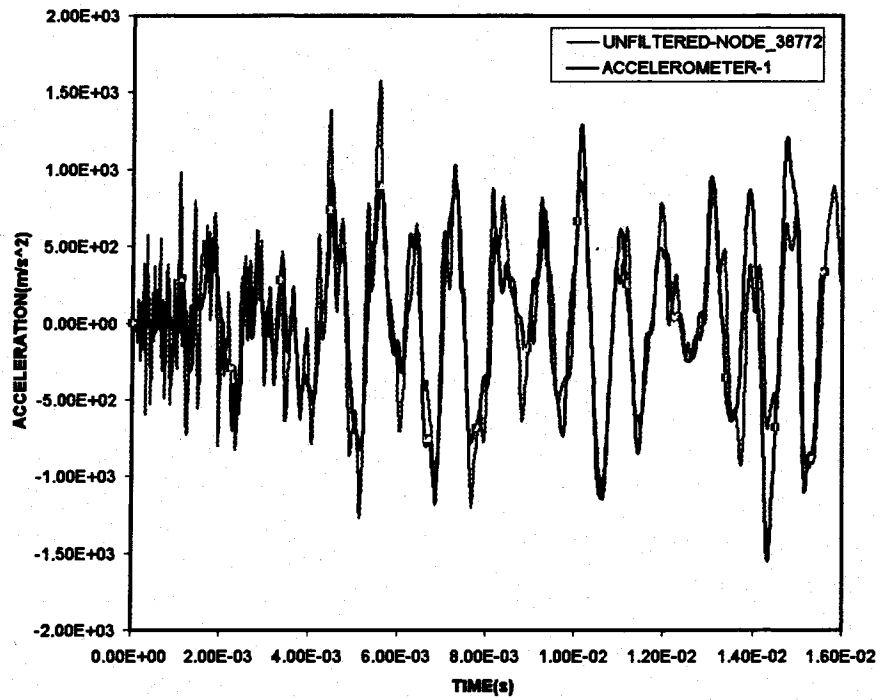
Figure 2-12(a) Finite element analysis comparisons using solid elements with experimental results (Acceleration Vs Time) obtained from aceelerometer-1
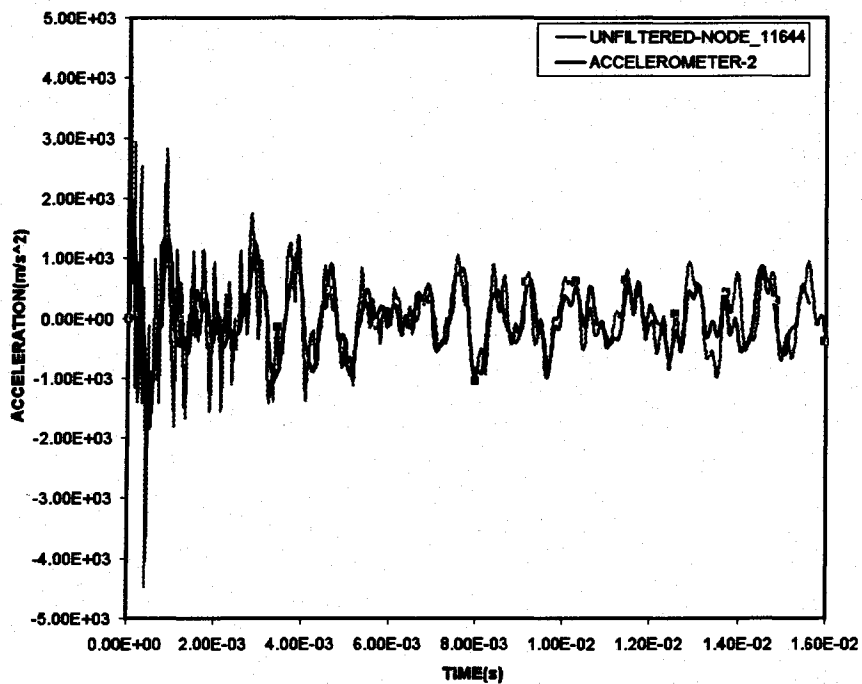
Figure 2-12(b) Finite element analysis using solid element model comparisons with experimental results (Acceleration Vs Time) obtained from aceelerometer-2

31

Similar analysis is performed using the shell element model, however the response of the node which corresponds to the accelerometer-2 form the experiment is not considered since the shell does not have a physical thickness and the node on which the load is being applied would be the same node which would correspond to accelleromerter-2 as the accelerometer is placed right behind the point of impact which. In the experimental setup the shell element model has a total of 10,400 elements and 10,659 nodes. Figure 2-13 shows the comparison of unfiltered results obtained from the finite element analysis with the experimental results.

EXPERIMENTAL Vs UNFILTERED FEA(SHELL)
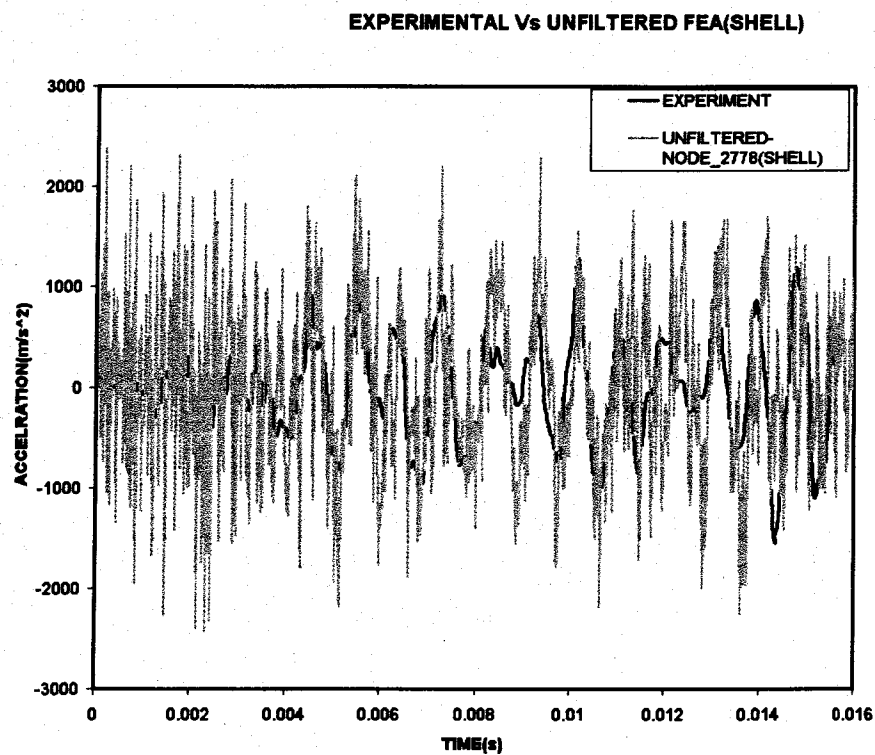
Figure 2-13 Comparison of acceleration response at node-2778 of the shell element model with the response obtained form acclerometer-1

Relative error between the experimental and finite element data is measured using the formula given below:

32

$$\text{Relative error} = \sum \frac{\text{Absolute } (a_{exp}) - \text{Absolute}(a_{fea})}{\sum \text{Absolute } (a_{exp})}$$

In the above formula, (a_{exp}) and (a_{fea}) represents the acceleration data obtained from the experiment at each time step from the experiment and finite element analysis respectively. Relative error is being used due to the fact that there is a phase shit that is present between the experiment and finite element analysis, as seen from the respective graphs. Table 2-4 shows the relative error calculated from the experimental and finite element data showed in Figures 2-12 and 2-13. Relative error is being used due to the fact that there is a phase shit that is present between the experiment and finite element analysis results.

Table 2-4 Relative Error Calculated from the Unfiltered Data.

	RELATIVE % ERROR (OVERALL)
SOLID ELEMENT MODEL	
ACCELEROMETER-1	8.06
ACCELEROMETER-2	6.31
SHELL ELEMENT MODEL	
ACCELEROMETER-1	3.65
ACCELEROMETER-2	-

2.7 Filtering

A common practice in signal processing is to smooth data by eliminating high-frequency components. This is done using a low-pass filter. It is called a low-pass filter because it only keeps low-frequency components and eliminates high frequency components. Other types of filters are high-pass, band-pass, and band-stop. In order to specify which frequencies are to be removed, cutoff frequencies must be defined. For low- and high-

pass filters, only a single cutoff frequency is necessary. For low-pass filters, frequencies below the cutoff frequency are passed, while the opposite is true for high-pass filters. Band-pass and band-stop filters require two cutoff frequencies, a low and a high. For a band-pass filter, only frequencies between the two cutoff frequencies are passed, while for a band-stop filter, only frequencies outside this range are passed [17].

Node number 2778 of the shell element model corresponds to the location of accelerometer-1 on the hat section. Initially various values were used for filtering starting from 3500 Hz but the FEA results start matching with the experimental results when the data is filtered up to 2500 Hz. Frequencies beyond 2500 Hz are filtered using HYPERGRAPH. This validates the specifications of the impact hammer which shows that the impact hammer has a frequency range of 1-2500 Hz. Graphs in Figure 2-14(a) and 2-14(b) show the comparison between the filtered experimental and finite element data of the solid element model and Figure 2-14(c) shows the comparisons with the shell element model.

EXPERIMENT Vs FEA
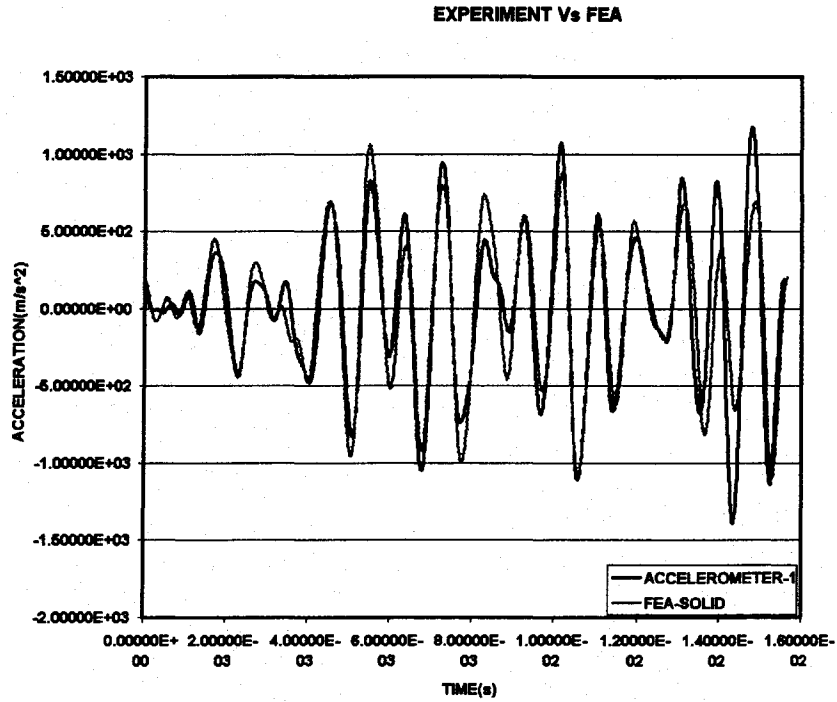
Figure 2-14(a) Finite element analysis comparisons using solid element (filtered) with experimental results (Acceleration Vs Time) obtained from accelerometer-2

EXPERIMENT VS FEA
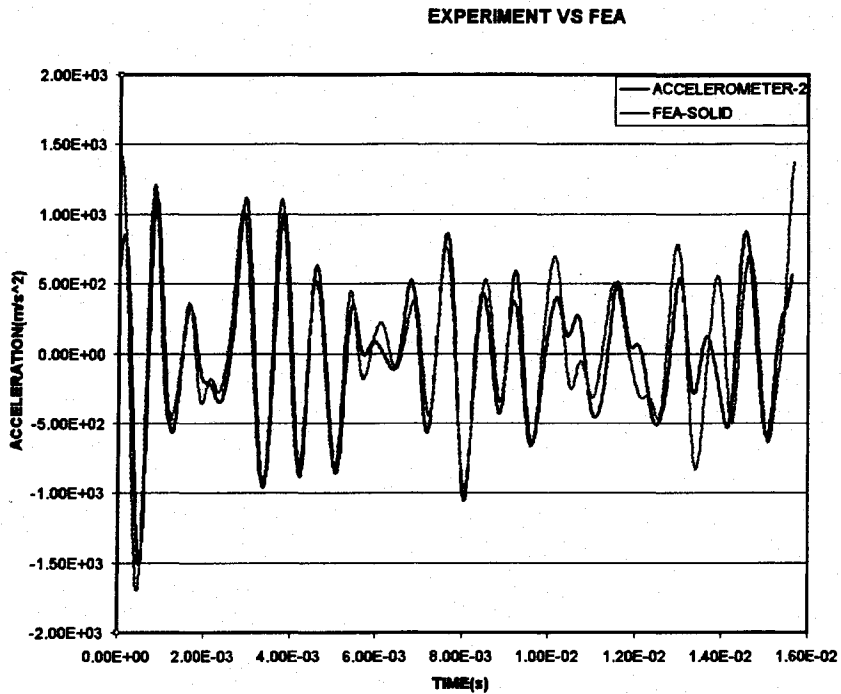
Figure 2-14(b) Finite element analysis comparisons using solid element (filtered) with experimental results (Acceleration Vs Time) obtained from accelerometer-2

35

EXPERIMENT Vs FEA
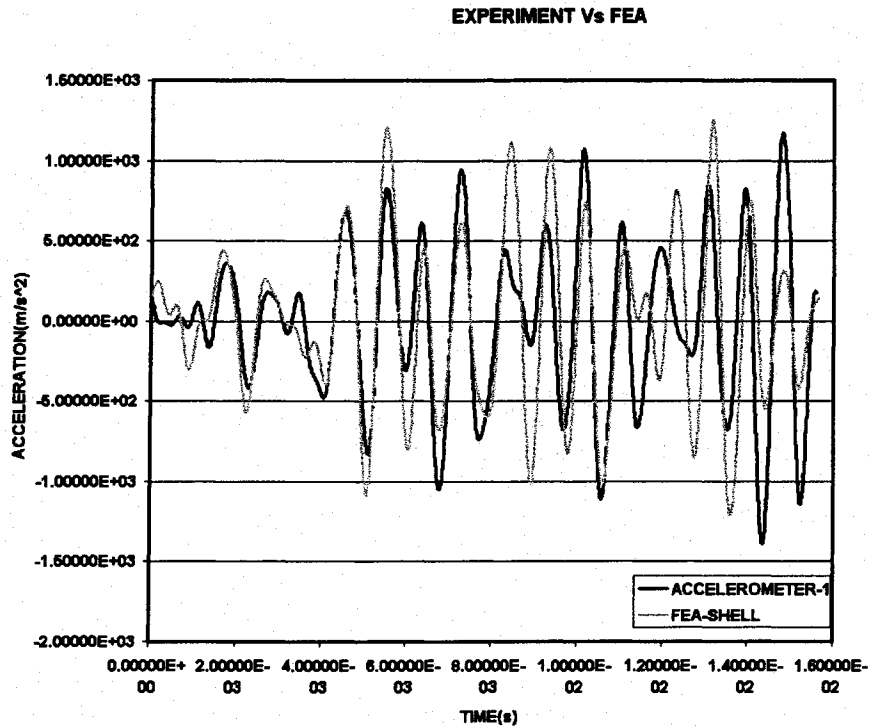
Figure 2-14(c) Finite element analysis comparisons using shell elements (filtered) with experimental results (Acceleration Vs Time) obtained from aceelerometer-1

It can be seen from the above graphs that there is good agreement between the finite element and experimental results when the FEA data is filtered beyond 2500 Hz. The solid element model is more representative of the actual model (experiment) where as slight discrepancies can be observed with the shell element model where the amplitudes are slightly higher then those obtained from the experiment. Figure 2-15 gives a clear picture of the comparison between all the three cases, experimental, finite element solid model and finite element shell model. Relative error is also calculated for the filtered data, which is shown in the Table 2-5.

36

Table 2-5 Relative error calculated from the filtered data

	RELATIVE % ERROR (OVERALL)
SOLID ELEMENT MODEL	
ACCELEROMETER-1	5.89
ACCELEROMETER-2	5.64
SHELL ELEMENT MODEL	
ACCELEROMETER-1	1.48
ACCELEROMETER-2	-

From all the above discussion it would be safe to assume that the finite element analysis using shell elements or solid elements give very good representations of the actual dynamics response of the steel hat section in the frequency and acceleration domains shown. However the use of filtering is required in the higher frequency ranges beyond 2500 Hz.
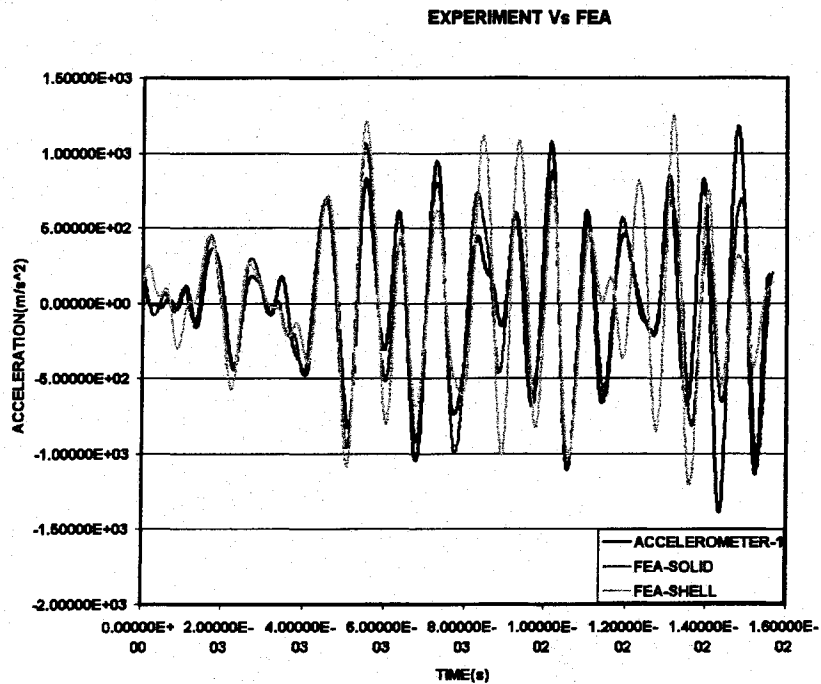
Figure 2-15 Comparison of filtered FEA results (shell and solid) with filtered experimental results

37

CHAPTER 3

ANALYSIS OF DOUBLE HAT SECTION ADHESIVELY BONDED WITH

CONTINUOUS SPACERS

3.1 Modal Analysis

Modal analysis is performed on adhesively bonded hat sections separated by

continuous spacers. Two different adhesives are examined in this process, epoxy and

super glue the two hat sections and later super glue is used. This is done to determine

which of the glues is stiffer. The reason behind using the continuous spacer is the fact

that the horizontal flat plates of the hat section are not completely flat so to avoid gaps

between the horizontal flat plates when glued together and to define a uniform contact

surfaces between the top and bottom hat sections the spacers are being used as seen in

Figure 3-1. Experimental setup is also similar to that of the single hat section, the glued

hat sections are hung to the frame with the help of steel wires. The solid element model

uses 66,000 elements and 99,864 nodes and the shell element model consists of 20,200

elements and 20,706 nodes. The spacers between either side of the hat sections are

modeled in such a manner that they share common nodes with the horizontal flat plates of

both the hat sections. Corresponding to the solid element model the shell element model

has five integration points along its thickness. Shell and solid element models of the

glued hat sections are shown in the Figure 3-2.

38
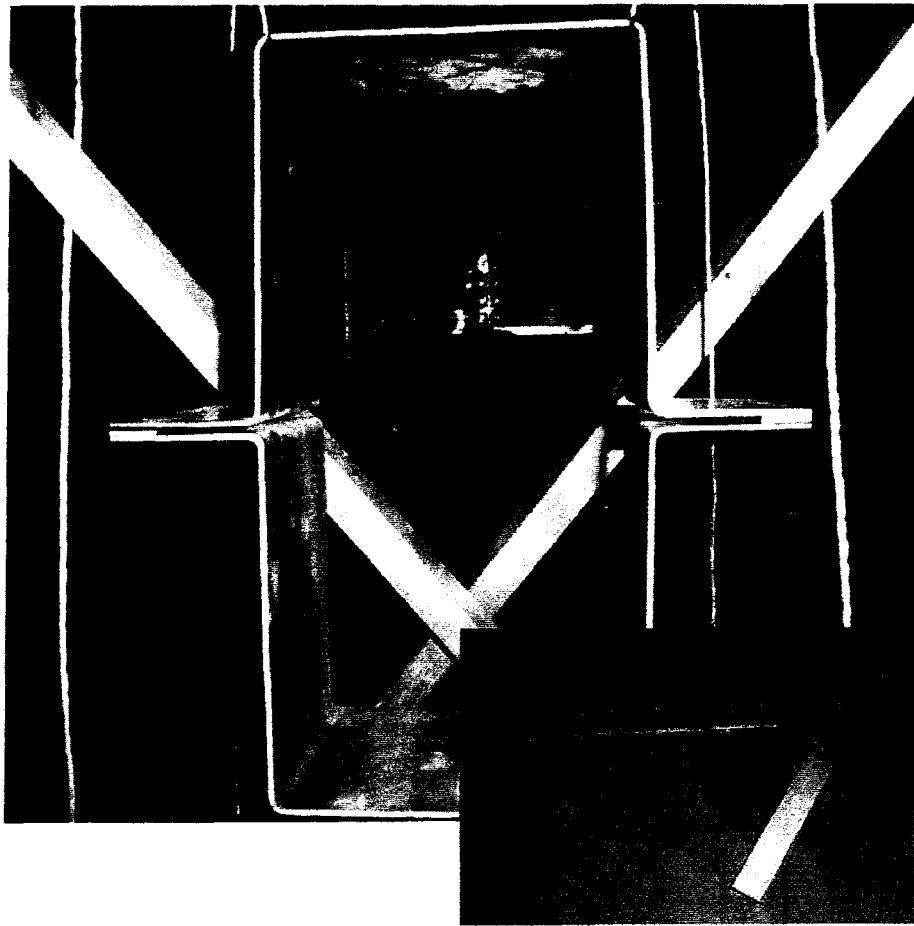
Figure 3-1 Adhesively bonded hat sections with continuous spacers.

39
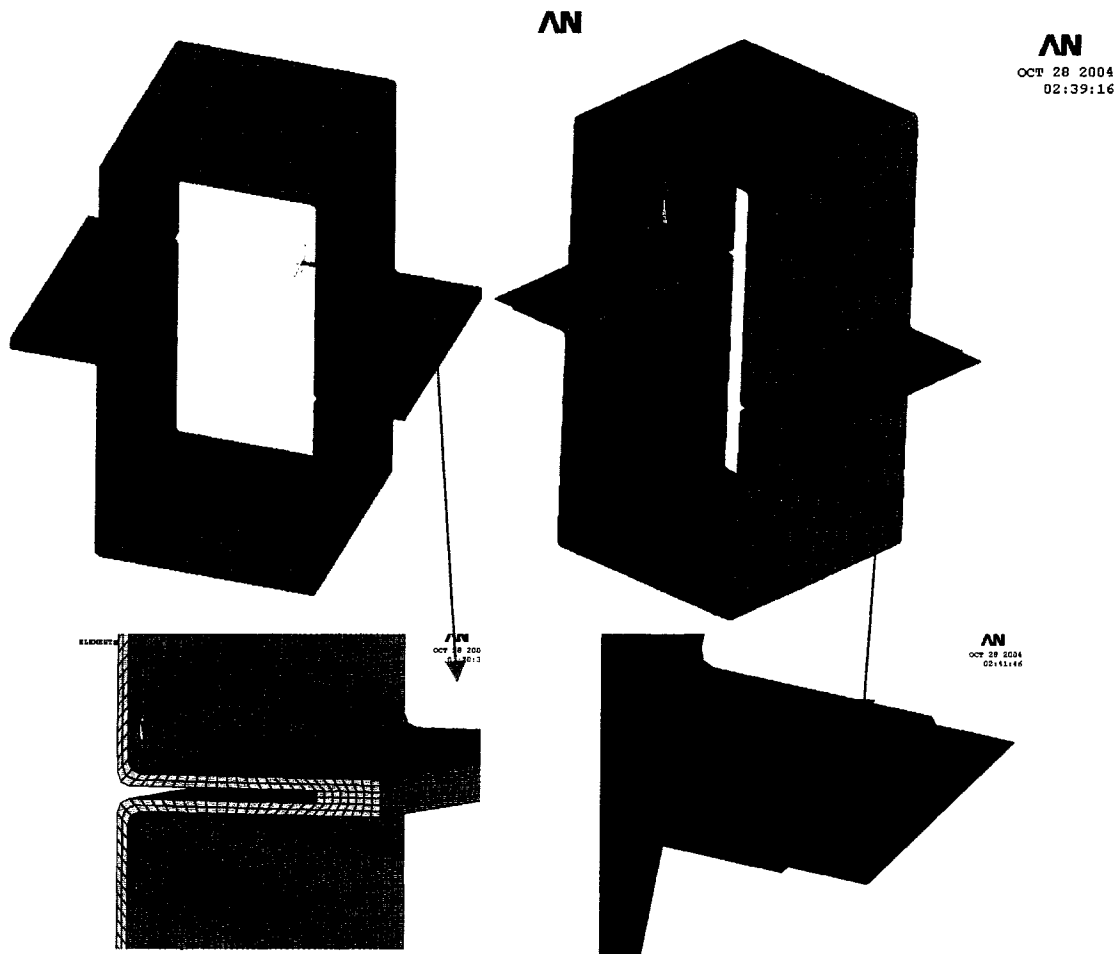
Figure 3-2 Finite element models of the glued double hat sections.

As can be seen from the Figure 3-2, the shell element model has two horizontal flat plates converging at the spacer; the spacer is given thrice the original thickness to account for the thickness of the upper and lower horizontal flat plates, the reason for considering this model is explained while describing the contacts in the explicit analysis of the jointed hat section. The mode shapes are extracted by performing modal analysis on the structure and depending upon the mode shapes the accelerometers are placed on

40

the hat sections (locations of maximum deflection). Two configurations are also used hare. The first configuration has the accelerometers on the edge of the horizontal flat plates and is impacted on the top by the hammer where as the second configuration has the accelerometers on the vertical edges of the hat sections and is impacted on one of vertical sides of the hat section. Both the configurations can be seen in Figure 3-3.
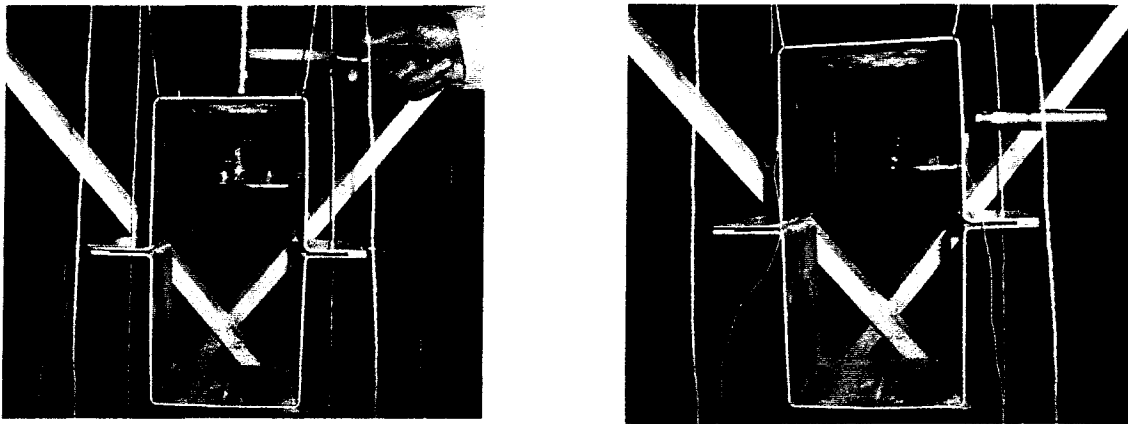
Figure 3-3 Configurations of the glued double hat sections, showing the accelerometers. in both the figures accelerometer-1 is placed on the left and accelerometer-2 to the right

Modal analysis experiments in both configurations were performed two times on each of the adhesively bonded structures (epoxy and superglue). Figure 3-4 shows the FFT results obtained from the experiments. It is observed that both the configurations yielded the same results; the natural frequencies for the structure obtained from both the configurations were the same. Data from a single accelerometer and configuration are shown from both the cases as all the frequencies were recorded by both the accelerometers.

41

CONFIGURATION1
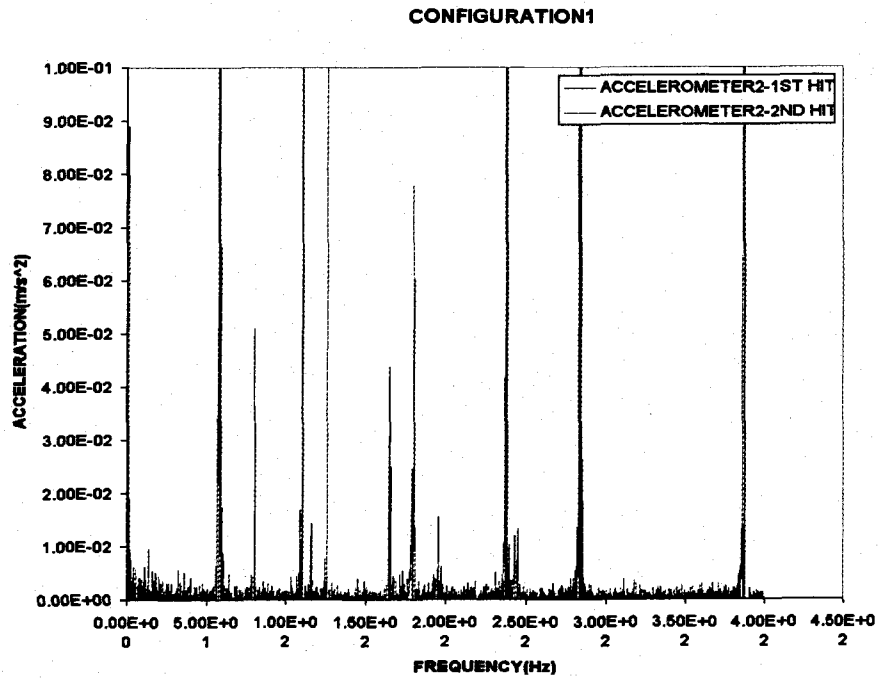
Figure 3-4(a) Fundamental frequencies for the two jointed hat sections (epoxy) with continuous spacers as measured by accelerometer-1.

CONFIGURATION1
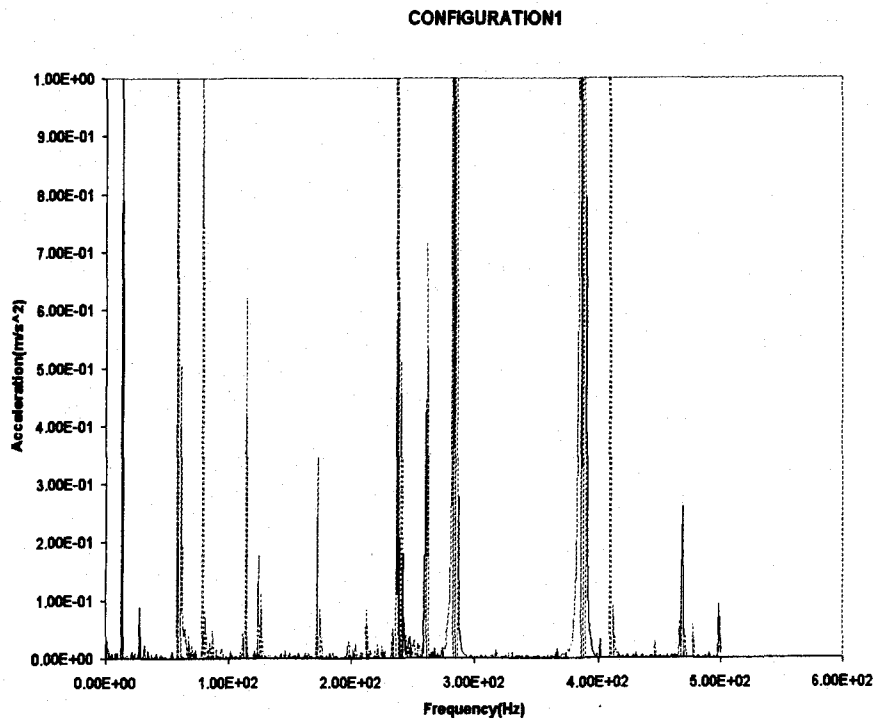
Figure 3-4(b) Fundamental frequencies for the two jointed hat sections (super glue) with continuous spacers as measured by accelerometer-1.

42

Comparison between the values of natural frequencies obtained from the experiments and the finite element analysis, which includes both solid and shell element models of the hat section, is shown in Table 3-1. Table-3-2 shows the percentage error between the experimental and finite element results.

Table 3-1 Comparisons of experimental and finite element results

MODE #	EXPERIME- -NTAL EPOXY (Hz)	EXPERIMEN- -NTAL SUPER GLUE (Hz)	SOLID MODEL (Hz)	SHELL MODEL (Hz)
7	58	58	61	61
8	80	78	79	79
9	110	115	116	116
10	116	125	121	120
11	126	128	130	128
12	165	173	176	175
13	180	213	216	217

43

Table 3-2 Errors between experimental and finite element results

Mode #	% Error with respect to Epoxy		% Error with respect to Super Glue	
	Solid	Shell	Solid	Shell
7	6.5	5.9	5.0	4.5
8	0.18	0.18	1.3	1.3
9	6.1	6.2	1.5	1.5
10	4.6	3.7	2.9	4
11	3.3	1.6	1.6	0.07
12	7.0	6.3	2.1	1.4
13	18.3	20.7	1.5	2.0

As is evident from Table 3-2, the frequencies obtained from the finite element analysis are closer to the results obtained from the experiments conducted on super glue, the difference between the results from the super glue and FEA are smaller compared to the difference between epoxy and FEA. It is evident that super glue acts stiffer then epoxy, yielding better results. Similar pattern was observed in the results obtained from the single hat section where the first natural frequencies obtained from the experiment were approximately matching with the experimental results. It is also evident that super glue, being harder than epoxy, gives closer results to both the FEA models which assume perfect bonding between spaces and hat sections. This helps avoiding the complex task of modeling the glue.

44

3.2 Shock Transmission Though the Jointed Hat Section (Continuous Spacer)

Experiments were conducted on the jointed hat section with continuous spacers placing the accelerometers on either sides of the joint as shown in Figure 3-5. Accelerometer-1 is placed at the center on the opposite side of the impact and accelerometer-2 is placed is placed on the bottom hat section also at the center, the aim is to record the shock propagation before and after the joint.
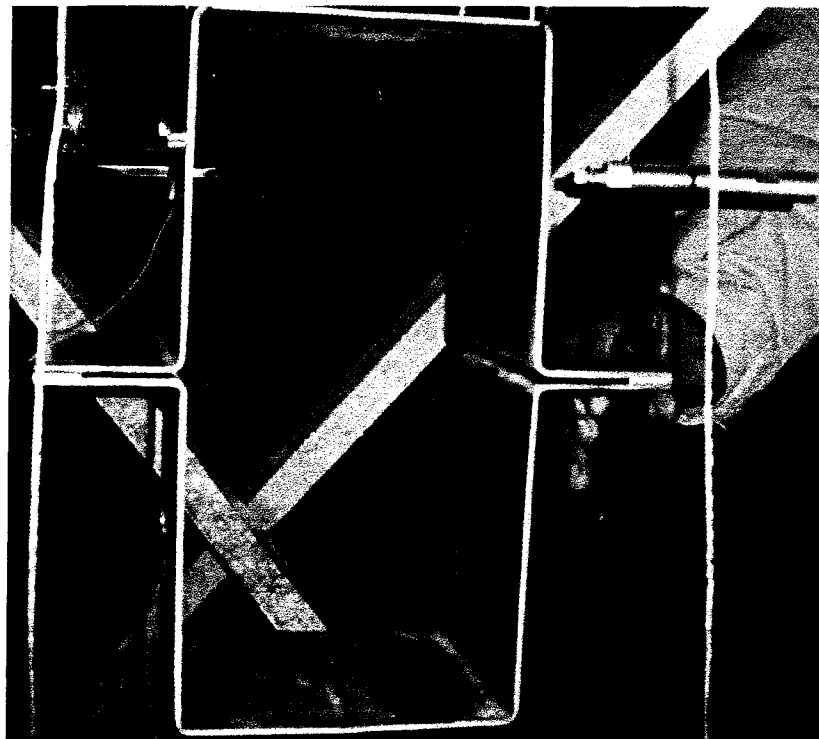
Figure 3.5- Placement of the accelerometers and point of impact

Accurate modeling of contact interfaces between the two hat sections is crucial to the prediction capability of the finite element simulations. Interfaces can be defined three dimensionally as triangular and quadrilateral segments of the elements that comprise each

45

side of the interface. One of the interfaces is designated as the slave side, and the other is designated as the master side. Nodes lying in those surfaces are referred to as slave and master nodes, respectively. The slave nodes are constrained to slide on the master surface after the impact and must remain on the master surface until a tensile force develops between the node and the surface [18].

The solid element model of the jointed hat section has 86,400 elements and 109,344 nodes; there are four elements through the thickness direction. The shell element model has a total of 20,400 elements and 20,808 nodes. The FEA models assume a perfect connection between the spacers and the horizontal flat plates (glue is not modeled) as they share the common nodes. "Shell thickness offsets" were used in order to define contacts between the spacers and the horizontal flat plates the contact command *CONTACT_TIED_SURFACE_TO_SURFACE was used initially. Use of this contact type with shell elements resulted in unrealistically soft behavior as rotational degrees of freedom of the slave node are not constrained. To avert this, the flange joints are modeled with the two horizontal flat plates converging at the spacer. The spacer is given thrice the original thickness to account for the thickness of the upper and lower horizontal flat plates as shown in Figure 3-2. Run time for the analysis is 0.016 seconds, similar to that of a single hat section. The load curve obtained from the experiment, which is applied to the FEA model, is shown in Figure 3-6. Initially no filtering was used on the data obtained from the finite element analysis. Graphs comparing the accelerations obtained from the solid element model, accelerometer-1 and accelerometer-2 are shown in Figure 3-7. Node number 71,361 corresponds to the location of the accelerometer-1 and node

46

number 113,997 corresponds to the location of the acceleromerter-2 on the solid element model.

Similar analysis was performed on the shell element model in which Node number 2778 corresponds to the location of the accelerometer-1 and node number 22,719 corresponds to the location of the acceleromerter-2. Graphs comparing the accelerations obtained from the shell element model, accelerometer-1 and accelerometer-2 are shown in Figure 3-8(a) and (b).
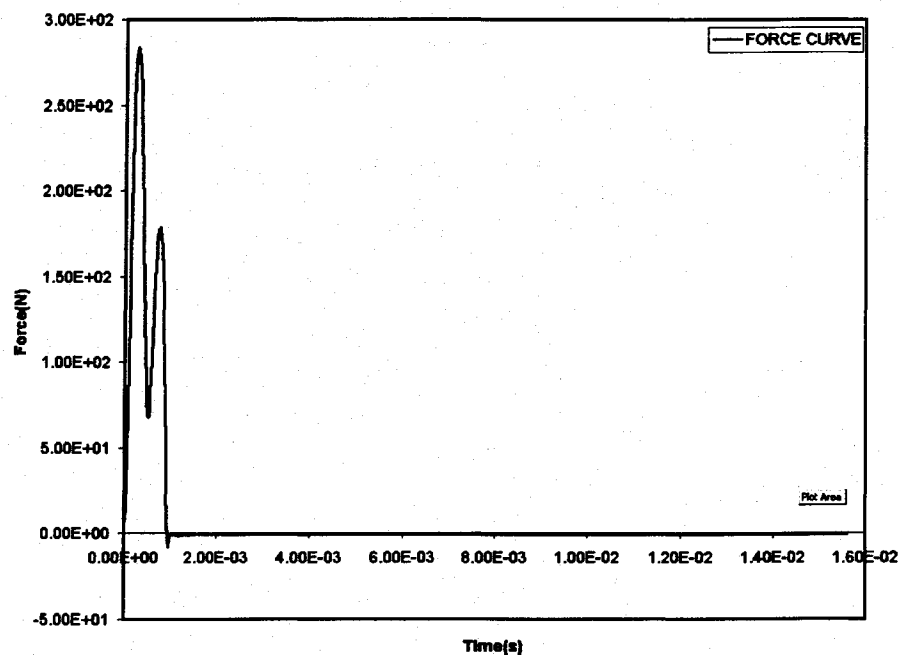
Figure 3-6 Load curve applied on the FEA models

47
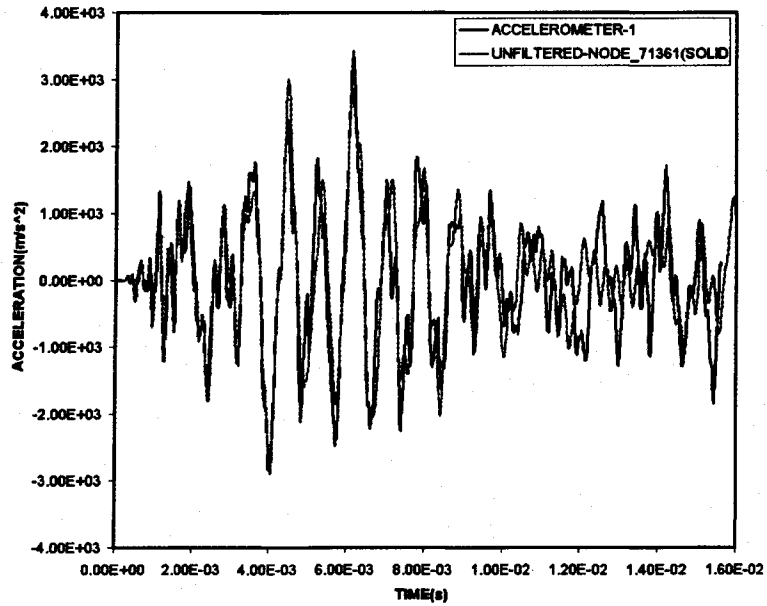
Figure 3-7(a) Finite element analysis comparisons of jointed double hat sections with continuous spacers using solid elements with experimental results (Acceleration Vs Time) obtained from aceelerometer-1.
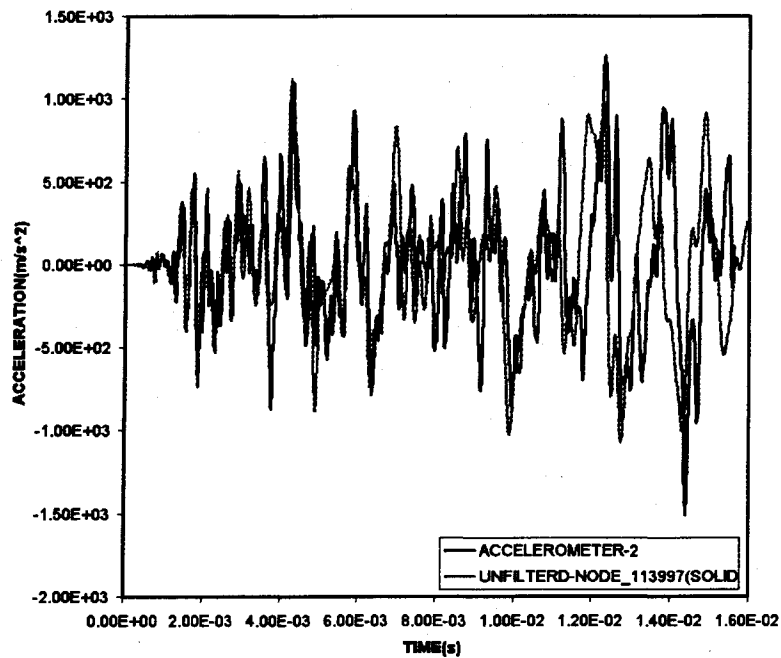
Figure 3-7(b) Finite element analysis comparisons of jointed hat sections with continuous spacers using solid elements with experimental results (Acceleration Vs Time) obtained from aceelerometer-2.

48
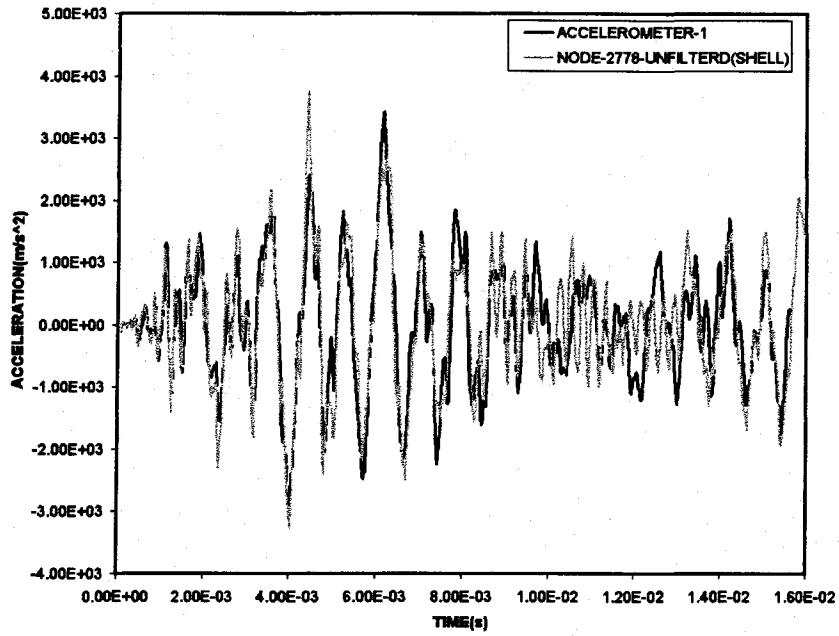
Figure 3-8(a) Finite element analysis comparisons of jointed double hat sections with continuous spacers using shell elements with experimental results (Acceleration Vs Time) obtained from aceelerometer-1
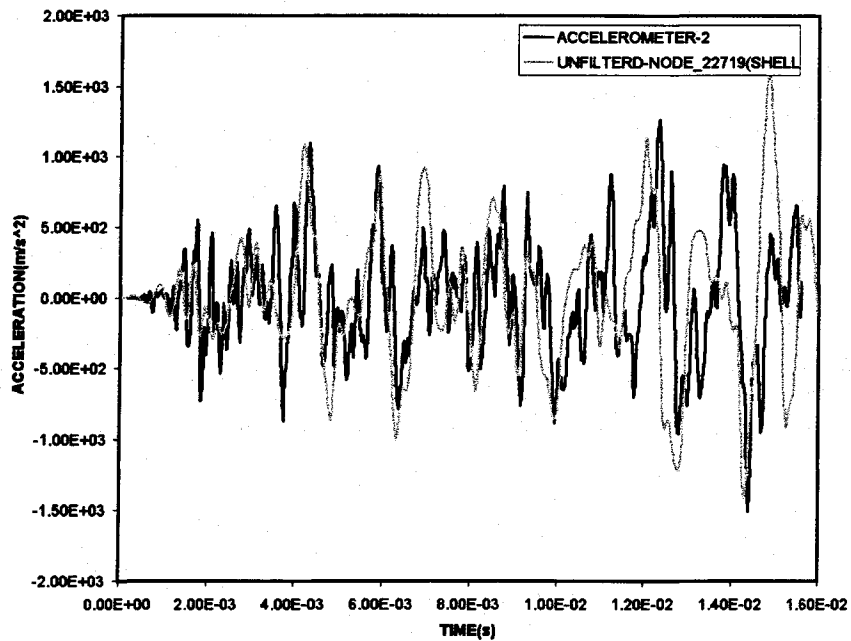
Figure 3-8(b) Finite element analysis comparisons of jointed double hat sections with continuous spacers using shell elements with experimental results (Acceleration Vs Time) obtained from aceelerometer-2

49

Figure 3-7 makes it evident that the finite element model generates almost the same acceleration response predicted from the experiments. For about 0.011 seconds both the responses over lap each other. Only after 0.011 seconds damping is observed in the finite element model in Figure 3.6(a). The discrepancies are augmented at node 113,997, which corresponds to the acclerometer-2; the magnitudes vary at some points even though they follow a similar pattern unlike node 71,361 where the acceleration magnitudes and the pattern are similar to the experimental acceleration response.

Similar pattern is observed in Figure 3-8, which depicts the comparison between the shell element model responses with that of the experiment, the node corresponding to accelerometer-1 has the identical acceleration pattern to the experimental results and starts to diverge from about 0.011 seconds. The most conspicuous difference being the magnitude, which is slightly higher then the response obtained from the solid element model. Akin is the response from the node corresponding to accelerometer-2 it shows more discrepancies as the time increases. Relative error between the experimental and finite element analysis data is calculated using the formula shown in Chapter 2, error in the finite element analysis models is also calculated with respect to the experiment for the peak amplitudes which are of utmost importance in shock analysis. Table 3-3 shows the relative error between experiment and finite element analysis.

Table 3-3 Relative error calculated for the unfiltered data

	RELATIVE % ERROR (OVERALL)	RELATIVE ERROR (PEAK AMPLITUDES)
SOLID ELEMENT MODEL		
ACCELEROMETER-1	9.36	0.1689
ACCELEROMETER-2	5.52	0.2214
SHELL ELEMENT MODEL		
ACCELEROMETER-1	52.32	0.3586
ACCELEROMETER-2	25.55	0.1190

As it was done for the single hat section, the experimental and finite element acceleration responses are filtered beyond 2500 Hz (the role and process of filtering was explained in chapter 2 .The filtered data is compared with the experimental results, which are shown in Figure 3-9 and 3-10. As it can be seen there is not much significant difference between the filtered and unfiltered data from the jointed hat sections where as there was a significant difference when the finite element analysis acceleration response was filtered in the single hat section. The comparisons between FEA results including solid and shell element models and experimental results are shown in Figure 3-11.

The results from the single hat section show more congruity between the finite element and experimental results when compared to the jointed hat sections. The main reason behind this is the fact that the single hat section is a continuous structure, and the shock travels along the structure uninterrupted. The Finite element analysis model proves to be efficient when dealing with continuous structures with out involving complexities like joints. The jointed hat sections are two separate structures, which are connected to

51

each other using spacers. The discontinuity in the structure causes the divergence of finite element analysis and experimental results, which can be seen from, Figure 3-9(b).

The results from the shell and solid finite element models approximately overlap each other but there is a small magnitude difference observed between them, which can be seen in Figures 3-10(a) and (b). The solid element model being stiffer then the shell element model behaves more like the actual structure where as the shell model being an approximate representation of the structure shows small discrepancies in the magnitudes. Relative error is also calculated for the filtered data, which is shown in the Table 3-4.

Table 3-4 Relative error calculated for the filtered data

	RELATIVE % ERROR (OVERALL)
SOLID ELEMENT MODEL	
ACCELEROMETER-1	8.36
ACCELEROMETER-2	4.77
SHELL ELEMENT MODEL	
ACCELEROMETER-1	65.5
ACCELEROMETER-2	40.8
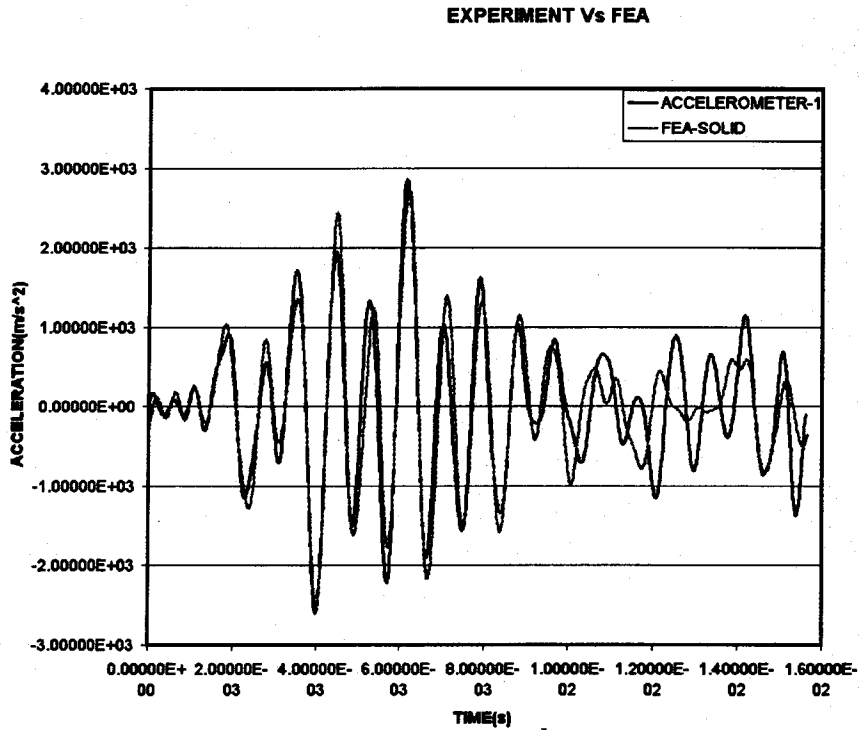
Figure 3-9(a) Filtered FEA comparisons using solid elements with experimental results (Acceleration Vs Time) obtained from aceelerometer-1
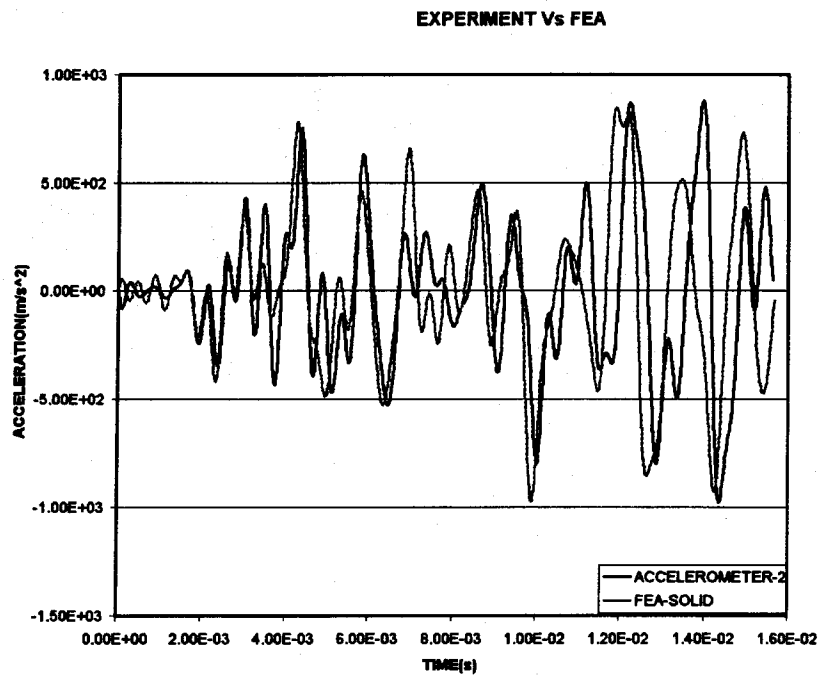
Figure 3-9(b) Filtered FEA comparisons using solid elements with experimental results (Acceleration Vs Time) obtained from aceelerometer-2

53
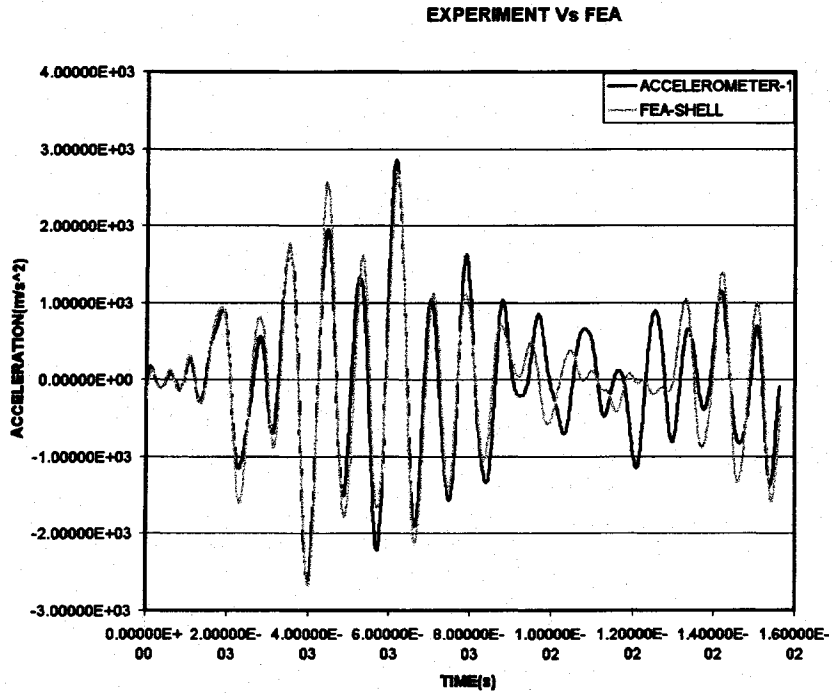
Figure 3-10(a) Filtered FEA comparisons using shell elements with experimental results (Acceleration Vs Time) obtained from aceelerometer-1
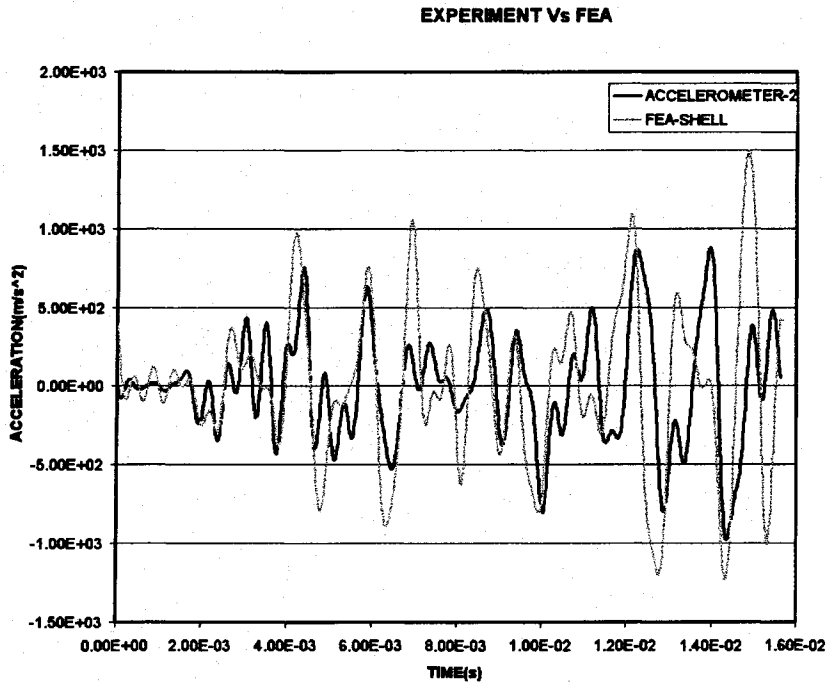
Figure 3-10(b) Filtered FEA comparisons using solid elements with experimental results (Acceleration Vs Time) obtained from aceelerometer-2

54
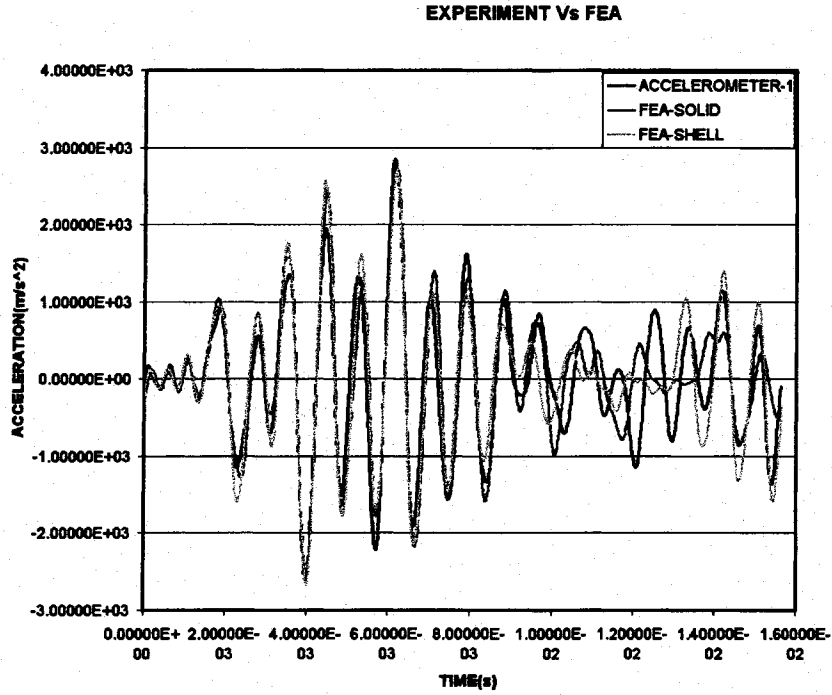
Figure 3-11(a) FEA comparisons using solid elements and shell elements with experimental results obtained from aceelerometer-1
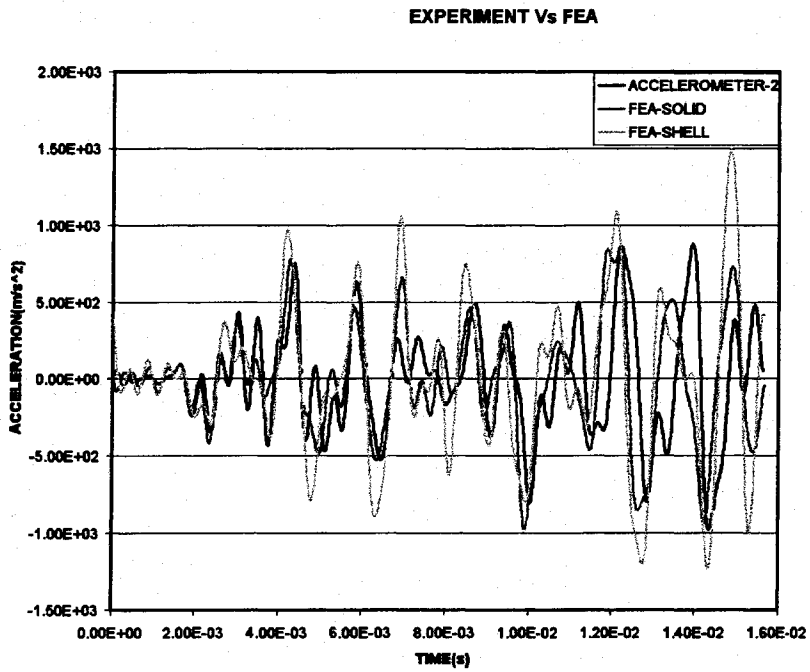
Figure 3-11(b) FEA comparisons using solid elements and shell elements with experimental results obtained from aceelerometer-2

55

CHAPTER 4

ANALYSIS OF ADHESIVELY BONDED HAT SECTIONS WITH

INTERMITTENT SPACERS

4.1 Modal analysis

In this section we examine the two steel hat sections which are glued together and are separated using intermittent spacers, which are 19.05 millimeters long; 19.05 millimeters wide and 2.654 millimeters thick and are placed along the length of the hat sections as shown in Figure 4-1. The objective of using intermittent spacer is to study the behavior of the shock when transmitted through an intermittent joint. Super glue was used to glue the hat sections together as it was seen in the analysis of single spacer, super glue proved to furnish better results when compared to epoxy. Even here two configurations are used, the first configuration has the Accelerometers on the edge of the horizontal flat plates and is impacted on the top of the hammer where as the second configuration has the accelerometers on the vertical edges of the hat sections and is impacted on one of vertical sides of the hat section, both the configurations can be seen in Figure 3-3. It was observed that both the configurations yielded the same results, the experimental FFT results from the jointed hat section with intermittent spacer is shown in Figure 4-2.

56

Figure 4-1 Jointed hat sections with intermittent spacers

57
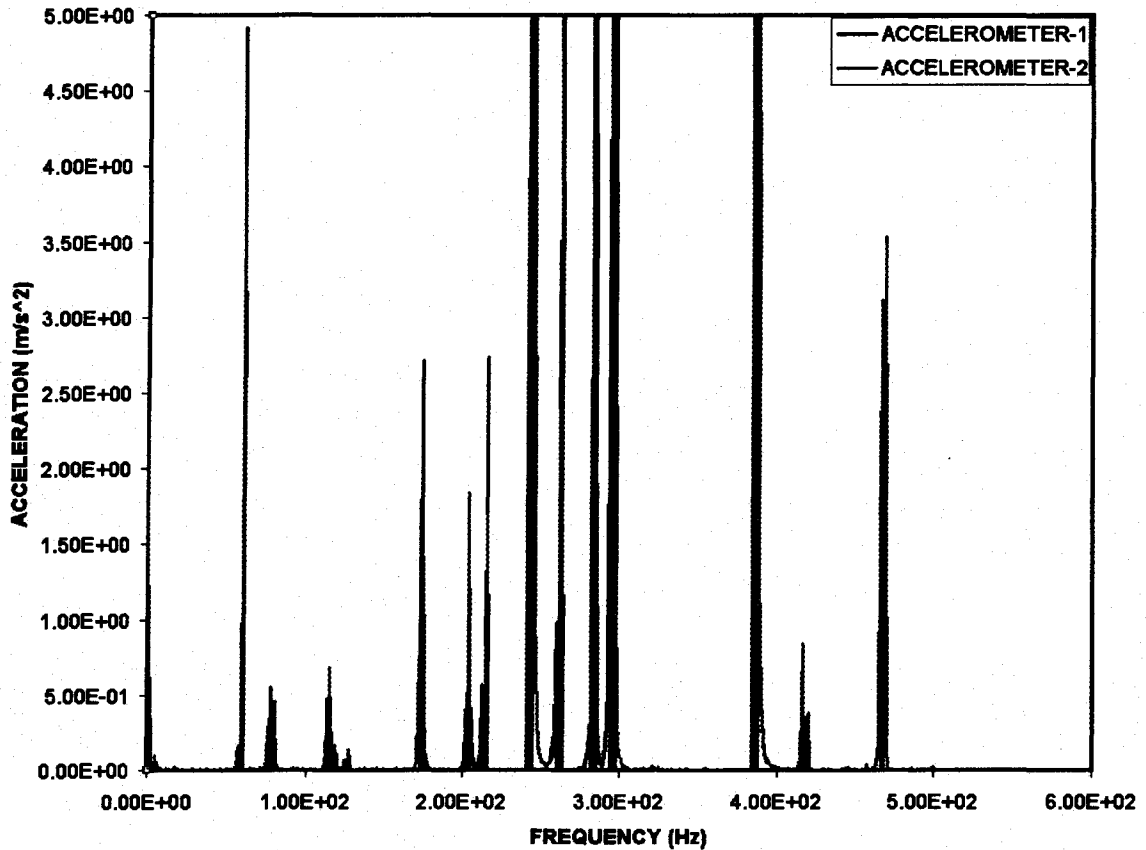
Figure 4-2 Fundamental frequencies for the two jointed hat sections with intermittent spacers as measured by accelerometer-1 and 2.

The finite element modal analysis of the jointed hat sections with intermittent spacers is performed using ANSYS. Both solid and shell elements are considered for the analysis, contacts between the spacers and the hat section horizontal flat plates have been defined by merging the nodes in order to make perfect contact between the two in case of the solid element model and for the shell element model the spacers have been considered as a single area and are given thrice the thickness to account for the two horizontal flat plates on either sides of the spacer similar to the case of single spacer. The finite element models of the shell and solid element models are shown in Figure 4-3.

58
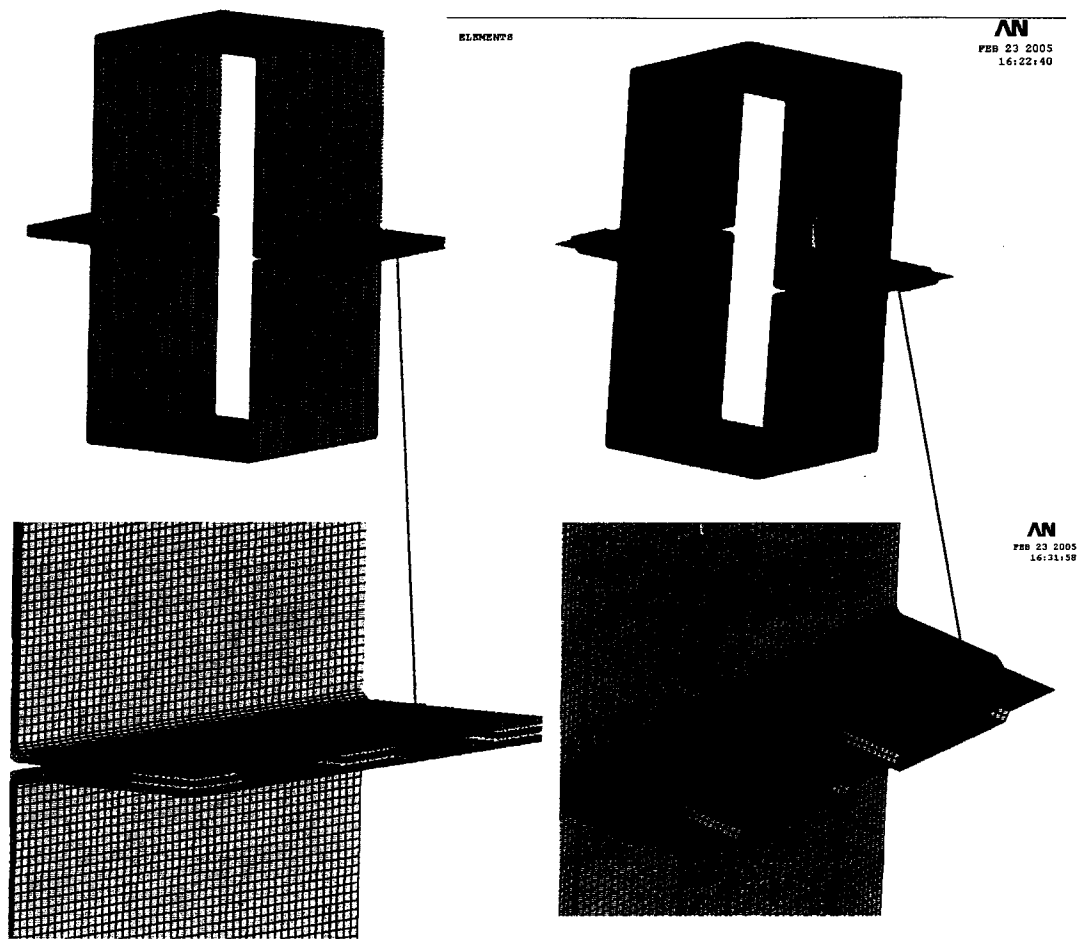
Figure 4-3 FEA models of the jointed hat section with intermittent spacers

The solid element model has 88,800 elements and 114,308 nodes and the shell element model has 34,792 elements and 35,324 nodes. Table 3 shows the natural frequencies obtained from the experiment and the finite element analysis (shell and solid element models).

59

Table 4-1 Comparison of experimental and finite element results

MODE #	EXPERIMENTAL (Hz)	SOLID MODEL (Hz)	SHELL MODEL (Hz)	% ERROR SOLID	% ERROR SHELL
7	60	62	61	4.8	3.0
8	80	79	79	0.2	0.2
9	115	116	116	1.2	1.0
10	126	125	121	0.5	3.8
11	128	131	128	2.5	0.27
12	174	178	174	2.6	0.27
13	204	226	221	11.1	8.6
14	215	237	235	10.2	9.3
15	243	254	258	4.6	6.3
16	263	290	288	10.5	9.6

As it can be seen form the above table all the natural frequencies match fairly well. After the sixth natural frequency the error starts increasing as seen in Table-3. The incongruity at the higher frequencies can be attributed to the damping, which did not have considerable effect on the finite element results when included but has its significance in real life. So it is quite evident that the finite element analysis is not accurately duplicating the effect of the experiment. One can observe that the mode number begins with number 7 due to the fact that the first six modes are rigid body motions.

60

4.2 Shock Transmission through the Jointed Double Hat Section with Intermittent Spacers

Experiments are conducted on a jointed double hat sections with intermittent spacers shown in Figure 4-3, similar to those with continuous spacers. Both accelerometers are placed at the same locations as before i.e. accelerometer-1 is placed at the center on the opposite side of the impact and accelerometer-2 is placed is placed on the bottom hat section also at the center as it is shown in Figure 3-5. The double hat sections were subjected to hits with a calibrated impact hammer as shown in Figure 3-5. the force of impact versus time was recorded and the curve applied an input to the finite element model. Shock propagation, as accelerations versus time measured on the faces opposite to the point of impact as shown in Figure 3-5.

The solid element model of the jointed hat section with intermittent spacers has a total of 88,800 elements and 114,308 nodes with four elements along the thickness direction. The shell element model has a total of 20,400 elements and 20,808 nodes. FEA element type (for both shell and solid), material model and type of contacts used are practically the same used in the case of adhesively joined hat sections with continuous spacers. The load curve obtained from the experiment, which is applied to the finite element model, is shown in Figure 4-4.

61
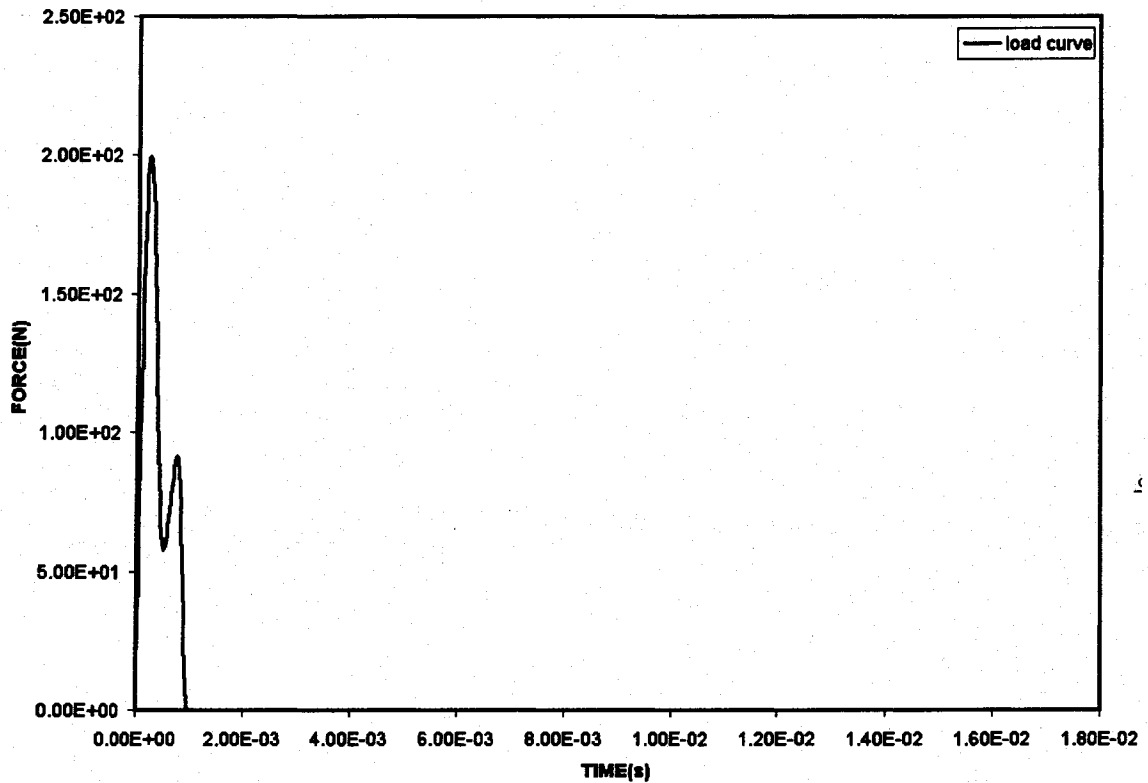
Figure 4-4 Load curve applied on the FEA models

Run time for the analysis is 0.016 seconds similar to the analysis of single and joined hat section with continuous spacers. Initially no filtering was done on the data obtained from the finite element analysis, graphs comparing the acceleration readings obtained from the solid element model with accelerometer-1 and accelerometer-2 are shown in Figure 4-5. Node number 29,140 corresponds to the location of accelerometer-1 and node number 111,823 corresponds to the location of acceleromerter-2 on the solid element model.

Similar analysis is performed on the shell element model in which Node number 13,743 corresponds to the location of the accelerometer-1 and node number 31,837 corresponds to the location of the acceleromerter-2. Graphs comparing the accelerations

62

obtained from the shell element model, with accelerometer-1 and accelerometer-2 are

shown in Figure 4-6.
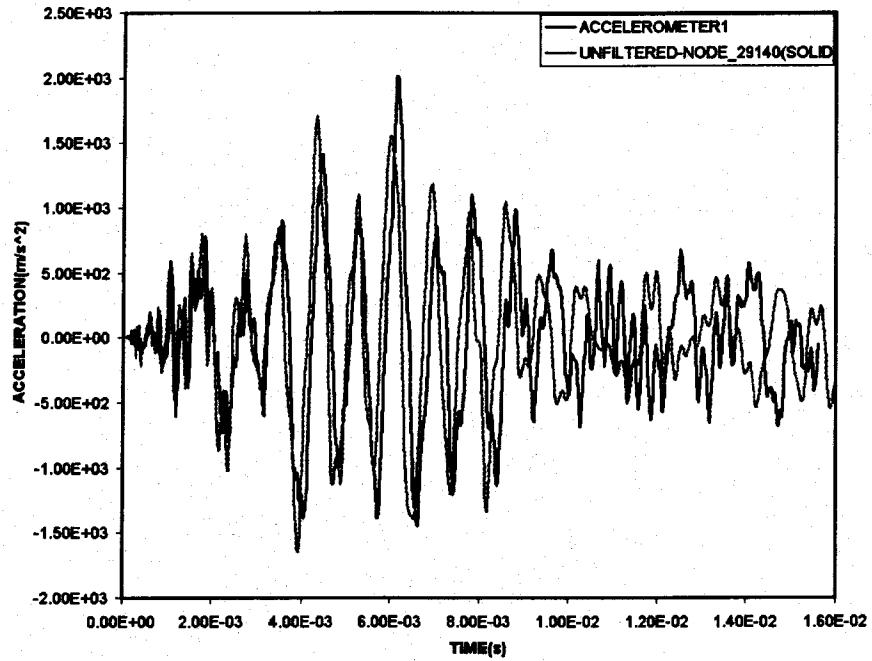
Figure 4-5(a) FEA comparisons of jointed double hat sections with intermittent
using solid elements with experimental results (Acceleration Vs Time) obtained from
aceelerometer-1

63
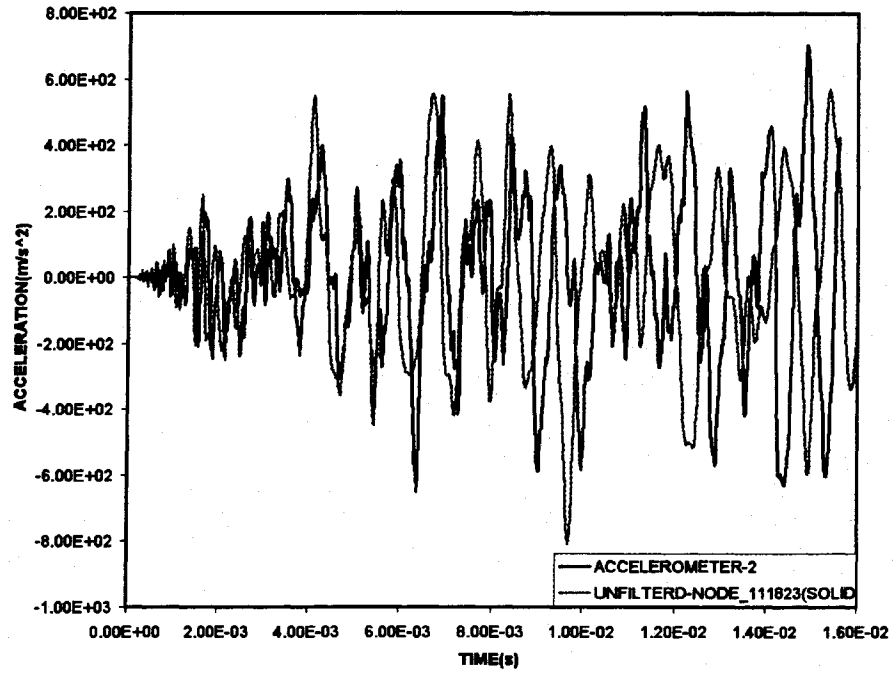
Figure 4-5(b) FEA comparisons of jointed double hat sections with intermittent spacers using solid elements with experimental results (Acceleration Vs Time) obtained from aceelerometer-2
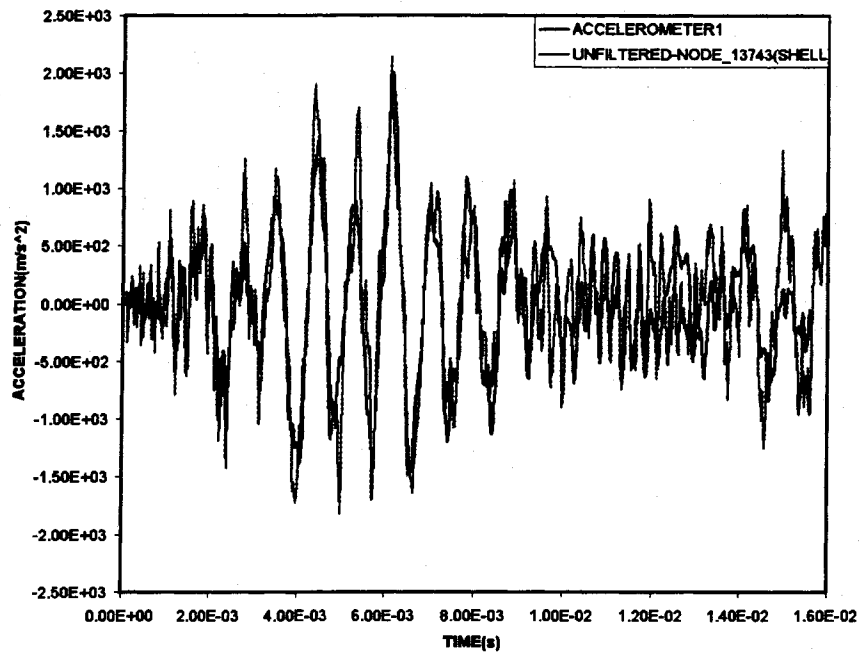
Figure 4-6(a) FEA comparisons of jointed double hat sections with intermittent spacers using shell elements with experimental results (Acceleration Vs Time) obtained from aceelerometer-1

64
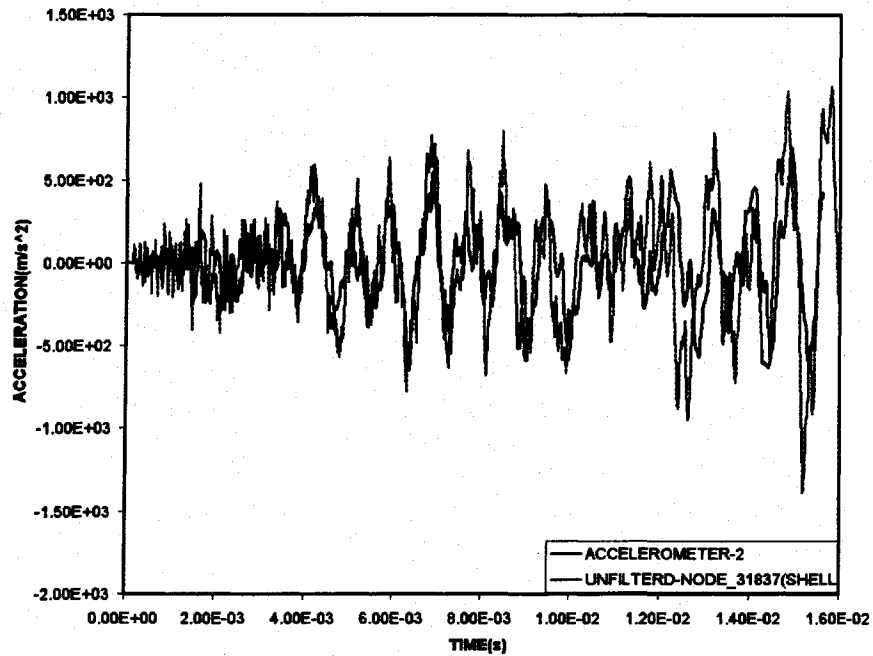
Figure 4-6(b) FEA comparisons of jointed double hat sections with intermittent spacers using shell elements with experimental results (Acceleration Vs Time) obtained from aceelerometer-2

As it can be seen from Figure 4-5 it is evident that the finite element model generates similar acceleration responses as of the experiments. The solid element model is comparable for 0.08 seconds, after which a phase shift and damping is observed in the finite element model. And similar to the case of jointed hat sections with single spacer the discrepancies are augmented at node 111,823, which corresponds to the acclerometer-2; the magnitudes vary at some points even though they follow a similar pattern unlike node 29,140 where the acceleration magnitudes and the pattern are similar to the experimental acceleration response till 0.08 seconds.

A much better pattern is observed in Figure 4-6, which depicts the comparison between the shell element model responses with that of the experiment, the node corresponding to accelerometer-1 has the identical acceleration pattern to the

65

experimental results and starts to diverge from about 0.011 seconds. The most conspicuous difference being the magnitude, which is slightly higher then the response obtained from the solid element model. Akin is the response from the node corresponding to accelerometer-2 it shows more discrepancies as the time increases. Relative error between the experimental and finite element analysis data is calculated using the formula shown in Chapter 2, error in the finite element analysis models is also calculated with respect to the experiment for the peak amplitudes which are of utmost importance in shock analysis. Table 4-2 shows the relative error calculated for the overall experimental and FEA data along with relative error in peak amplitudes.

Table 4-2 Relative error calculated for the unfiltered data

	RELATIVE % ERROR (OVERALL)	RELATIVE ERROR (PEAK AMPLITUDES)
SOLID ELEMENT MODEL		
ACCELEROMETER-1	5.36	0.2
ACCELEROMETER-2	3.32	0.2
SHELL ELEMENT MODEL		
ACCELEROMETER-1	4.2	0.08
ACCELEROMETER-2	12.3	0.5

As it was done for the single hat section and the jointed hat section with single spacer, the finite element acceleration responses are filtered beyond 25,00Hz and compared with the experimental results which are shown in Figure 4-7 and 4-8, as it can be seen there is not much significant difference between the filtered and unfiltered data from the jointed hat sections where as there was a significant difference when the finite element analysis acceleration response was filtered in the single hat section. The

66

comparisons between FEA results including solid and shell element models and experimental results are shown in Figure 4-9. Table 4-3 depicts the overall relative error between experiment and FEA.

The differences between the finite element analysis and experimental results can be attributed to a lot of factors. Firstly, the accuracy of finite element analysis depends on the number of elements used. Secondly, the conditions in which the experiments are conducted are not replicated in the finite element analysis for instance damping, *DAMPING_GLOBAL card was used with a damping constant of 0.3 which was calculated using the first natural frequency of the structure to consider the damping effect but the results over lapped results from the model which did not consider damping.

EXPERIMENT Vs FEA
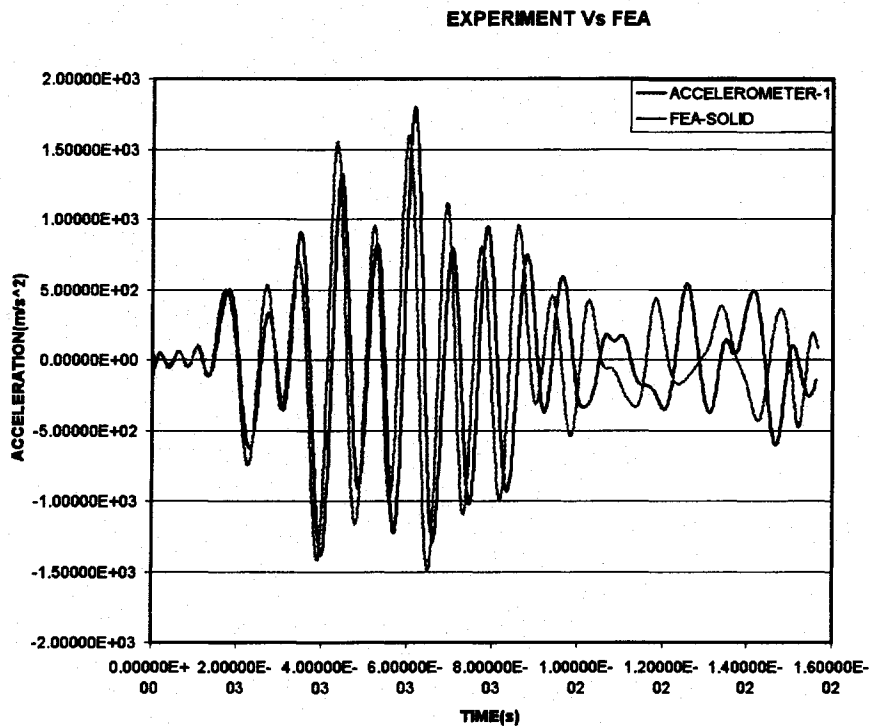
Figure 4-7(a) Filtered FEA comparisons using solid elements with experimental results (Acceleration Vs Time) obtained from aceelerometer-1

67

EXPERIMENT Vs FEA
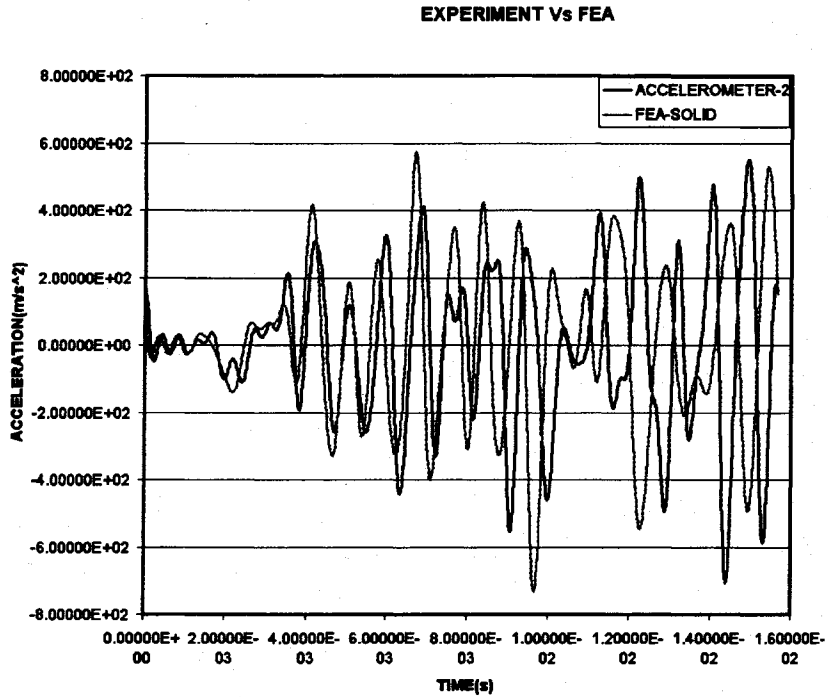
Figure 4-7(b) Filtered FEA comparisons using solid elements with experimental results (Acceleration Vs Time) obtained from aceelerometer-2

EXPERIMENT Vs FEA
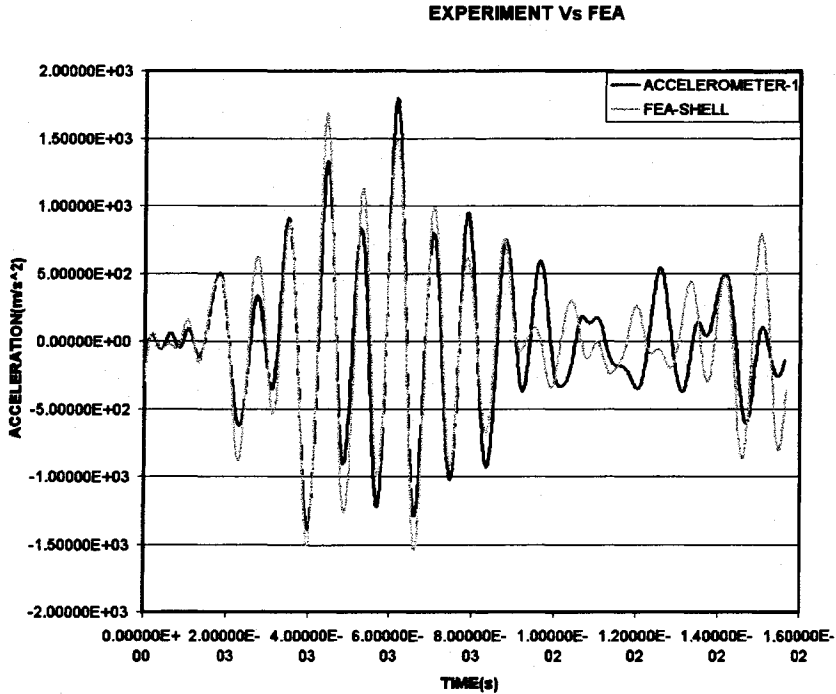
Figure 4-8(a) Filtered FEA comparisons using shell elements with experimental results (Acceleration Vs Time) obtained from accelerometer-1

68

EXPERIMENT Vs FEA
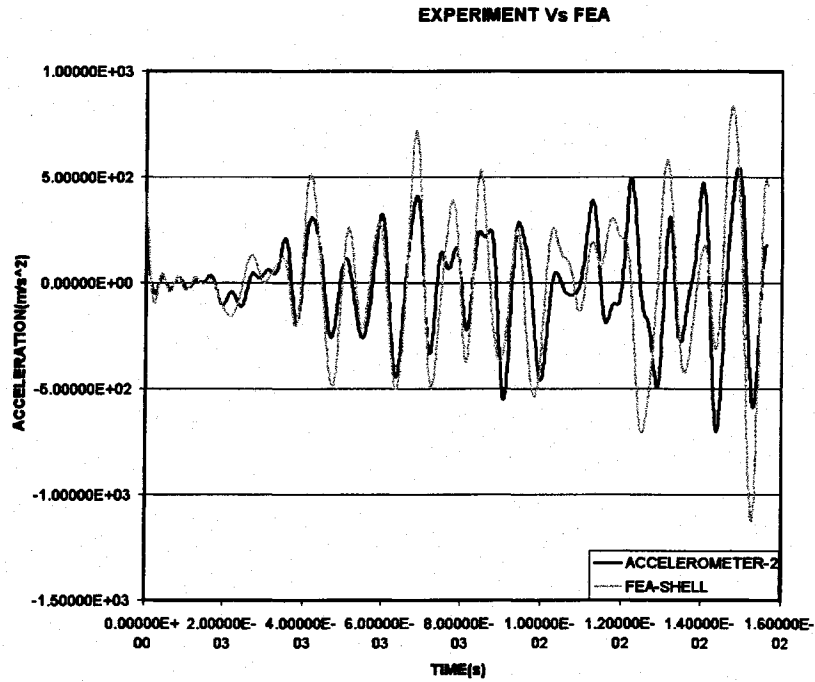
Figure 4-8(b) Filtered FEA comparisons using shell elements with experimental results (Acceleration Vs Time) obtained from accelerometer-2

EXPERIMENT Vs FEA
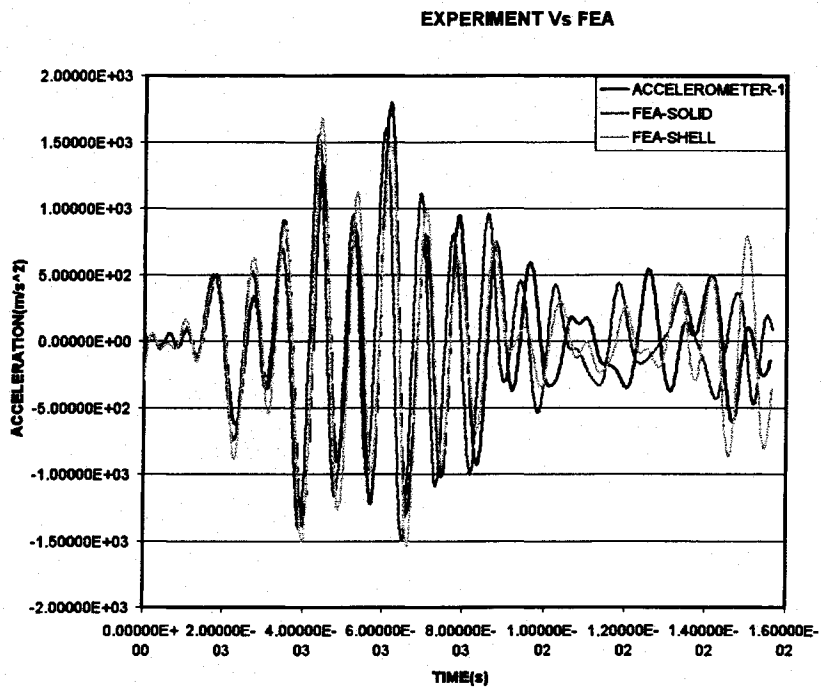
Figure 4-9(a) FEA comparisons using solid elements and shell elements with experimental results (Acceleration Vs Time) obtained from aceelerometer-1

69

EXPERIMENT Vs FEA
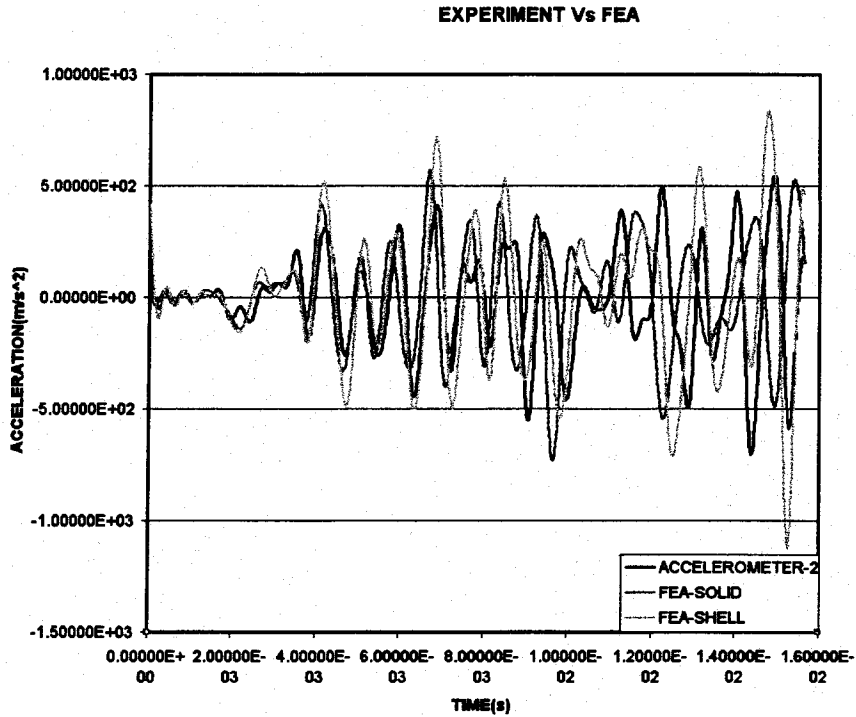
Figure 4-9(b) FEA comparisons using solid elements and shell elements with experimental results (Acceleration Vs Time) obtained from aceelerometer-2

Table 4-3 Relative error calculated for the filtered data

	RELATIVE % ERROR (OVERALL)
SOLID ELEMENT MODEL	
ACCELEROMETER-1	1.77
ACCELEROMETER-2	14.6
SHELL ELEMENT MODEL	
ACCELEROMETER-1	0.395
ACCELEROMETER-2	42.3

70

CHAPTER 5

ANALYSIS OF THE DOUBLE HAT SECTIONS WITH BOLTED JOINTS

5.1 Bolted Joint Configuration

The glued hat sections were separated from each other and two holes of diameter 0.006 m were drilled through the flanges on either side of the hat sections for fitting the steel bolts. Hexagonal headed bolts were used for this purpose, which have a nominal diameter of 0.005 m and have a bolt shank length and a bolt head height of dimensions 0.02 m and 0.003 m respectively. Steel washers with a hole diameter of 0.005 m with a thickness of 0.001 m were used to separate the hat sections; jointed hat sections with bolts are shown in Figure 5-1. Steel hexagonal nuts of dimensions 0.0035 m were employed to tighten the bolts, the dimensions of the nut; bolt and washer assembly is shown in Figure 5-2.

71
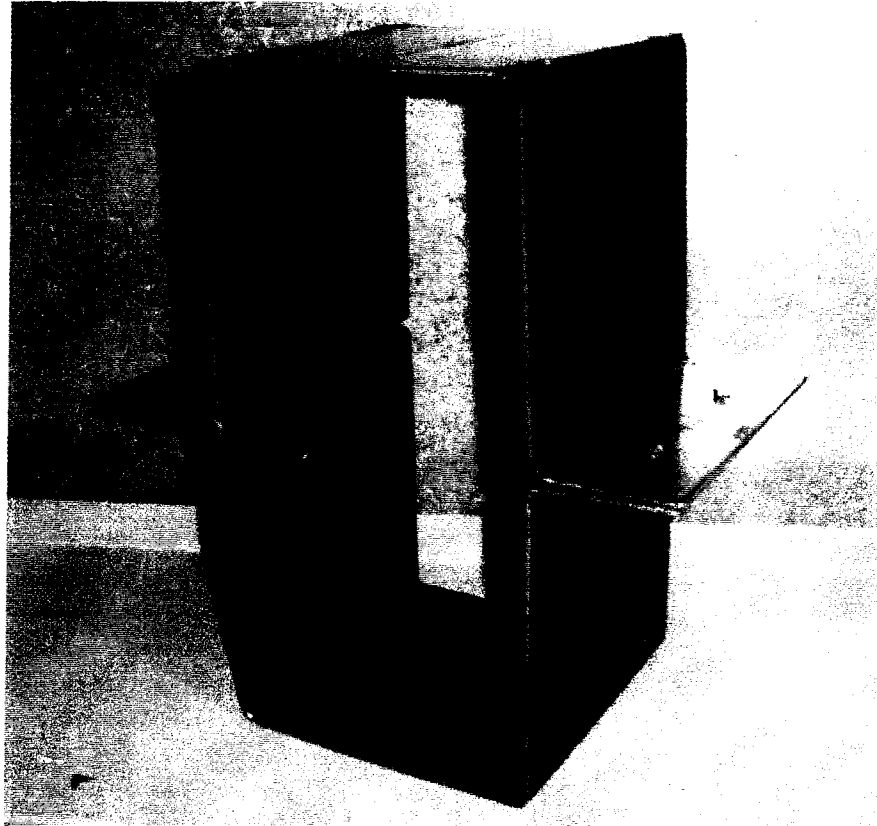
Figure 5-1 Double hat sections with bolted joints.

5.2 Selection of the 0.005 m bolt

Due to size of the jointed hat sections, larger sized bolts were avoided. To design

an appropriate bolt that can withstand the loads tending to separate the joined members

the following equations are used.

$$(F_t + F_i) < (A_t \times S_y), \text{ where}$$

$$F_i = K_i \times A_t \times S_p$$

$(F_t + F_i)$ being the total load applied on the bolt and $A_t^* S_y$ is maximum force the

bolt can withstand. F_i is the initial tensile force nearly equal to the full proof load, which

is defined as the maximum tensile force that does not produce a normally permanent set

and F_t is the total load taken in the bolt when the structure is subjected to external

72

loading. A_t is the tensile stress area of the threads, S_p is the proof strength of the material and K_i is a constant, usually specified in the range of 0.75 to 1.0 and S_y is the yield strength of the material.

An external load of 500 N was considered the maximum force that could be applied on the hat sections with the impact hammer since the load rating of the hammer is 440 N. The load carried by the bolts due to the applied external force is calculated by taking the moments with respect to the locations of the bolts on the structure. A_t, S_p and S_y were obtained from a standard machine design book and a bolt size of 0.0035 m was considered.

It was found that the force acting on each bolt was 593.70 N (considering two bolts) and the proof load was calculated to be 1576.35 N, resulting in a total load of 2169.25 N, which was less then the calculated maximum load of 2305.2 N, thus proving that a 0.0035 m bolt could be used to join two structures together when the applied external load is 500 N. The reason behind using the 0.005 m size bolt instead of a 0.0035 m is the fact that it is too small for handling while doing the experiments.
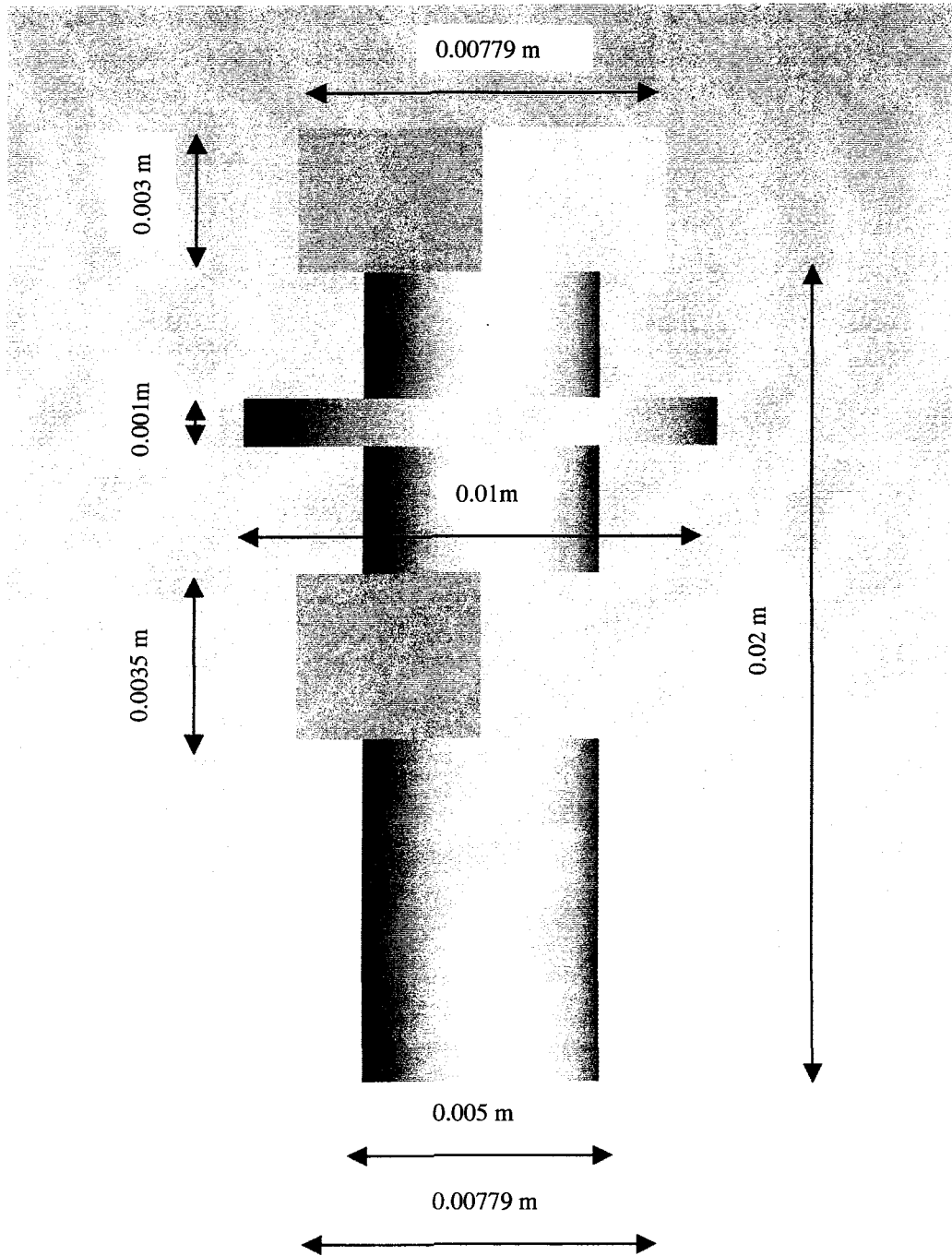
Figure 5-2 Dimensions of the nut, bolt and washer used in the joint of the double hat sections.

5.3 Modal Analysis of the Bolted Hat Sections

Finite element modal analysis is performed on the jointed hat sections with bolts using the finite element system analysis program ANSYS. A total of 63,665 elements and 42,909 nodes were used in the model, as shown in Figure 5-3. The hat sections are meshed with solid brick elements however due to the complexity of the geometry of the bolt and nut, tetrahedral elements had to be used in the model. Contacts are defined between the various jointed parts. A perfectly glued modeling option is used for this purpose.
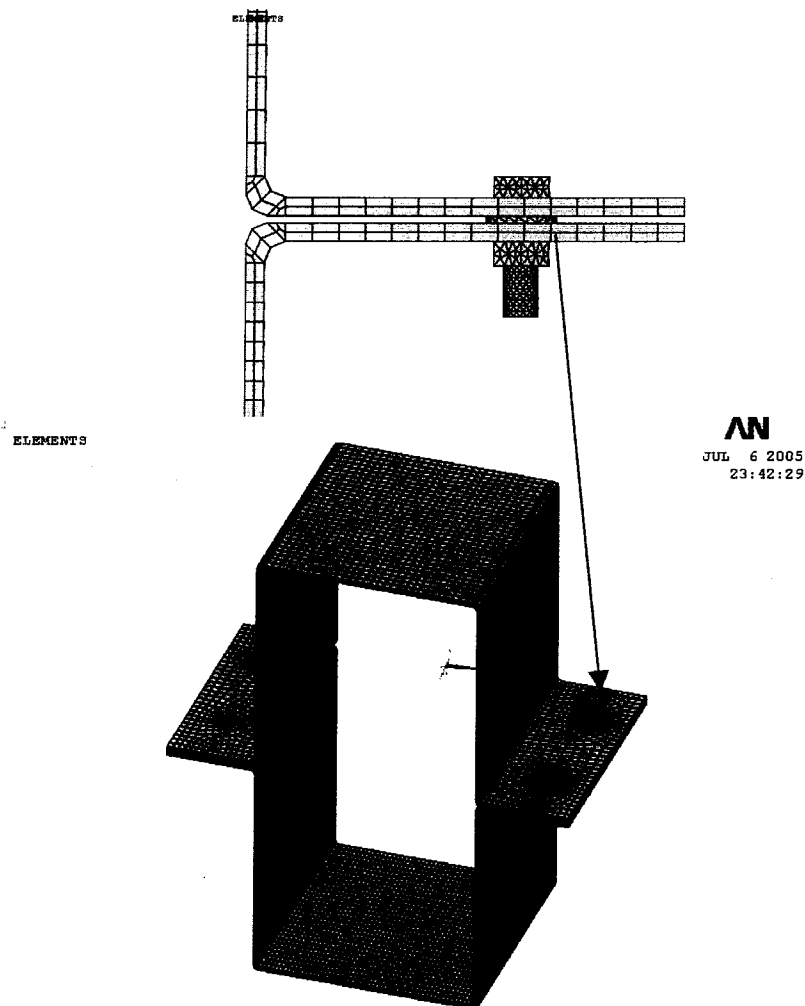
Figure 5-3 FE model of the jointed double hat section with bolts, using 3-d elements

75

Experiments similar to the adhesively jointed hat sections discussed earlier were conducted on the bolted hat section. FFT analysis of the bolted hat section is done using two configurations. The first configuration has the accelerometers on the vertical edges of the hat section and in the second configuration the accelerometers were placed on the edges of the horizontal flat plates. Both the configurations are shown in Figure 3-3 of chapter 3.

FFT analysis graphs of the bolted hat section for both configurations are shown in Figure 5-4. It is observed that most of the natural frequencies are excited in configuration-1 nevertheless there are a couple of natural frequencies, which are invisible in configuration-1. In configuration-2 the first three natural frequencies are less prominent when compared to configuration-1, the peaks are visible but not as prominently as seen in configuration-1. Comparison between experimental and finite element natural frequencies are shown in Table-5-1

76
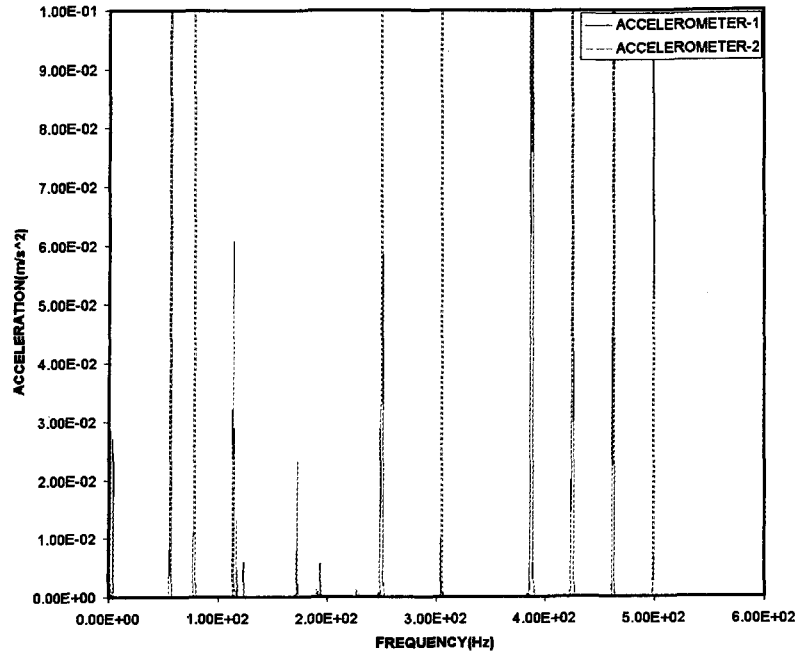
Figure 5-4(a) Fundamental frequencies for the two jointed hat sections with bolted joints as measured by accelerometer-1, placed on the vertical edge of the hat section.
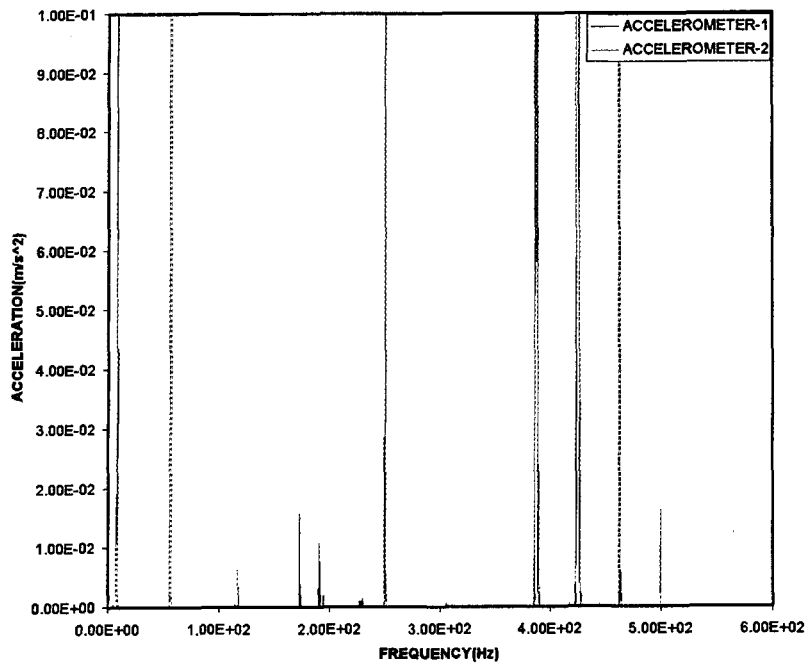
Figure 5-4(b) Fundamental frequencies for the two jointed hat sections with bolted joints as measured by accelerometer-2, placed on the horizontal edge of the hat section.

77

Table 5-1 Comparison of experimental and finite element results

MODE #	FEA (Hz)	EXPERIMEN -TAL (Hz)	%ERROR SOLID
7	60.0	56.3	6.6
8	80.6	79.4	1.5
9	114.9	114.2	0.6
10	123.3	124	0.5
11	128.6	-	-
12	177.5	173	2.6
13	201.0	194	3.6
14	215.4	-	-
15	251	251	0

5.4 Shock Transmission through the Bolted Joints

Experiments were conducted on the hat sections with bolted joints to determine the transient response in a similar fashion as the adhesively jointed hat sections. Accelerometers are placed on the upper and lower sides of the joints and the hat section is impacted at the opposite side as was done in the case of adhesively jointed hat sections.

Three cases are considered for the finite element analysis:

1. Complete solid element model

2. Hat sections made up of shell elements while the nut, bolt and washer with solid elements.

3. Hat sections and the washers modeled of shell elements while bolts are molded as beam elements and effect of the nuts are neglected.

Load curve obtained from the experiment which is applied on the finite element models is shown in Figure 5-5 .The solid model of case-1 has a total of 186,186 nodes and 143,504 elements respectively where as the model with shell element hat sections and solid element nuts, bolts and washers of case-2 has a total of 44,560 (43,264 shell elements and 1296 solid elements) elements and 37,364 nodes. The third model has a total of 2294 nodes and 2092 (2088 shell elements and 4 beam elements) elements. The three finite element models of the hat sections with bolted joints are shown in Figure 5-6.
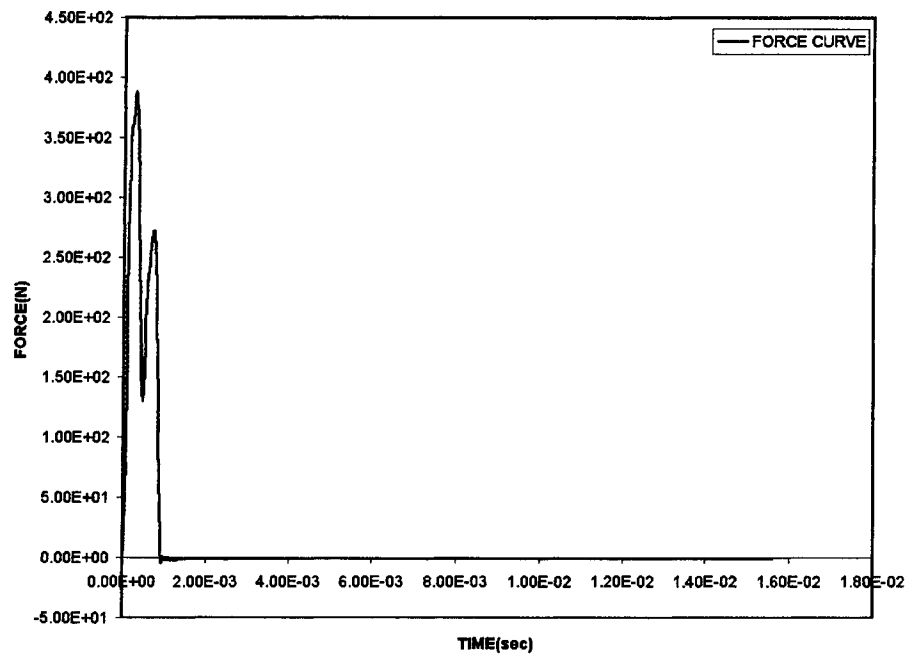
Figure 5-5 Load curve applied on the FE models

79
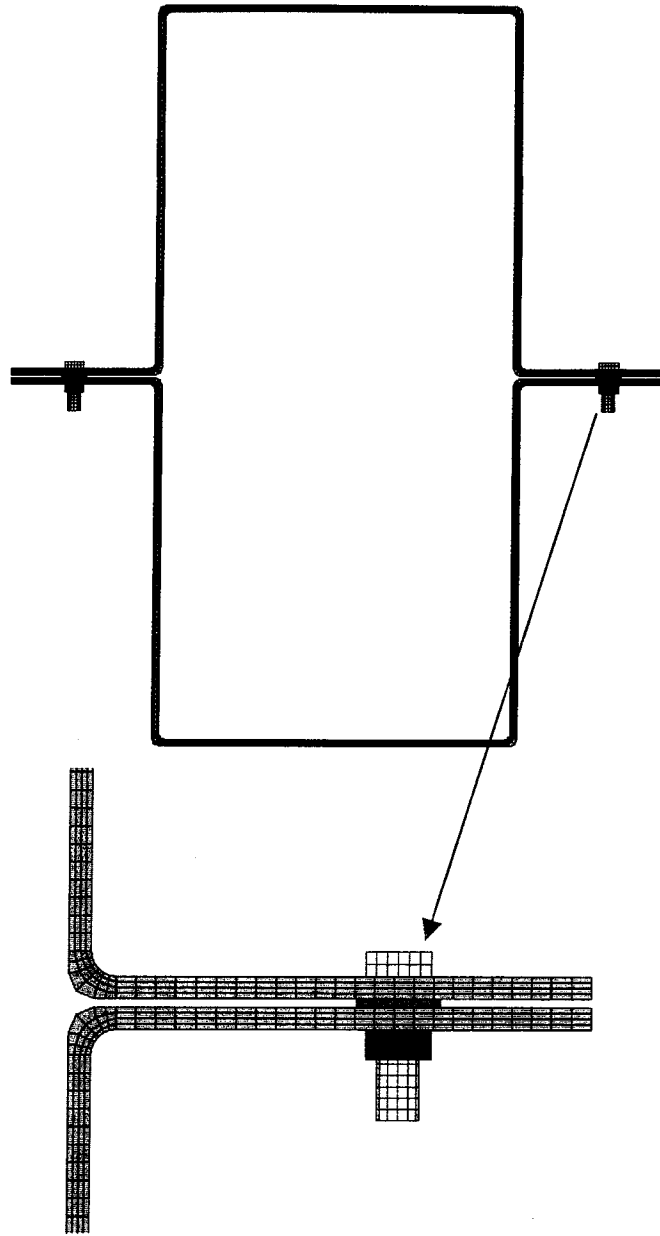
Figure 5-6(a) Case-1, FE model with solid elements of the bolted double hat sections.

80
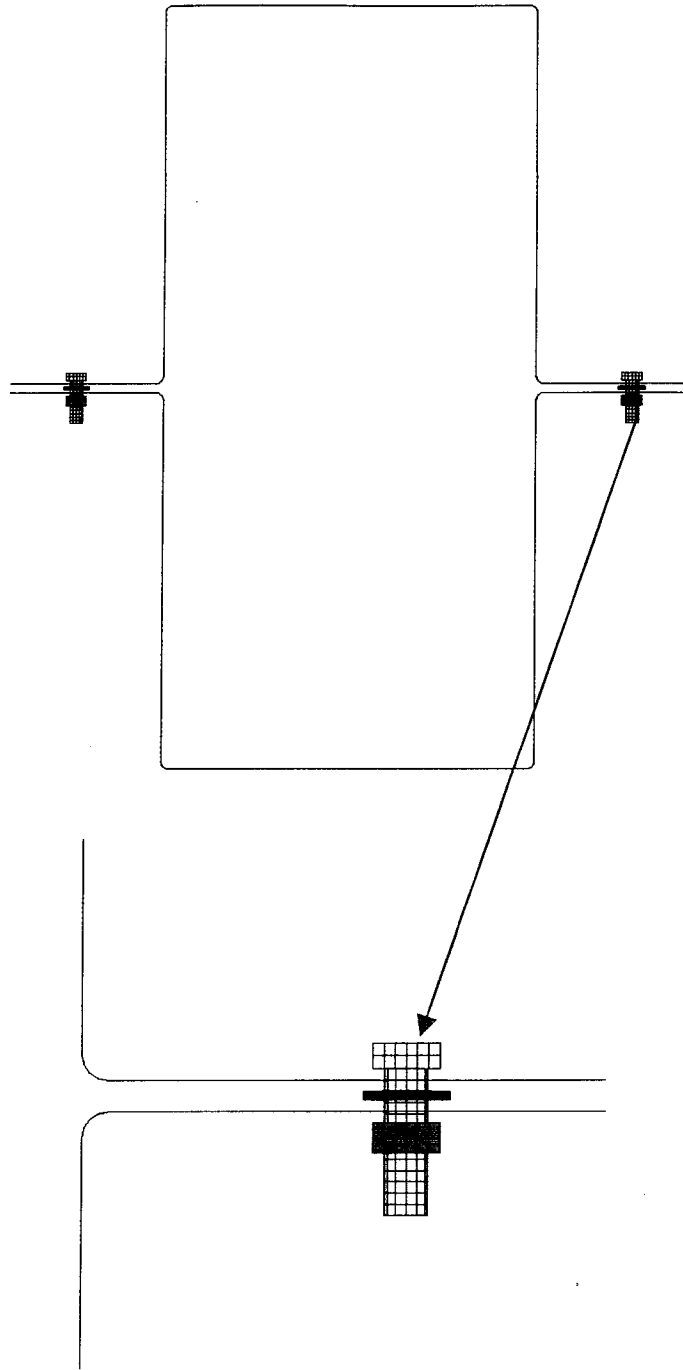
Figure 5-6(b) FE model of bolted double hat sections with shell element hat sections and solid element bolts, nuts and washers.
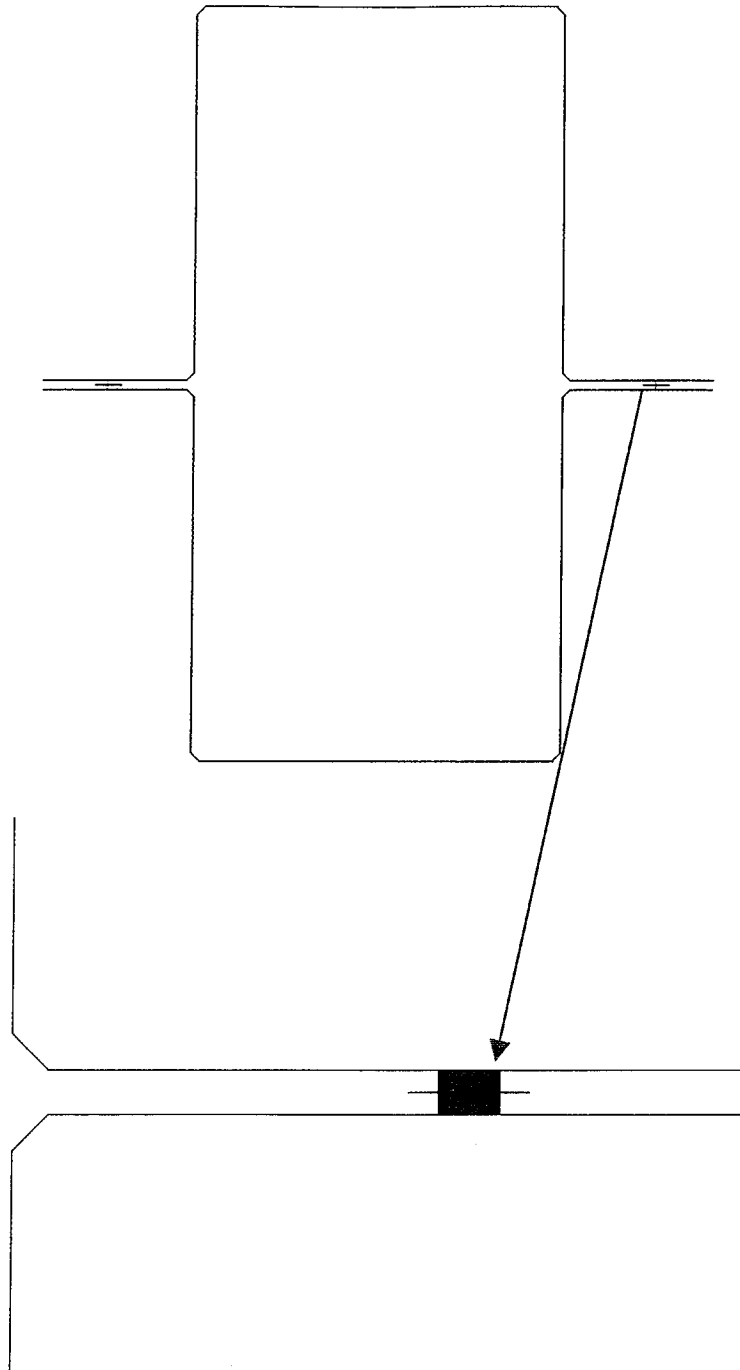
Figure 5-7(c) FE model of bolted double hat sections with shell element hat sections and beam element bolts and washers modeled with shell element.

As was done in the adhesively jointed hat sections, the bolted hat sections have four elements along the thickness direction in the solid element model. To duplicate the effect of using four solid elements in the model thickness; five integrations points were used along the thickness direction for the shell element model.

Accurate modeling of contact interfaces between the two hat sections is crucial to the prediction capability of the finite element simulations. Interfaces can be defined three dimensionally as triangular and quadrilateral segments of the elements that comprise each side of the interface. One of the interfaces is designated as the slave side, and the other is designated as the master side. Nodes lying in those surfaces are referred to as slave and master nodes, respectively. The slave nodes are constrained to slide on the master surface after the impact and must remain on the master surface until a tensile force develops between the node and the surface.

Contacts were defined between the components using part id numbers for the solid element model. Contact type *CONTACT_TIED_SURFACE_TO_SURFACE was used for the solid element model since the maximum force applied on the hat section by the hammer is 400 N, which does not cause any appreciable deformations in the structure nor result in loosening of the bolt. Thus, there is a perfectly tight contact between all the components, which move in unison. The a master and slave components defined in the contact surfaces, which were used for the solid element model, are shown in Table 5-2

83

Table 5-2 Master and slave surfaces in the solid element model

MASTER SURFACE	SLAVE SURFACE
Hat section	Bolt
Hat section	Washer
Hat section	Nut
Bolt	Washer
Bolt	Nut

Similar to the solid element model, contacts were defined between the various components of the shell element model. In order to account for the shell thickness offset the contact types *CONTACT_TIED_SURFACE_TO_SURFACE_OFFSET and *CONTACT_AUTOMATIC_SURFACE_TO_SURFACE ware used. Part ids were considered for defining the contact components similar to the solid element model. The master and slave components defined in the contact surfaces with the contact type used, for the shell element model, are shown in Table 5-3.

84

Table 5-3 Master and slave surfaces in the shell element model

MASTER SURFACE	SLAVE SURFACE	CONTACT TYPE
Hat section	Bolt	Tied_surface_surface_offset
Hat section	Washer	Tied_surface_surface_offset
Hat section	Nut	Tied_surface_surface_offset
Bolt	Washer	Automatic_surface_surface
Bolt	Nut	Automatic_surface_surface

The shell element model with the beam elements acting as the bolts is modeled in such a manner that the one-dimensional beams share their nodes with the shell elements on either sides of the beam. An orientation key point is defined on a plane, which is parallel to the beam, to define the local orientation of the beam element. The cross section of the beam is defined by using the card *SECTION_BEAM, the card and the parameters used to define the card are specified below.

```
*SECTION_BEAM
$HMNAME PROPS        3BEAM
       3       1     1.0     2.0     1.0     0.0
       5       5     0.0     0.0
```

A Hughes-Liu element with cross section integration (which is the default beam element formulation) is used to define the beam. As tubular (circular) cross-section is used to define the beam, both inner and outer diameters are given the same value, 5 to make it represent a solid cylinder.

*TIED_SHELL_EDGE_TO_SURFACE_BEAM_OFFET contact card was initially used to define contacts between the washer and the bolt, which resulted in initial

85

penetration of the washer into the bolt. This problem was taken care by the use of the contact card *CONTACT_TIED_SURFACE_TO_SURFACE_OFFSET which was defined between upper flange, lower flange and the washer. There was no penetration observed and the horizontal flat plates and washer moved together.

There is an incongruity here as there was no instability observed due to the use of *CONTACT_TIED_SURFACE_TO_SURFACE_OFFSET for shell elements which was quite prevalent in the case of adhesively jointed hat sections with spacers (both continuous and intermittent). Due to the shell thickness offset considerations which is a theoretical modeling phenomena where one cannot see the contact interface, but relative motion between the two shell surfaces begins when the invisible top surface of the bottom shell plate which is at half the distance from the shell surface and which behaves as the mid surface of the actual 3-D structure comes in contact with the invisible bottom surface of the top shell plate. Shell surfaces are supposed to have very small separation between them (LS DYNA manual) if tied contacts are ever to be used which might be the reason for the instabilities observed in the adhesively joined hat section models as the distance between the spacers (master) and hat section horizontal flat plates (slaves) was 0.002654m where as in the present case of shell element model with beam element acting as bolt the separation between washer and the horizontal flat plates of the hat section is 0.001m.

The node number corresponding to the locations of accelerometer-1 and accelerometer-2 in the solid element model is 44,821 and 139,276 respectively. The comparisons between the experimental and finite element analysis for the solid element model is shown in Figure 5-7. Similarly the node numbers 6,129 and 37,171 correspond

86

to the locations of accelerometer-1 and accelerometer-2 in the shell element model with solid element nut, bolt and washer. The comparisons between the experimental and finite element analysis for this model is shown in Figure 5-8.

Similar approach, which was applied for the shell element model with solid element nut, bolt, and washer, is applied to the shell element model with beam element bolts. Node numbers 4188 and 5277 of the second shell element model (with the beam element bolt) correspond to the accelerometer-1 and accelerometer-2 respectively. The finite element and experimental comparisons are shown in Figure 5-9. It can be seen from the graphs that the finite element prediction does not match with the experimental response, there is not only a difference seen in the magnitudes but it is also observed that they do not follow a similar pattern.

87
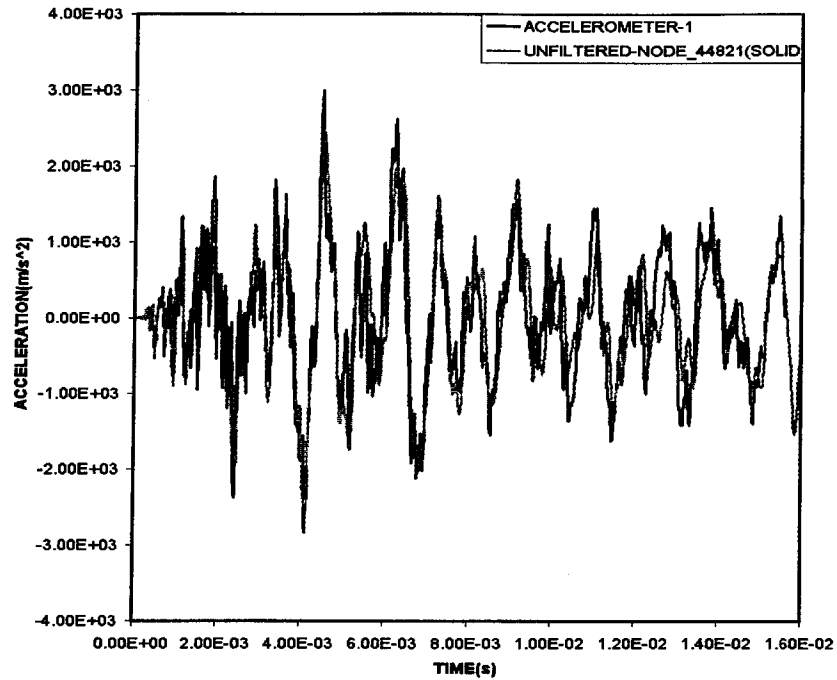
Figure 5-7(a) FEA comparisons of bolted double hat sections using solid elements with experimental results (Acceleration Vs Time) obtained from aceelerometer-1

Figure 5-7(b) FEA comparisons of bolted double hat sections using solid elements with experimental results (Acceleration Vs Time) obtained from aceelerometer-2

88

Figure 5-8(a) FEA comparisons of bolted double hat sections using shell element hat sections and solid element bolts, nuts and washers with experimental results (Acceleration Vs Time) obtained from acelerometer-1
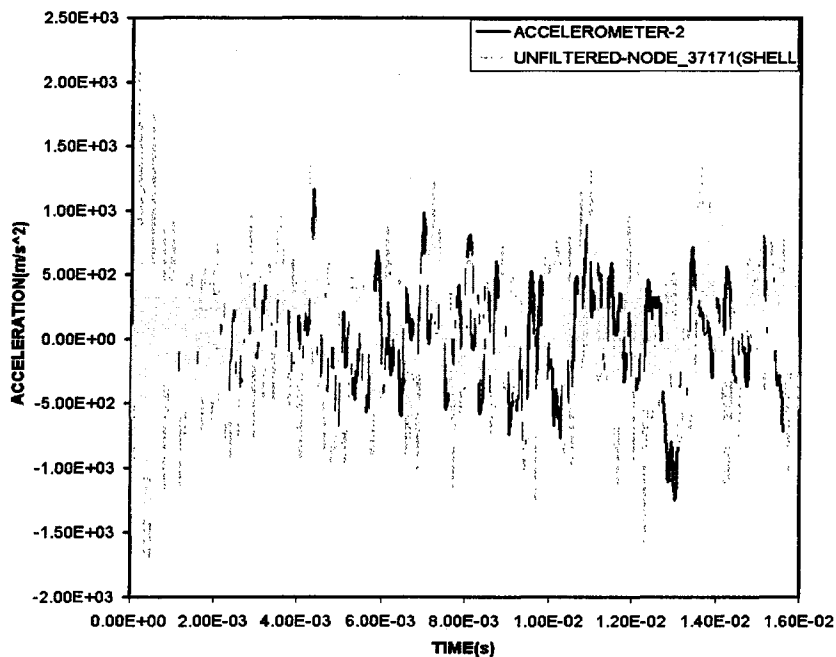
Figure 5-8(b) FEA comparisons of bolted double hat sections using shell element hat sections and solid element bolts, nuts and washers with experimental results (Acceleration Vs Time) obtained from acelerometer-2

89
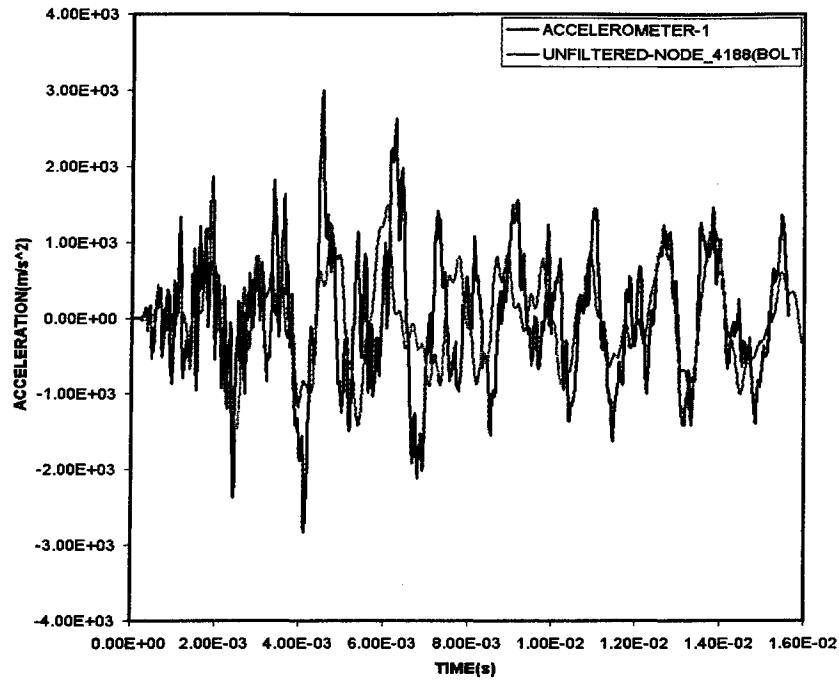
Figure 5-9(a) FEA comparisons of bolted double hat sections using shell element hat sections and beam element bolts and shell element washers with experimental results (Acceleration Vs Time) obtained from accelerometer-1
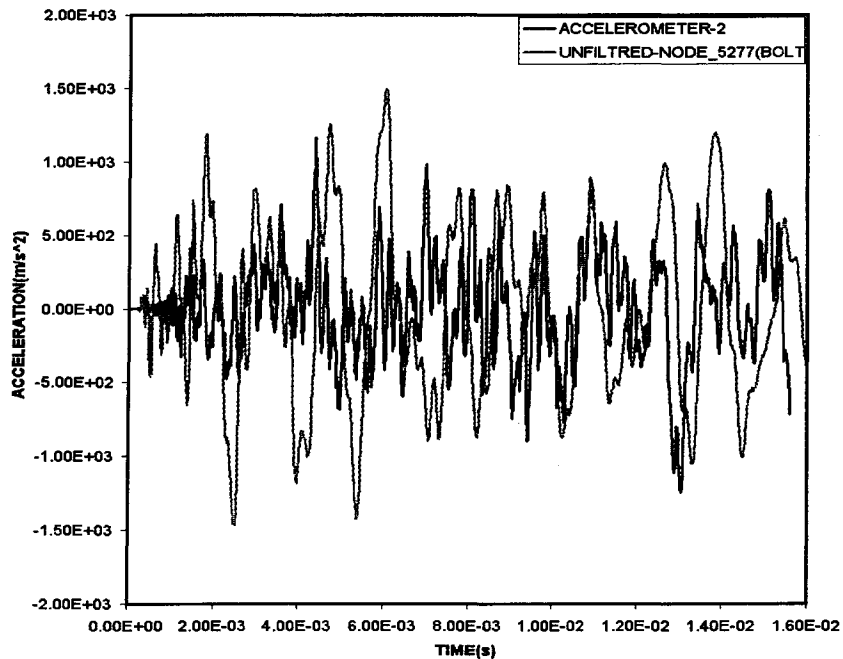
Figure 5-9(b) FEA comparisons of bolted double hat sections using shell element hat sections and beam element bolts and shell element washers with experimental results (Acceleration Vs Time) obtained from accelerometer-2

90

As it can be seen from Figure 5-7, the finite element analysis predicts almost the same response at the node 44,821 as accelerometer-1, the prediction follows similar pattern for the node 139,276 for about 0.01 seconds after which discrepancies creep in and a phase shift is observed. Nevertheless the amplitudes remain almost the same, which are most important since damages to components in vehicles due to shock are a function of the magnitudes of the accelerations that the components are subjected to. Relative error between the experimental and finite element analysis data was calculated using the formula shown in Chapter 2, error in the finite element analysis models is also calculated with respect to the experiment for the peak amplitudes which are of utmost importance in shock analysis.

Similar patterns were observed in the shell element model where the finite element analysis predicts the response well that corresponds to the response picked up by Accelerometer-1 although initial disturbances are observed. It is difficult to compare the response from node 37,171 and accelerometer-2 as much disturbance was observed. As was done for previous cases, the finite element analysis and experimental responses are filtered beyond 2500Hz (filtering is discussed in Chapter 3), the comparisons for the solid element model are shown in Figure 5-10 and the comparisons for the shell element model solid washer, nut and bolt are shown in Figure 5-11. Table 5-4 shows the relative error calculated for the overall experimental and FEA data along with relative error in peak amplitudes.

Table 5-4 Relative error calculated for the unfiltered data

	RELATIVE % ERROR (OVERALL)	RELATIVE ERROR (PEAK AMPLITUDES)
SOLID ELEMENT MODEL		
ACCELEROMETER-1	15.56	0.1866
ACCELEROMETER-2	32.25	0.2042
SHELL ELEMENT MODEL		
ACCELEROMETER-1	52.32	0.003
ACCELEROMETER-2	45.24	0.1452

EXPERIMENT Vs FEA
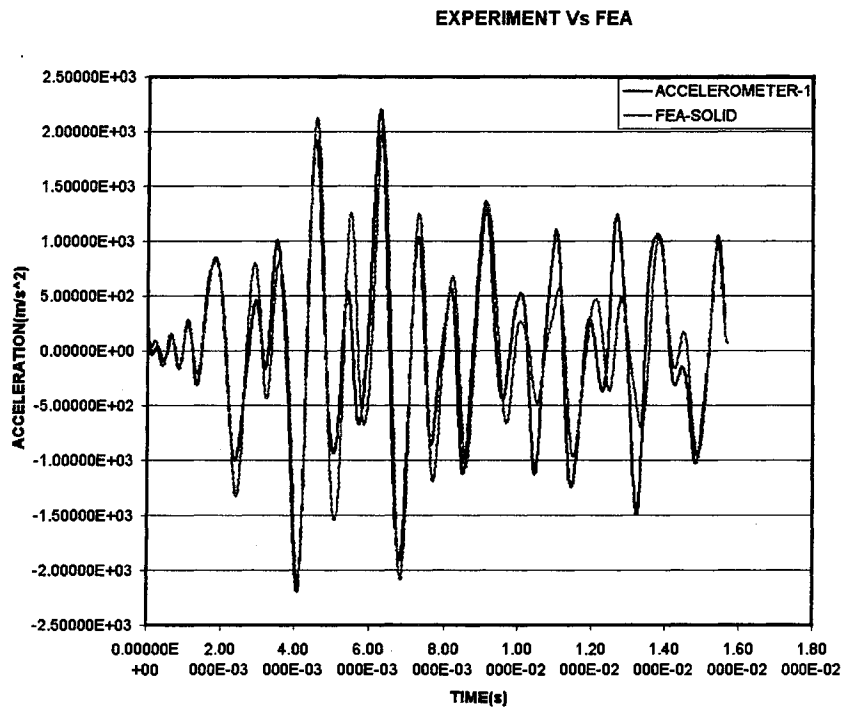
Figure 5-10(a) Filtered FEA comparisons using solid elements with experimental results (Acceleration Vs Time) obtained from aceelerometer-1

92
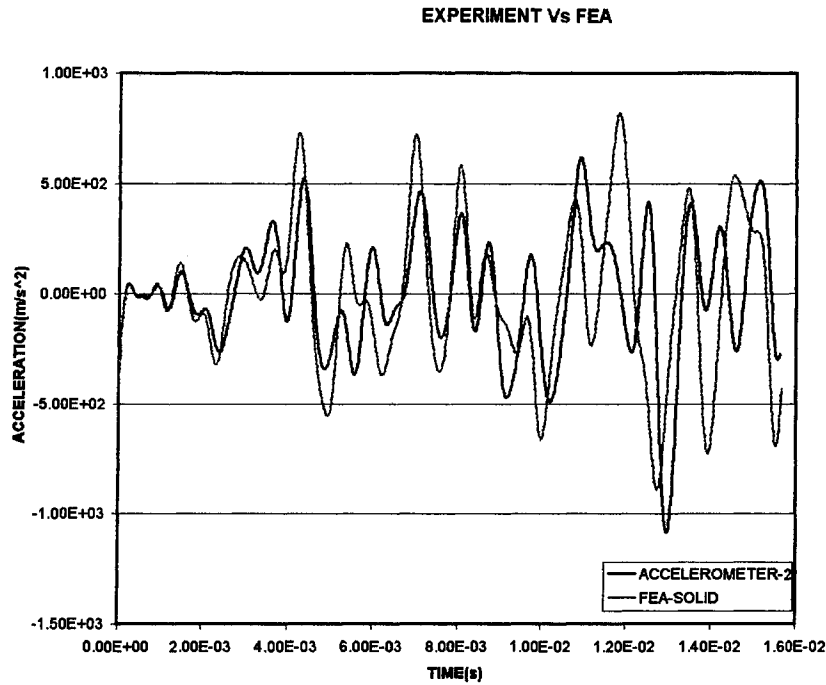
Figure 5-10(b) Filtered FEA comparisons using solid elements with experimental results (Acceleration Vs Time) obtained from aceelerometer-2
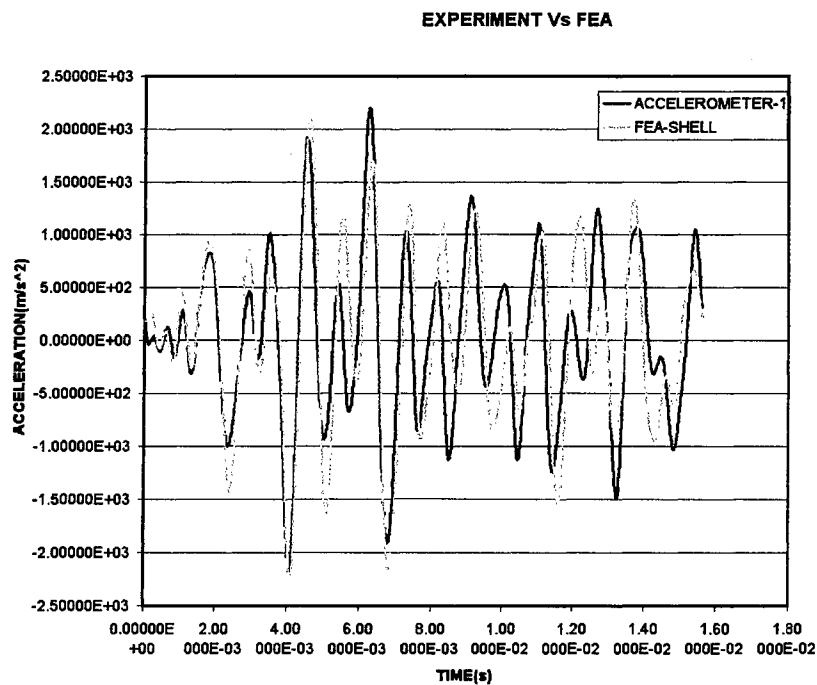
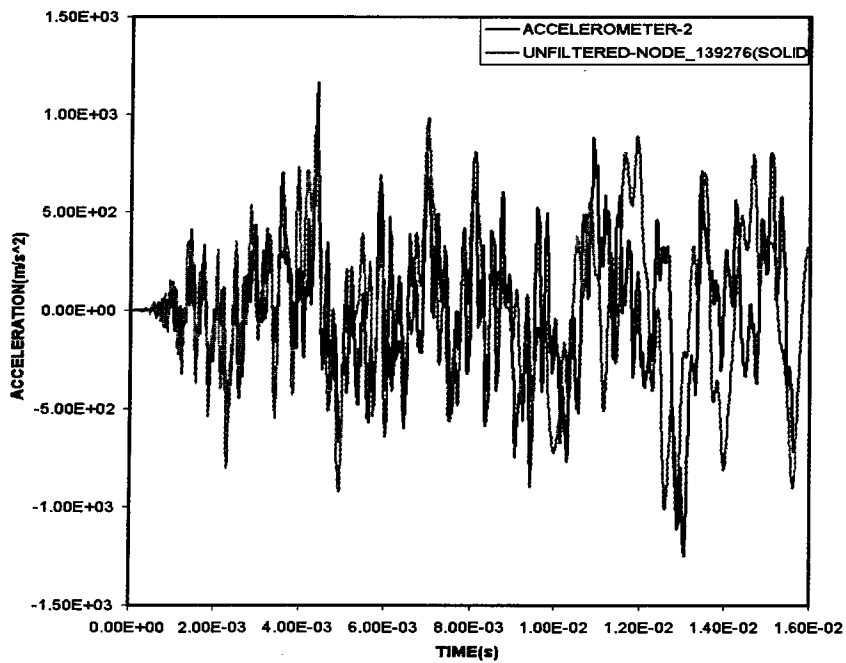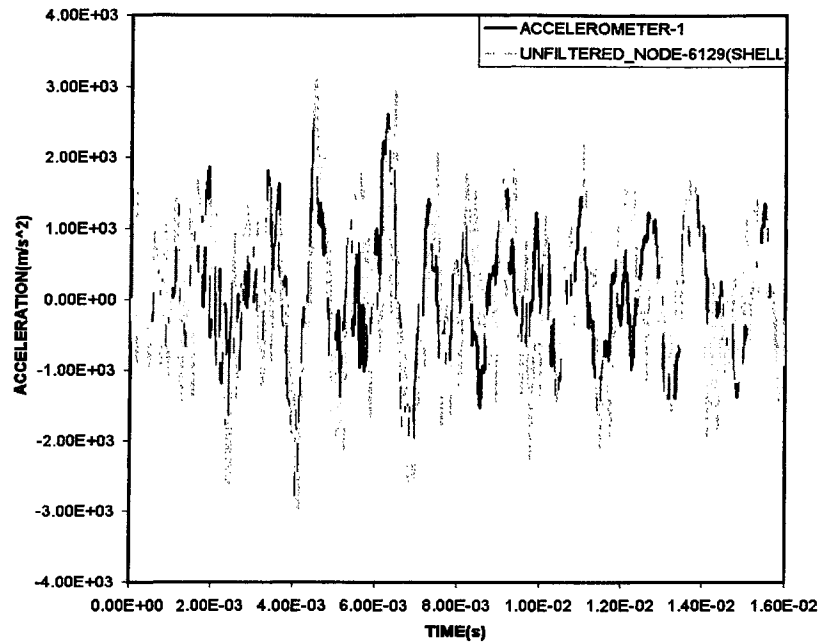Figure 5-11(a) Filtered FEA comparisons using shell element hat sections and solid element bolts, nut and washers with experimental results (Acceleration Vs Time) obtained from aceelerometer-1

93
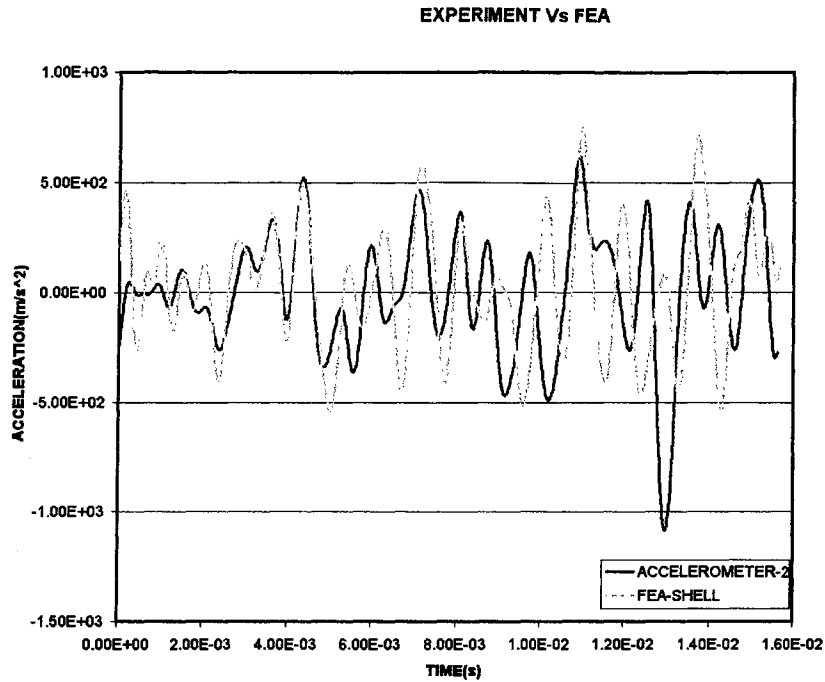
Figure 5-11(b) Filtered FEA comparisons using shell element hat sections and solid element bolts, nut and washers with experimental results (Acceleration Vs Time) obtained from aceelerometer-2

From Figures 5-0 and 5-11 it can be said again that the solid element model better characterizes the experiment than the shell element model. It can be seen from Figure 5-7(b) and 5-10(b) that, when the data is filtered to 2500 Hz, significant peaks are lost in the solid element model due to which the filtered data looks incongruous with the experimental results. In the shell element model unwanted noise can be removed when the Finite element data are filtered to 2500Hz as it can be seen in Figures 5-8(b) and 5-11(b).

The finite element results from the adhesively jointed double hat sections with spacers (both, continuous and intermittent) show better congruity with the experimental results when compared to the double hat sections with bolts. The reason behind this might be the area of contact between the two hat sections. In the case of adhesively

94

jointed double hat section the structure behaves relatively more like a continuous structure when compared to the double hat sections with bolted joints. This enables the finite element analysis to better predict the shock response in the adhesively jointed hat sections.

From Figure 5-9(a) and (b) it is evident that the beam element representation of the bolt does not duplicate the effect of shock propagation through an actual bolted joint. Figure 5-9(a), which represents the comparison between the response from accelerometer-1 and the response of the node corresponding to the location of accelerometer-1 is totally invalid as accelerometer-1 is located on the hat section which has been impacted with the hammer and technically the finite element analysis response should approximate the experimental results as the impact node and the measurement node (location of accelerometer-1) lie on a s structure without any discontinuities.

As it can be seen from the Figures 5-12(a) and (b), the solid element model approximates the experimental results better then the shell element model due to the reasons discussed in chapter 4. Table 5-5 depicts the overall relative error between experiment and FEA.

95

EXPERIMENT Vs FEA
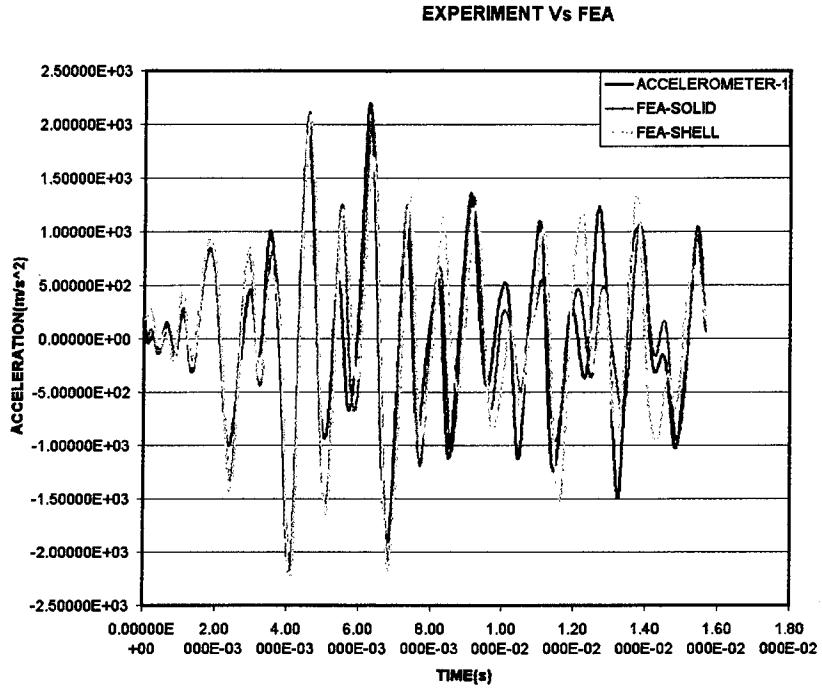
Figure 5-11(a) FEA comparisons using solid elements and shell elements with experimental results (Acceleration Vs Time) obtained from aceelerometer-1

EXPERIMENT Vs fFEA
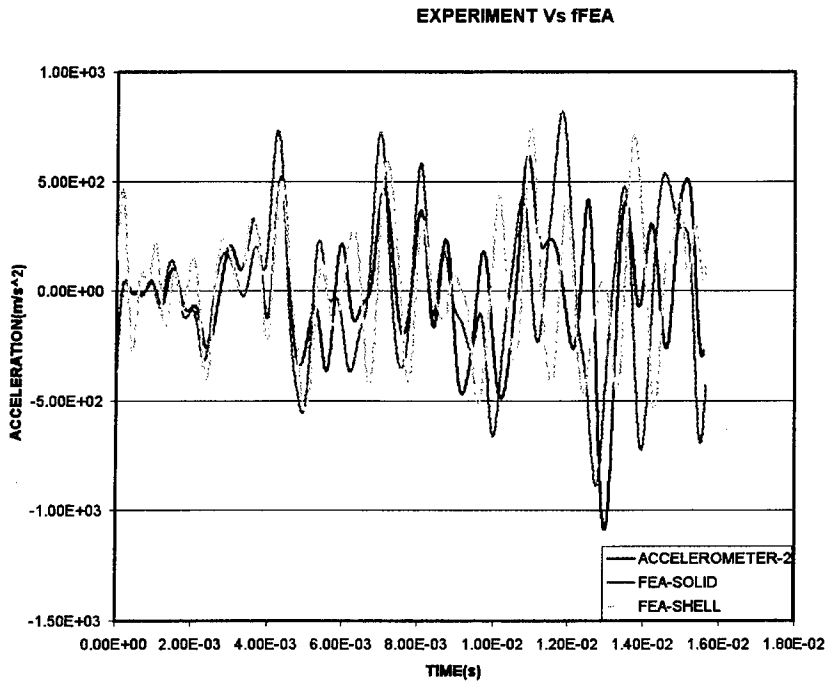
Figure 5-11(b) FEA comparisons using solid elements and shell elements with experimental results (Acceleration Vs Time) obtained from aceelerometer-2

96

Table 5-5 Relative error calculated for the filtered data

	RELATIVE % ERROR (OVERALL)
SOLID ELEMENT MODEL	
ACCELEROMETER-1	7.31
ACCELEROMETER-2	17.1
SHELL ELEMENT MODEL	
ACCELEROMETER-1	12.2
ACCELEROMETER-2	24.73

97

CHAPTER 6

SHOCK RESPONSE SPECTRUM ANALYSIS

Shock tests were performed to validate that a structure or a mechanism can support transient vibrations encountered during its life in a genuine environmental setting. Shock Response Spectrum is one of the shock testing formats. Shock Response Spectrum (SRS) analysis is, by definition, the maximum response of a series of Single Degree of Freedom (SDOF) systems, which have different mass, M_i, springs stiffness, K_i and damping devices, C_i. Each component (SDOF) has a different resonance frequency, $F_r = 1/ (2*\Pi)*\sqrt{K/M}$ So that every resonance frequency of possible interest is represented. The transient acceleration is enforced on the series of SDOF platform, each of the SDOF components will respond with its own unique acceleration transient. The peak response acceleration level is then computed for each SDOF component. The set of all peak levels is seen to be representative of the severity of each of the SDOF systems shock transient. This set of peak levels can be collected together to form a spectrum across the frequency range of interest [19]. This is the SRS. The process is pictured in Figure 6-1.

98
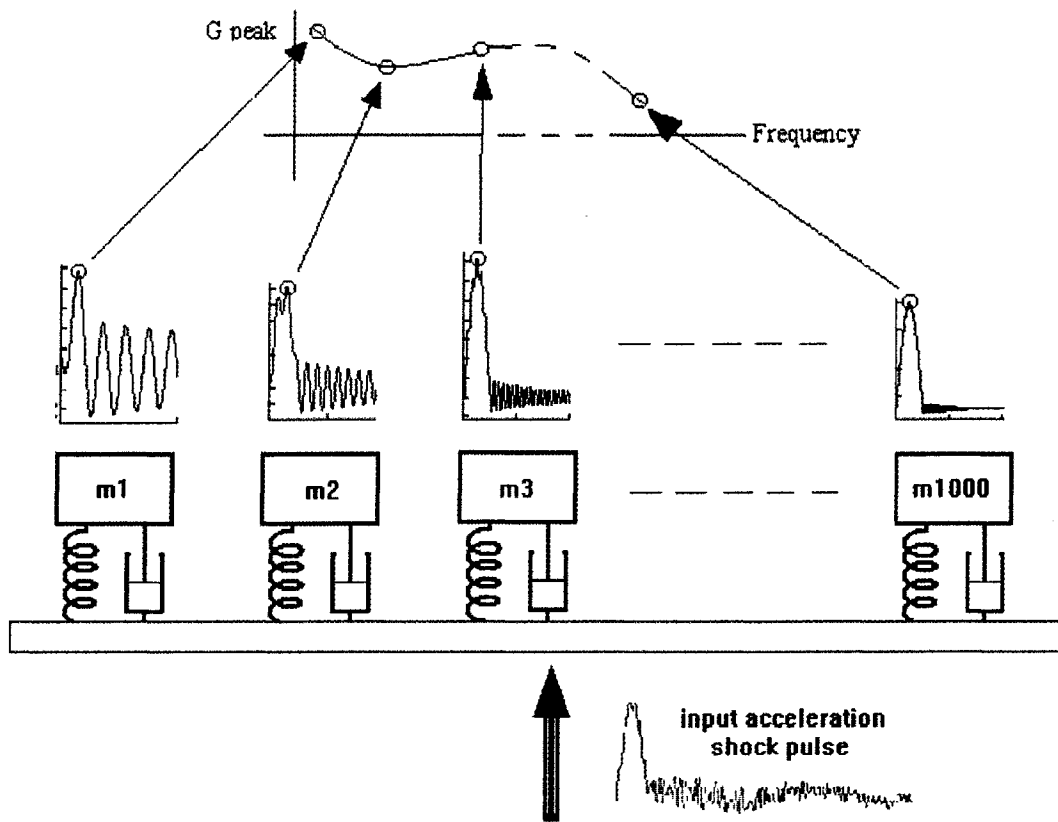
Figure 6-1 The SRS concept [19]

The Army Research Labs provided a comprehensive MATLAB code for the Shock Response Spectrum, which was used to determine the SRS for the acceleration responses presented in the previous chapters. The data obtained from both the accelerometers in all the cases was fed into the Mat lab program, which generated a set of graphs comparing the shock response spectrum of experimental and finite element analysis data.

99

6.1 Shock Response Spectrum Analysis Results of Single Hat Section.

The Experimental and finite element analysis acceleration responses obtained from the single hat section previously shown in Figures 2-9 and 2-10 are fed into the Mat lab program resulting in the graphs shown in Figures 6-2 and 6-3. Figure 6-2(a) depicts the shock response spectrum comparison between the experimental response from accelerometer-2 and the FEA response at the corresponding node. The worst frequency is around 1082.4 Hz in both the experiment and finite element analysis even though there is a slight difference seen in the amplitude, the experiment shows an amplitude of 7726.5 m/s^2 where as the finite element result shows an amplitude of 6820 Hz. Similar pattern is observed in Figure 6-2(b) which represents the comparison between the experimental response from accelerometer-1 and the FEA response at the corresponding node. The worst frequency is about 1082.4 Hz but there is a slight magnitude difference between the experiment and finite element analysis, the experiment shows an amplitude of 5679.5 m/s^2 where as the finite element result shows an amplitude of 5399.1 Hz.

Comparison of Shock response spectrum of the shell element model with the experiment is shown in Figure 6-3. The finite element analysis acceleration response is obtained from the node, which corresponds to the location of accelerometer-1. As it can be seen from Figure 6-3, the shell element model replicates the experiment, the shock response spectrum curves from the experiment and finite element analysis shell model overlap.

100
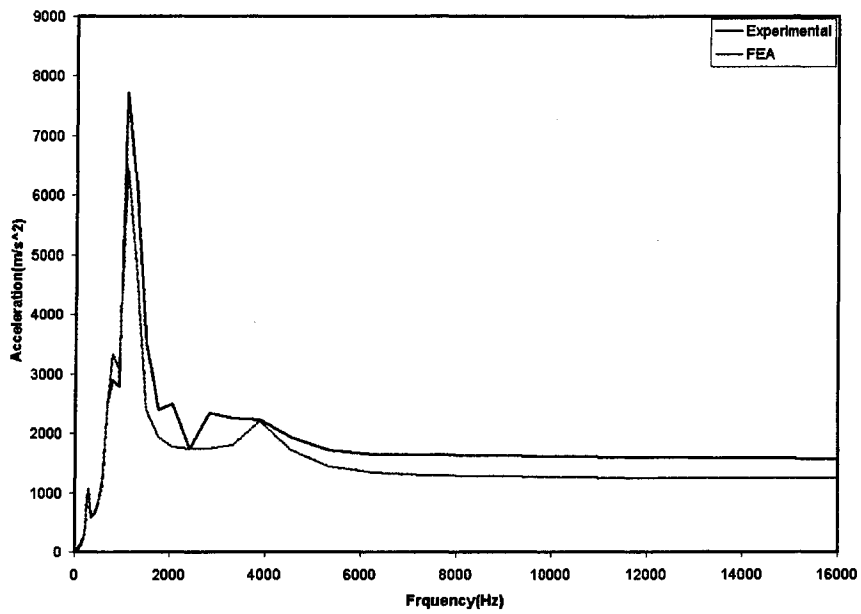
Figure 6-2(a) SRS analysis comparisons between FEA model using solid elements and experimental Results for a single hat section from accelerometer-1
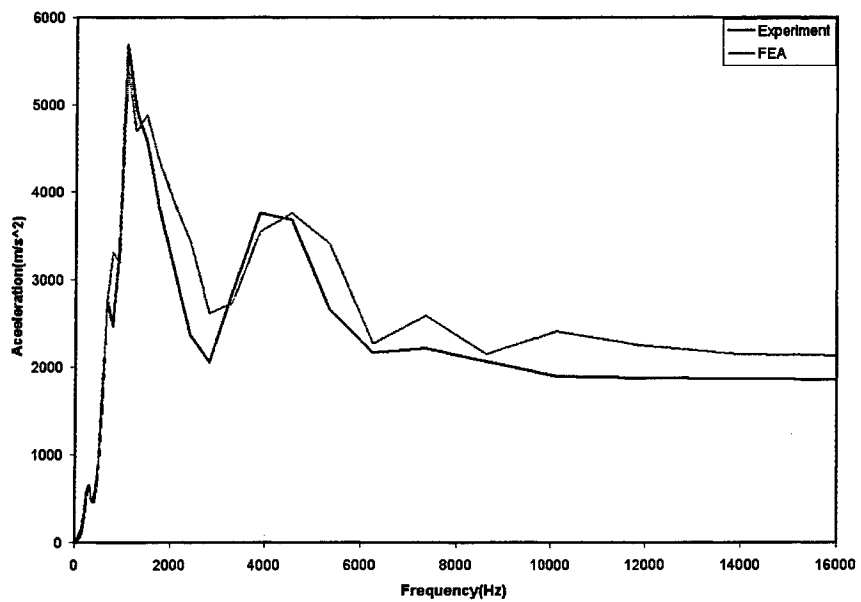
Figure 6-2(b) SRS analysis comparisons between FEA model using solid elements and experimental Results for a single hat section from accelerometer-2

101
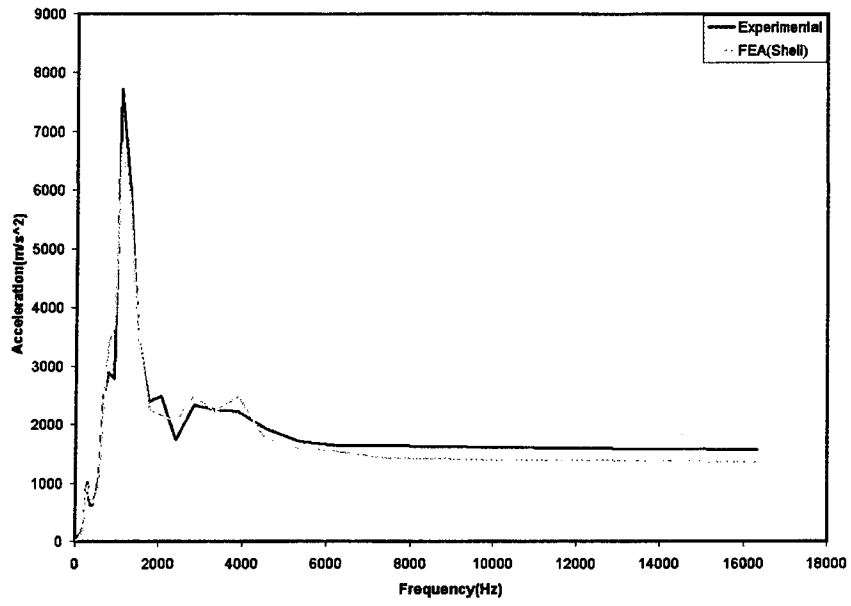
Figure 6-3 SRS analysis comparisons between FEA model using shell elements and experimental results for a single hat section from accelerometer-1

102

6.2 Shock Response Spectrum Analysis Results of Adhesively Bonded Double Hat Sections with Continuous Spacers.

Figures 6-4 and 6-5 depict the shock response spectrum comparisons between the experiment and finite element analysis of the adhesively bonded double hat sections with continuous spacers. Figure 6-4(a) depicts the shock response spectrum comparison between the experimental response from accelerometer-1 from the experiment and the response at the node, which corresponds to the location of accelerometer-1 in the finite element solid model. As it can be seen, the worst frequency is again close to 1082.4 Hz in both the experiment and finite element analysis and there is very little difference seen in the amplitude, which is around 13320 m/s^2. Figure 6-4(b) represents the comparison between the experimental response from Accelerometer-2 from the experiment which predicted a worse frequency of 670.4 Hz and the response at the node, which corresponds to the location of accelerometer-2 in the finite element model, where the worst frequency is about 786.4 Hz, there is an error of little over 14% recorded in the finite element analysis . There also exists a magnitude difference between the experiment and finite element analysis, the finite element result shows a peak amplitude of 4515.3 m/s^2 where as the experimental result shows a peak amplitude of 3725.9 m/s^2.

Comparison of Shock response spectrum of the shell element model with the experiment is shown in Figure 6-5. The finite element analysis acceleration response is obtained from the node, which corresponds to the location of accelerometer-1. As it can be seen from Figure 6-5(a), the shell element model replicates the experiment till a frequency of 3000 Hz after which a difference in magnitudes is observed even though the peak amplitudes correspond to a frequency of 1082.4 Hz on the x-axis. However the

103

comparison becomes a little complicated in Figure 6-5(b) even though the worst frequency in both the cases is 670.4 Hz. In the comparison of experimental response from accelerometer-2 and the response at the node, which corresponds to the location of accelerometer-2 in the finite element shell model, there is not only a huge difference between the finite element analysis and experimental peak amplitudes, the finite element analysis shows a peak amplitude of 5637.5 m/s^2 where as the experimental result shows a peak amplitude of 3725.9 m/s^2 but also a phase difference can be observed in the comparison after a frequency of 2000 Hz.

Figure 6-4(a) Shock Response Spectrum Analysis Comparisons Between FEA Model using Solid Elements and Experimental Results of Glued Double Hat Sections with Continuous Spacers from Accelerometer-1.

104

Figure 6-4(b) SRS analysis comparisons between FEA model using solid elements and experimental results of glued double hat sections with continuous spacers from accelerometer-2

Figure 6-5(a) SRS analysis comparisons between FEA model using shell elements and experimental results of glued double hat sections with continuous spacers from accelerometer-1

105

Figure 6-5(b) SRS analysis comparisons between FEA model using shell elements and experimental results of glued double hat sections with continuous spacers from accelerometer-2

106

6.3 Shock Response Spectrum Analysis Results of the Adhesively Bonded Double Hat Sections with Intermittent Spacers.

Figures 6-6 and 6-7 show the shock response spectrum comparisons between the experiment and finite element analysis of adhesively bonded double hat sections with intermittent spacers. Figure 6-6(a) depicts the shock response spectrum comparison between the experimental response from accelerometer-1 and the response at the node, which corresponds to the location of accelerometer-1 in the finite element solid model. As it can be seen, the worst frequency is close to 1082 Hz in both the experiment and finite element analysis and there is very little difference seen in the amplitude, which is around 8,260 m/s^2. Figure 6-6(b) represents the comparison between the experimental response from accelerometer-2 and the response at the node, which corresponds to the location of accelerometer-2 in the finite element model, where the worst frequency is about 1082 Hz. There is not much amplitude difference observed between the finite element and experimental shock response spectrum in this case when compared to the previous case (continuous spacers) where there is a considerable amplitude difference observed. The experiment shows a peak amplitude of 3220 m/s^2 where as the finite element result shows a peak amplitude of 2853 Hz.

Comparison of Shock response spectrum of the shell element model with the experiment is shown in Figure 6-7. The finite element analysis acceleration response is obtained from the node which corresponds to the location of accelerometer-1. As it can be seen from Figure 6-7(a), the experiment shows a peak amplitude of 8233 m/s^2 where as the finite element result shows a peak amplitude of 8726 m/s^2 which correspond to the worst frequency of 1082.4 Hz in both the cases. It can be observed that the finite element

107

analysis replicates the experiment till a frequency of 3000 Hz after which a difference in magnitudes is observed. Figure 6-7(b) depicts the comparison between the experimental response from accelerometer-2 and the response at the node, which corresponds to the location of accelerometer-2 in the finite element shell model. The worst frequency is again at 1082.4 Hz in both experiment and finite element analysis. As it was seen in the previous case (continuous spacer) there is not only a huge difference between the finite element analysis and experimental peak amplitudes, the finite element analysis shows a peak amplitude of 4556.3 m/s^2 where as the experimental result shows a peak amplitude of 3220 m/s^2 but also a phase difference can be observed in the comparison after a frequency of 2000 Hz.
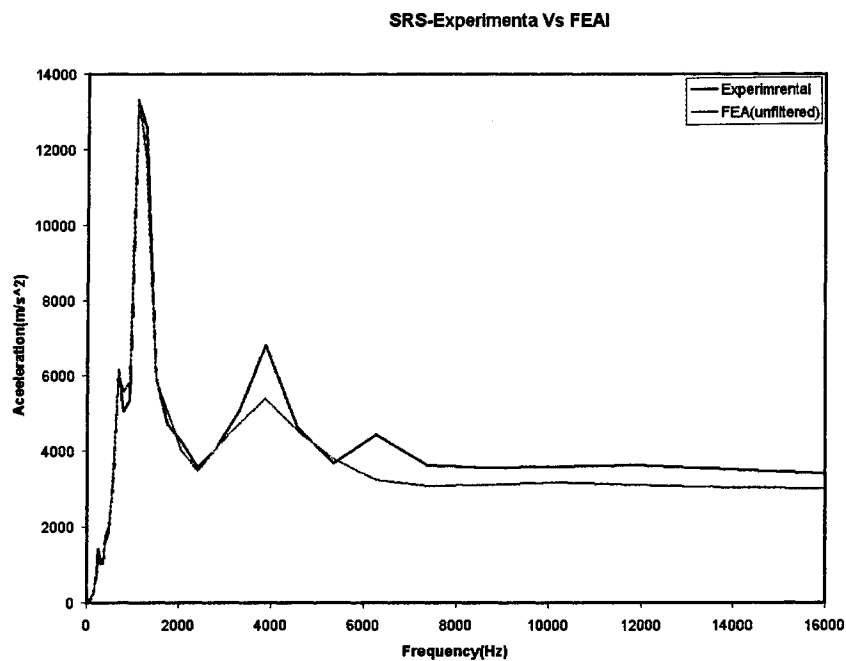

Figure 6-6(a) SRS analysis comparisons between FEA model using solid elements and experimental results of glued double hat sections with intermittent spacers from accelerometer-1

108

Figure 6-6(b) SRS analysis comparisons between FEA model using solid elements and experimental results of glued double hat sections with intermittent spacers from accelerometer-2
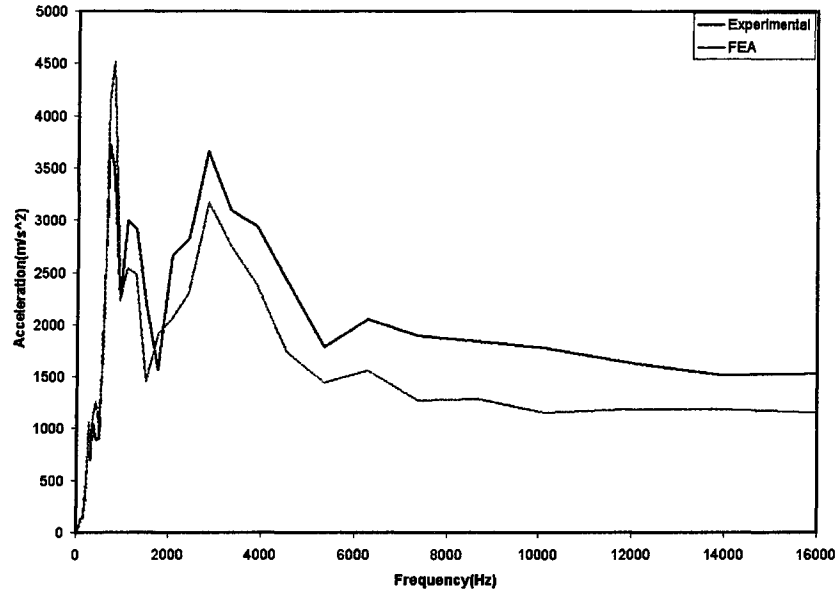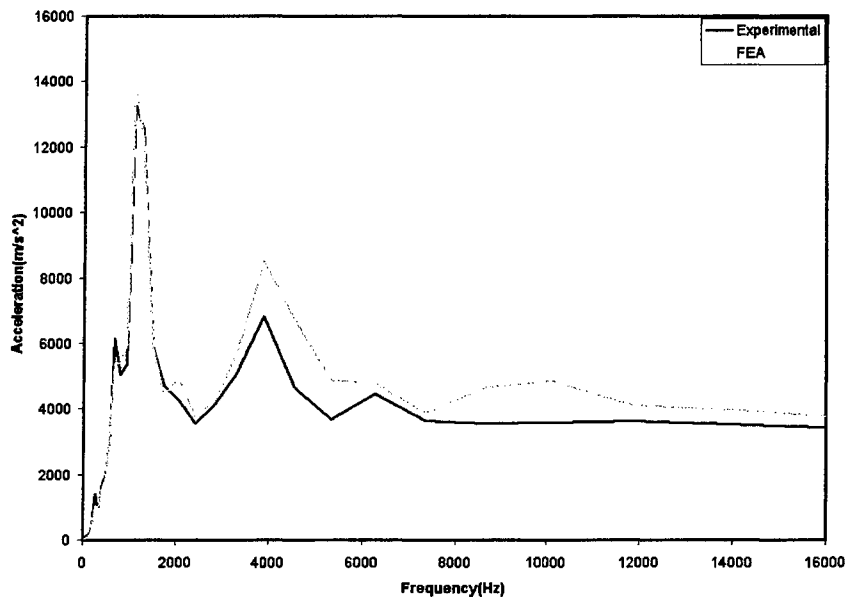

Figure 6.7(a) SRS analysis comparisons between FEA model using shell elements and experimental results of glued double hat sections with intermittent spacers from accelerometer-1

109

Figure 6.7(b) SRS analysis comparisons between FEA model using shell elements and experimental results of glued double hat sections with intermittent spacers from accelerometer-2
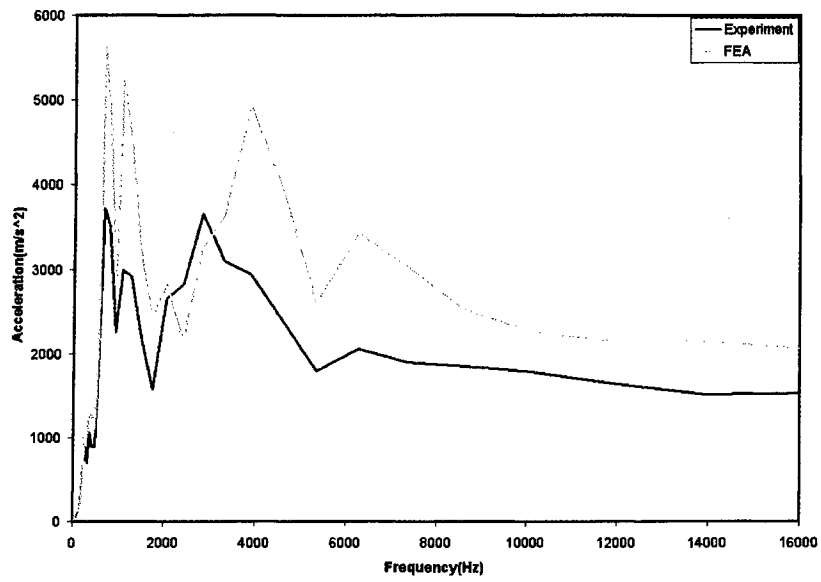
110

6.4 Shock Response Spectrum Analysis Results of Bolted Double Hat Sections.

Shock response spectrum comparisons between the experiment and finite element analysis of double hat sections with bolted joints are depicted in Figures 6-8 and 6-9. Figure 6.8(a) depicts the shock response spectrum comparison between the experimental response from accelerometer-1 from the experiment and the response at the node, which corresponds to the location of accelerometer-1 in the finite element solid model. As it can be seen, the worst frequency is close to 1082.4 Hz, the experiment shows a peak amplitude of 9934.8 m/s^2 where as the finite element result shows a peak amplitude of 11,710 Hz. Figure 6-8(b) represents the comparison between the experimental response from accelerometer-2 and the response at the node, which corresponds to the location of accelerometer-2 in the finite element model, where the worst frequency is about Hz and the experiment shows a peak amplitude of 1082.4 Hz. There is a phase shift that can be observed between the finite element and experiment along with the amplitude difference. The finite element result shows a peak amplitude of 4038 m/s^2 where as the experimental result shows a peak amplitude of 3450 m/s^2, the corresponding frequencies to these amplitudes are 786.46 Hz and 1082.4 Hz respectively.

Comparison of Shock response spectrum of the shell element model with the experiment is shown in Figure 6-9. The finite element analysis acceleration response is obtained from the node, which corresponds to the location of accelerometer-1. As it can be seen from Figure 6-9(a), the experiment shows a peak amplitude of 9,934.8 m/s^2 where as the finite element result shows a peak amplitude of 11,315 m/s^2 which correspond to the worst frequency of 1,082 Hz in both the cases. It can be observed that the finite element analysis replicates the experiment till a frequency of 9,000 Hz after

111

which a difference in magnitudes is observed. Figure 6-7 (b) depicts the comparison between the experimental response from accelerometer-2 from the experiment and the response at the node, which corresponds to the location of accelerometer-2 in the finite element shell model. In this case the worst frequency is again at 1082.4 Hz in both experiment and finite element analysis with slightly different peak amplitudes but the congruity is completely lost after a frequency of 3000 Hz.
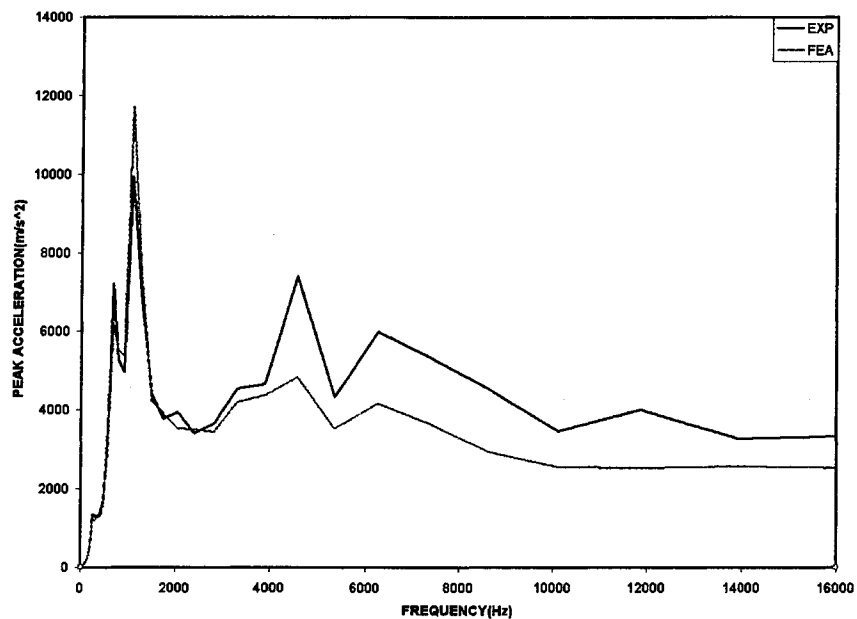
Figure 6-8(a) SRS Analysis comparisons between FEA model using solid elements and experimental results of bolted double hat sections from accelerometer-1

112
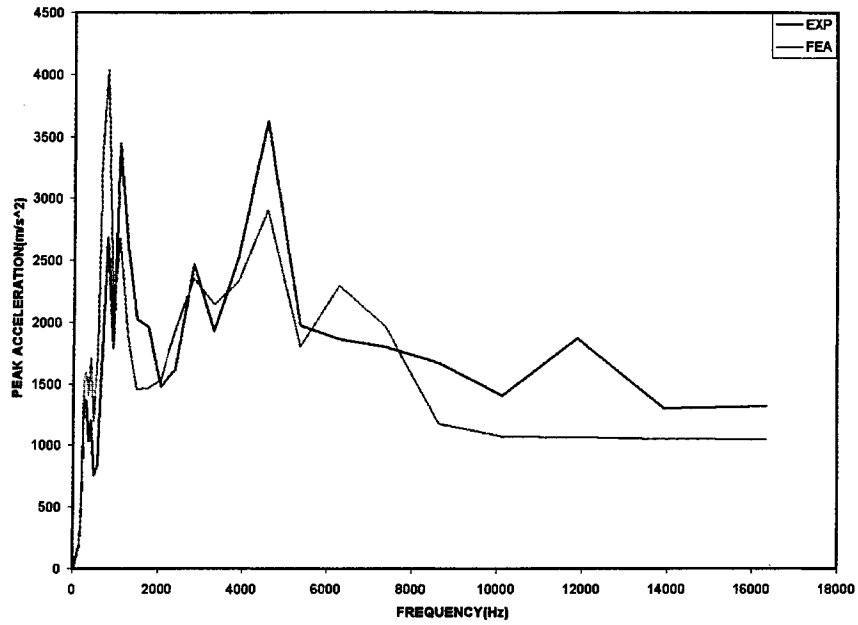
Figure 6-8(b) SRS Analysis comparisons between FEA model using solid elements and experimental results of bolted double hat sections from accelerometer-2
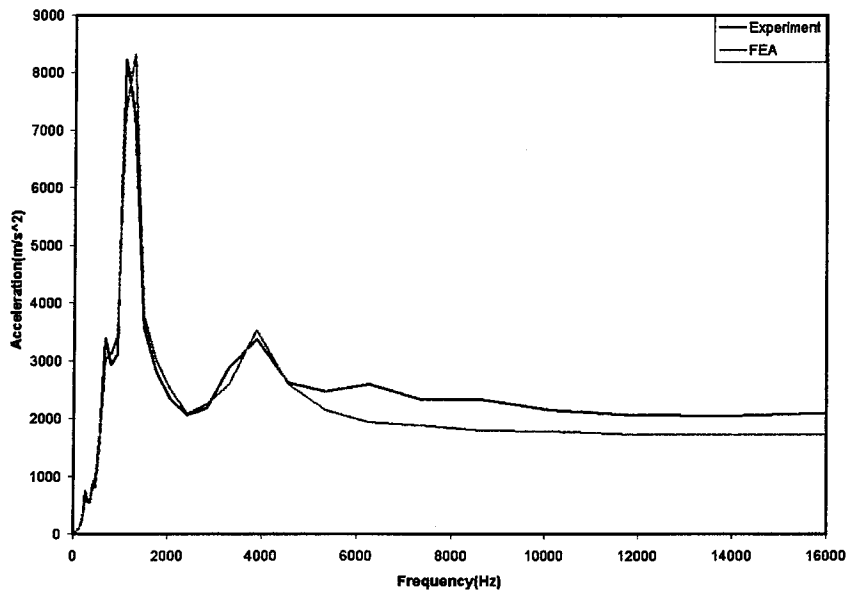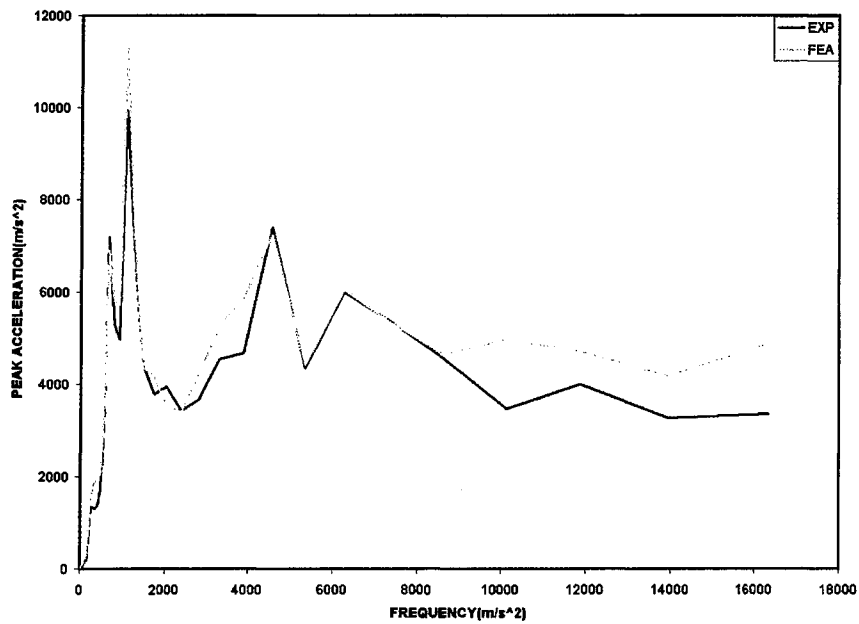

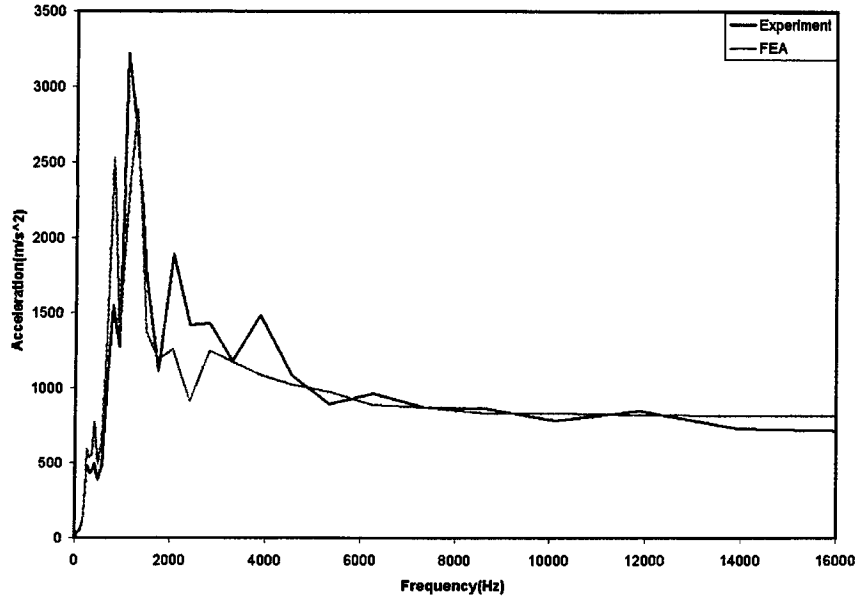Figure 6-9(a) SRS Analysis comparisons between FEA model using shell elements and experimental results of bolted double hat sections from accelerometer-1

113
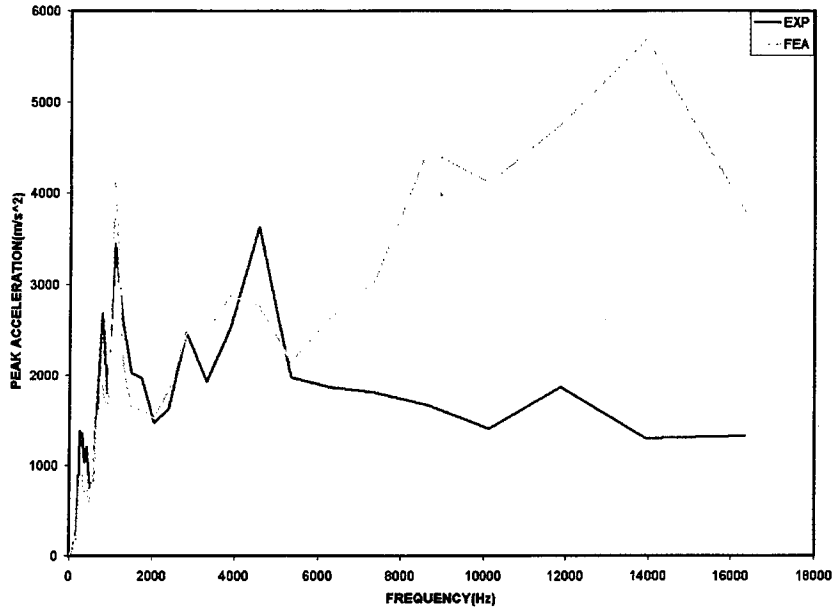
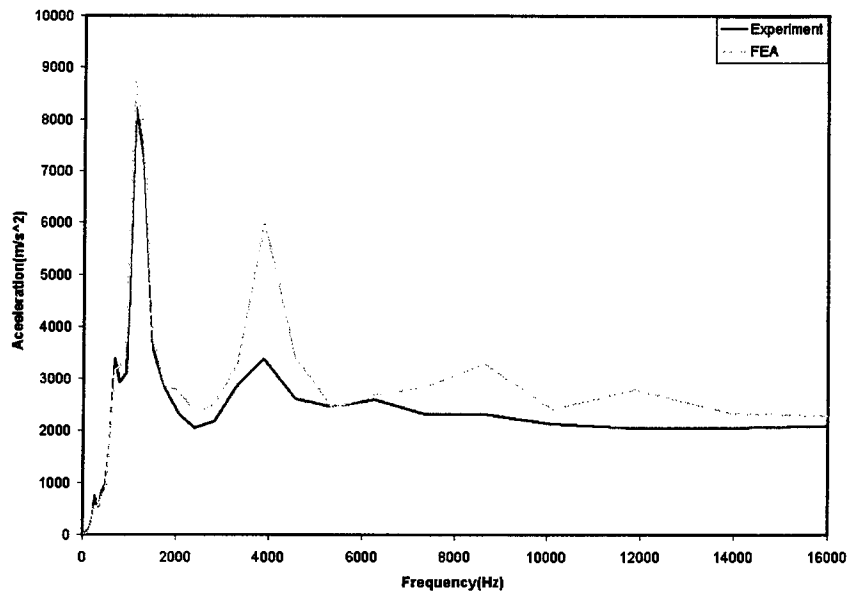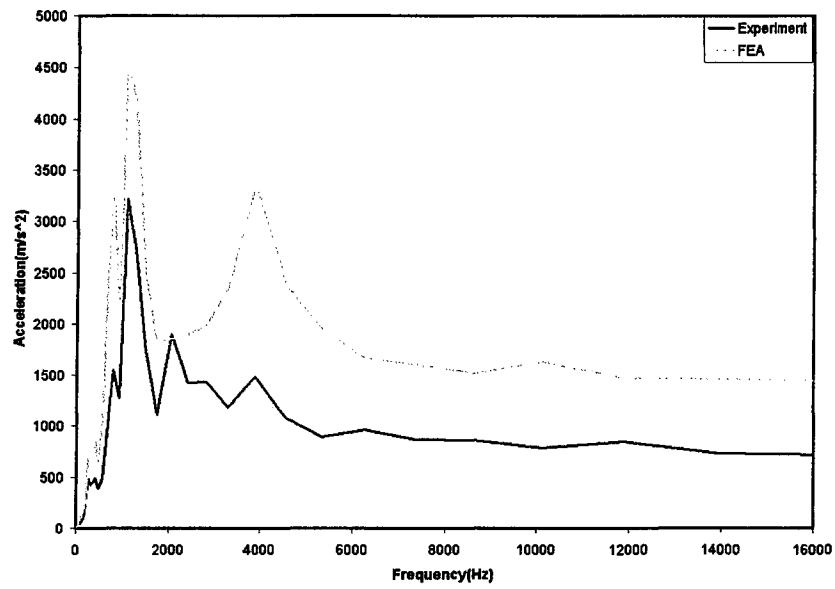Figure 6-9(b) SRS Analysis comparisons between FEA model using shell elements and experimental results of bolted double hat sections from accelerometer-2

114

6.5 Investigation of SRS Results:

As it can be seen from the shock response spectrum comparisons between experiment and finite element analysis, congruity is maintained when the structure is continuous as in the case of single hat section; both shell and solid element finite element analysis results show good agreement with the experimental results. Discrepancies can be observed when joints are introduced.

For the double hat section with continuous spacers and intermittent spacers a typical phenomena is observed, shock response spectrum results from accelerometer-1 and the node corresponding to accelerometer-1 in both shell and solid element finite element models show good agreement as there is no discontinuities in the structure to disturb the shock propagation. But high amplitudes greater then those of the experiment are observed in the finite element solid and shell models for the double hat sections with continuous spacers. It can also be observed that even though there is a magnitude difference between finite element shell and solid element models and the experiment, the solid element model has better correlation with the experiment then the shell element model. Similar pattern is observed for the double hat sections with intermittent spacers for the node corresponding to accelerometer-1 in the finite element shell and solid models. There is a bigger difference with the node corresponding to accelerometer-2 in both shell and solid element models. The shock response from the node corresponding to accelerometer-2 in the solid element model has lesser peak amplitude then the experiment unlike the solid element model of double hat section with continuous spacer where the finite element analysis peak amplitude was larger then that of the experiment. But the shell element model continues to show a similar trend as of the previous case, the finite

115

element analysis peak amplitude is larger then that of the experiment. In both the cases of adhesively jointed double hat sections, solid element proves to be a better approximation to the experiment.

Unlike the previously discussed shock response spectrum from adhesively joined double hat sections, the shock response spectrum from double hat sections with bolted joints have distinctive results. Shock response spectrum results from accelerometer-1 and the node corresponding to accelerometer-1 in both shell and solid element finite element models show good agreement with the experiment but discrepancies are observed at the location of accelerometer-2 in both shell and solid element models. Phase difference is observed in the comparison between the solid element model and the experiment, which was not predominant in the previous cases even though they follow a similar pattern. In the shell element model the worst frequency is again at 1200 Hz in both experiment and finite element analysis with slightly different peak amplitudes but the congruity is completely lost after a frequency of 3000 Hz.

CHAPTER 7

CONCLUSIONS AND FUTURE WORK

7.1 Conclusions

Modal analysis of the single hat section and jointed double hat sections (both adhesive and bolted joints) shows that experimental and finite element analysis results have good agreement. The finite element analysis proves to be proficient in replicating the structural behavior of the hat sections. Both the shell and solid element models in all the cases generate almost the same frequencies.

The results from the single hat section show more congruity between the finite element and experimental results when compared to the jointed hat sections. The main reason behind this is the fact that the single hat section is a continuous structure, and the shock travels along the structure uninterrupted. It can be said from Table 3-2 that super glue proves to be better then epoxy as the error is much lower when compared to epoxy. The jointed hat sections are two separate structures, which are connected to each other using spacers and bolts. The discontinuity in the structure causes the divergence in the higher frequencies between the finite element analysis and experimental results.

In the case of adhesively jointed double hat sections (both, with continuous and intermittent spacers) the finite element model generates similar acceleration responses as of the experiments, the solid element model is comparable for 0.08 seconds, after which

117

phase shift and damping are observed in the finite element model. Discrepancies are augmented at the node, which corresponds to acclerometer-2. The magnitudes vary at some points even though they follow a similar pattern unlike the node, which corresponds, to accelerometer-1 where the acceleration magnitudes and the pattern are similar to the experimental acceleration response till 0.08 seconds.

The finite element results from the adhesively jointed double hat sections with spacers (both, continuous and intermittent) show better congruity with the experimental results when compared to the double hat sections with bolts. The reason behind this might be the area of contact between the two hat sections. In the case of adhesively jointed double hat section the structure behaves relatively more like a continuous structure when compared to the double hat sections with bolted joints. This enables the finite element analysis to better predict the shock response in the adhesively jointed hat sections.

A much better pattern is observed in the comparison between the shell element model responses with that of the experiment in the case of intermittent spacers, the node corresponding to accelerometer-1 has the identical acceleration pattern to the experimental results and starts to diverge from about 0.011 seconds. The most conspicuous difference being the magnitude, which is slightly higher than the response obtained from the solid element model. Akin is the response from the node corresponding to accelerometer-2, which shows more discrepancies as the time increases.

The comparisons between finite element analysis and experimental results are slightly out of the league in the case of the jointed double hat section with bolted joints when compared with the results from adhesively jointed double hat sections (both

intermittent and continuous spacers). The finite element analysis predicts almost the same response at the node, which corresponds to accelerometer-1 in both shell and solid models but the prediction slightly differs for the node, which corresponds to accelerometer-2 in both the shell and solid model. The data from the shell model, had to be filtered to 2500 Hz to compare with the experimental results. The finite element analysis prediction follows similar pattern for about 0.01 seconds after which discrepancies creep in and a phase shift is observed, nevertheless the amplitudes remain almost the same which are most important since damages to components in vehicles due to shock is a function of the magnitudes of the accelerations that the components are subjected to.

The beam element representation of the bolt in the double hat sections with bolted joints does not yield the desired results, the comparison between the experiment and finite element are divergent.

7.2 Investigation of SRS Results:

In the shock response spectrum comparisons between experiment and finite element analysis, congruity is maintained when the structure is continuous as in the case of single hat section; both shell and solid element finite element analysis results show good agreement with the experimental results. Discrepancies can be observed when joints are introduced.

For the double hat section with continuous spacers and intermittent spacers a typical phenomena is observed, shock response spectrum results from accelerometer-1 and the node corresponding to accelerometer-1 in both shell and solid element finite

119

element models show good agreement as there is no discontinuities in the structure to disturb the shock propagation but high amplitudes greater than those obtained from the experiment are observed in the finite element solid and shell models for the double hat sections with continuous spacers. It can also be observed that even though there is a magnitude difference between finite element shell and solid element models and the experiment, the solid element model has better correlation with the experiment then the shell element model. Similar pattern is observed for the double hat sections with intermittent spacers for the node corresponding to accelerometer-1 in the finite element shell and solid models, the difference being with the node corresponding to accelerometer-2 in both shell and solid element models. The shock response from the node corresponding to accelerometer-2 in the solid element model has lesser peak amplitude than the experiment unlike the solid element model of double hat section with continuous spacer where the finite element analysis peak amplitude was larger then that of the experiment. But the shell element model continues to show a similar trend as of the previous case, the finite element analysis peak amplitude is larger then that of the experiment. In both the cases of adhesively jointed double hat sections, solid element proves to be a better approximation to the experiment.

Unlike the previously discussed shock response spectrum from adhesively joined double hat sections, the shock response spectrum from double hat sections with bolted joints have distinctive results. Shock response spectrum results from accelerometer-1 and the node corresponding to accelerometer-1 in both shell and solid element finite element models show good agreement with the experiment but discrepancies are observed at the location of accelerometer-2 in both shell and solid element models. Phase difference is

120

observed in the comparison between the solid element model and the experiment, which was not predominant in the previous cases even though they follow a similar pattern. In the shell element model the worst frequency is again at 1082.4 Hz in both experiment and finite element analysis with slightly different peak amplitudes but the congruity is completely lost after a frequency of 3000 Hz.

7.3 Future Work:

The future work in this task includes determining the various factors, which are influencing the phase shift that is occurring after 10 milli seconds in the time history comparisons between the experimental and finite element analysis. Main focus will be on efficiently modeling various joints for structures, which can accurately predict the shock response. As it was seen in the case of adhesively jointed hat sections, results from super glue and epoxy were reasonably different. It might be interesting to know the physics of adhesive joints by modeling the adhesive layer in the finite element model.

So far different joint configurations have been studied under different loading conditions. The future work will include comparisons of the responses obtained from all the joint configurations when subjected to a single loading function. This will help us in understanding the physics of each joint and the amount of damping the joints are causing in the structure.

Future work may also focus on the experimental and finite element studies of larger double hat sections (quarter inch hat sections) and hats of composite materials, such as fiberglass composites. Intermittently welded double hat sections may also be considered. Another important study will be the shock transmission in a long aluminum

121

plate hanging from above by cables to investigate the geometrical effects on shock

transmission. Other test may include high impacts using the air gun available at UNLV

APPENDIX


```
*KEYWORD
$$ HM_OUTPUT_DECK created 16:42:22 06-06-2005 by HyperMesh
Version 7.0
$$ Ls-dyna Input Deck Generated by HyperMesh Version  : 7.0
$$ Generated using HyperMesh-Ls-dyna 970 Template Version :
7.0
*CONTROL_TERMINATION
$$    ENDTIM      ENDCYC       DTMIN      ENDENG      ENDMAS
        0.016
*CONTROL_HOURGLASS
$$       IHQ          QH
           2
*CONTROL_ENERGY
$$      HGEN        RWEN      SLNTEN       RYLEN
           2
$$DATABASE_OPTION -- Control Cards for ASCII output
*DATABASE_NODOUT
1.5300E-05               1
*DATABASE_BINARY_D3PLOT
$$ DT/CYCL        LCDT        BEAM       NPLTC
1.6000E-04
*DATABASE_BINARY_D3DUMP
$$ DT/CYCL
10000
*NODE
        1            -113.5        -14.346              115.5
        2 -113.1650616622        -14.346    114.2500012962
        3 -112.2499982781        -14.346    113.3349399501
        4            -111.0        -14.346  113.00000489966
        5 -109.7500017219        -14.346    113.3349399501
        6 -108.8349383377        -14.346    114.2500012962
*MAT_PLASTIC_KINEMATIC
$HMNAME MATS          1steel
        17.7800E-09  200000.0       0.33       315.0

*PART
$HMNAME COMPS         16bolt
```


123

```
$HMCOLOR COMPS        16        11

            16         1         1
$HMNAME COMPS         17washer
$HMCOLOR COMPS        17         5

            17         1         1
$HMNAME COMPS         18nut
$HMCOLOR COMPS        18         7

            18         1         1
$HMNAME COMPS         19top_section
$HMCOLOR COMPS        19         2

            19         1         1
*SECTION_SOLID
$HMNAME PROPS         1solid
            1
*CONTACT_TIED_SURFACE_TO_SURFACE
$HMNAME GROUPS        1hat_bolt
$HMCOLOR GROUPS        1        11
$           1
            16        19         3         3


*CONTACT_TIED_SURFACE_TO_SURFACE
$HMNAME GROUPS        2hat_washer
$HMCOLOR GROUPS        2        11
$           2
            17        19         3         3


*CONTACT_TIED_SURFACE_TO_SURFACE
$HMNAME GROUPS        3hat_nut
$HMCOLOR GROUPS        3        11
$           3
            18        19         3         3


*CONTACT_TIED_SURFACE_TO_SURFACE
$HMNAME GROUPS        4bolt_washer
$HMCOLOR GROUPS        4        11
$           4
            17        16         3         3


*CONTACT_TIED_SURFACE_TO_SURFACE
```

124

```
$HMNAME GROUPS        5bolt_nut
$HMCOLOR GROUPS         5       11
$           5
            18        16          3          3


*ELEMENT_SOLID
        17        16         13          1         21         20          2
2        22        22
        19        16          4         14         23         25          3
3        24        24
        22        16         16         13         20         30         14
14        23        23
        24        16         15         11         32         26         12
12        27        27
        25        16         17          5
*LOAD_NODE_POINT
$HMNAME LOADCOLS         1auto1
$HMCOLOR LOADCOLS        1        1
    95151            1          1          1          0
*DATABASE_HISTORY_NODE
$HMNAME OUTPUTBLOCKS          2HISTORY
    44821    139276
*DEFINE_CURVE
$HMNAME CURVES          1curve1
$HMCOLOR CURVES          1        1
$HMCURVE        1      0 curve1
        1            0        1.0        1.0        0.0
0.0            0
0.00E+00,  2.52E+00
1.53E-05,  8.86E+00
3.05E-05,  2.38E+01
4.58E-05,  4.63E+01
6.10E-05,  8.97E+01
7.63E-05,  1.54E+02
9.16E-05,  2.11E+02
1.07E-04,  2.59E+02
1.22E-04,  2.99E+02
1.37E-04,  3.29E+02
1.53E-04,  3.45E+02
1.68E-04,  3.57E+02
1.83E-04,  3.61E+02
```

REFERENCES

1. Gupta A.D, J.M. Santiago and H.L.Wisniewski, "Shock Damage to Sensitive Components in an Armored Vehicle", Computers in Engineering- Vol-2, ASME 1982.

2. Gaul L, and J.Lenz, "Nonlinear Dynamics of Structures Assembled by Bolted Joints", Acta Mechanics 125, 169-181(1997).

3. Ibrahim R.A, C.L.Pettit., "Uncertainties and Dynamic Problems of Bolted joints and other Fasteners", Journal of Sound and Vibration 279 (2005) 857-936.

4. Belingardi G, L.Goglio_, M.Rossetto, "Impact behaviour of bonded built-up beams: experimental results", International Journal of Adhesion & Adhesives 25 (2005) 173-180.

5. Erpolat S, I.A. Ashcroft, A.D. Crocombe, M.M. Abdel-Wahab, "A study of adhesively bonded joints subjected to constant and variable amplitude fatigue", International Journal of Fatigue 26 (2004) 1189-1196.

6. Barnes T.A, I.R.Pashby, "Joining techniques for Aluminum Space frames used in Automobiles Part II-Adhesive bonding and Mechanical Fastener", Journal of Material Processing Technology 99(2000) 72-79.

7. Eskandarian A, D.Marazougui and N.E.Bedewi, "Impact Finite Element and Analysis of Slip-Base Sign Support Mechanism", Journal of Transportation Engineering, March-April 2000.

8. Semke W.H, G.D.Bibel, S.B.Gaurav, A.L.Webster, S.Jarath, "Dynamic Response of a Pipe having Bolted Flange Connection with a Gasket", Engineering Technology Conference on Energy, Febuary 2005.

9. Songa Y, C.J. Hartwigsenb, D.M. McFarlanda, A.F. Vakakisb,c,L.A. Bergman, "Simulation of dynamics of beam structures with bolted joints using adjusted Iwan beam elements", Journal of Sound and Vibration 273 (2004) 249-276.

10. Forrest J.A, "Experimental modal analysis of three small-scale vibration isolator models", Journal of Sound and Vibration.

11. Sinha J K, A.R.Rao, R.I.K. Murthy, " Singnificance of Analytical modeling for Complete interpretation of Experimental modal Analysis: A Case Study", Nuclear Engineering and Design 220(2003) 91-97

12. Munsi A. S. M. Y., A. J. Waddell and C. A. walker, "Modal Analysis of a Lightweight Structure—Investigation of the Effects of the Supports on the Structural Dynamics", Mechanical Systems and Signal Processing (2002) 16(2}3), 273d284.

13. Vaziri A, H.N.Hashemi and H. R. Hamidzadeh, "Experimental and Analytical Investigations of the Dynamic Response of Adhesively Bonded Single Lap Joints", Journal of Vibration and Acoustics, January 2004, Vol. 126 / 85.

14. Sabuwala T, D.Linzell, T. Krauthammer, "Finite element analysis of steel beam to column connections subjected to blast loads", International Journal of Impact Engineering 31 (2005) 861–876.

15 Brüel&Kjær PULSE Help Manual.

16 Ansys 8.0 User Manual.

17 Hypermesh 7.0 User Manual.

18 Ls-Dyna 970 User Manual.

19 SRS View "Shock Response Spectrum Analysis"
www.signalanalysis.com/pdf.srs.pdf.

VITA

Graduate College
University of Nevada, Las Vegas

Karthik Doppala

Local Address:
    969 E Flamingo Road
    Apt#122
    Las Vegas NV 89119

Permanent Address:
    Plot # 478,
    Defence Colony, Sainikpuri (PO)
    Secunderabad,
    Andhra Pradesh INDIA 5000094

Degrees:
    Bachelor of Technology, Mechanical Engineering, 2003
    S.N.I.S.T, Jawahar Lal Technological University
    Hyderabad, INDIA

Thesis Title: Experimental and Finite element Studies of Shock Transmission through
Jointed Hat Sections

Thesis Examination Committee:
    Chairperson, Dr. Samaan Ladkany, Ph. D.
    Chairperson, Dr.Brendan J. O'Toole, Ph. D.
    Committee Member, Dr.Mohamed B Trabia, Ph. D.
    Committee Member, Dr. Samir Moujaes, Ph. D.
    Graduate College Faculty Representative, Dr Gerald Fredrick, Ph.D.

128